Oxidation States, Stability and Reactivity of Organoferrate Complexes

Tobias Parchomyk[†], Serhiy Demeshko[‡], Franc Meyer[‡] and Konrad Koszinowski[*†]

[†]Institut für Organische und Biomolekulare Chemie, Universität Göttingen, Tammannstraße 2, 37077 Göttingen, Germany

[‡]Institut für Anorganische Chemie, Universität Göttingen, Tammannstraße 4, 37077 Göttingen, Germany

Supporting Information

Table of Contents

1.) Effect of the Organyl Substituent

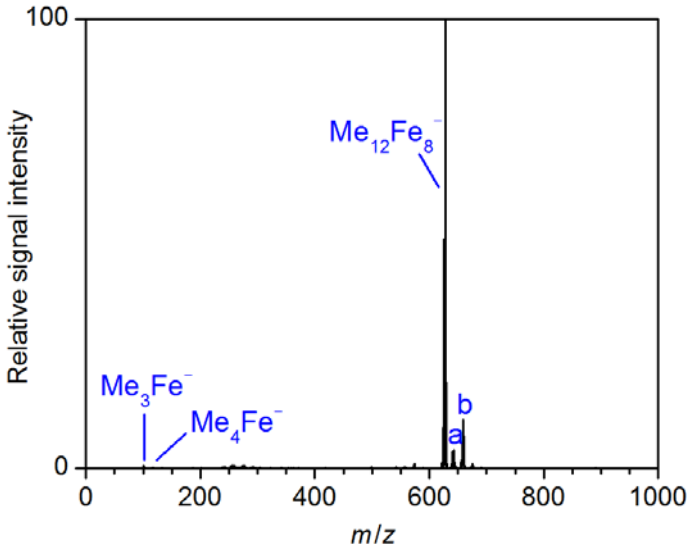

Figure S1. Negative-ion mode ESI mass spectrum of a solution of the products formed in the reaction of $FeCl_3$ (20 mM) with MeMgCl (4 equiv) in THF, a = $Me_{13}Fe_8^-$, b = $[Me_{12},Fe_8,O_2]^-$.

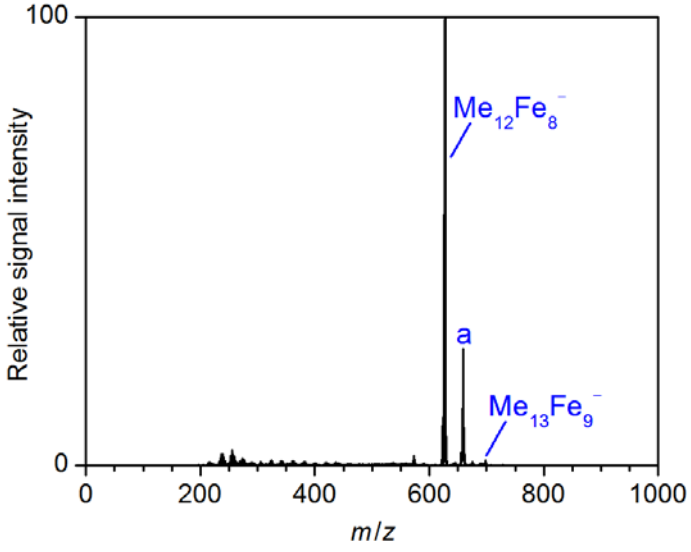

Figure S2. Negative-ion mode ESI mass spectrum of a solution of the products formed in the reaction of $FeCl_2$ (20 mM) with MeMgCl (4 equiv) in THF, a = $[Me_{12},Fe_8,O_2]^-$.

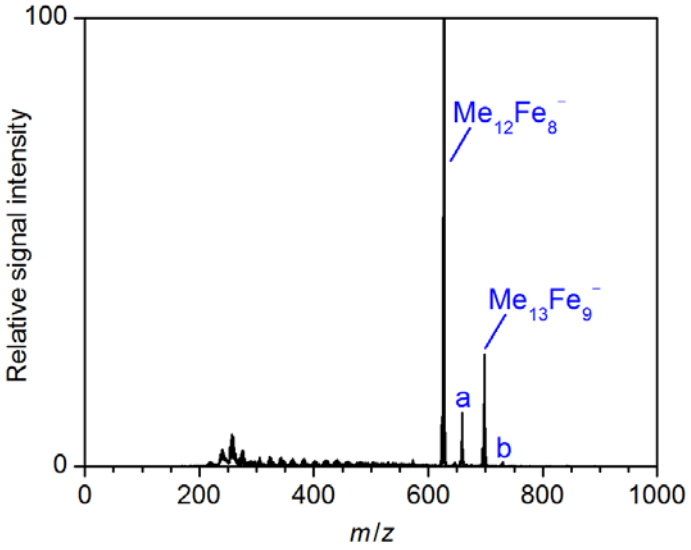

Figure S3. Negative-ion mode ESI mass spectrum of a solution of the products formed in the reaction of $Fe(OAc)_2$ (20 mM) with MeMgCl (4 equiv) in THF; a = $[Me_{12},Fe_8,O_2]^-$, b = $[Me_{13},Fe_9,O_2]^-$.

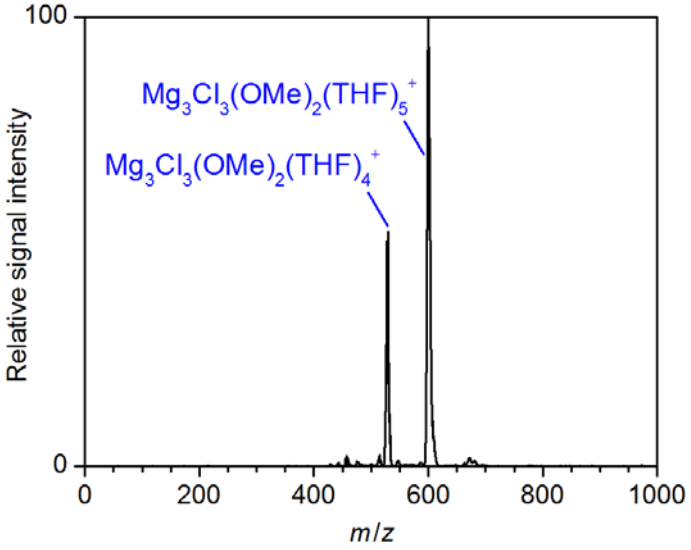

Figure S4. Positive-ion mode ESI mass spectrum of a solution of the products formed in the reaction of $FeCl_3$ (20 mM) with MeMgCl (4 equiv) in THF. The incorporated methoxide originates from traces of methanol as reported previously.[1,2]

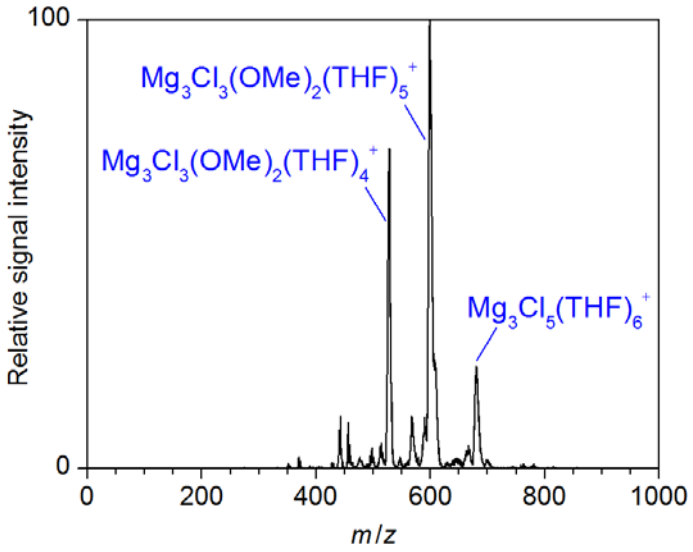

Figure S5. Positive-ion mode ESI mass spectrum of a solution of the products formed in the reaction of $FeCl_2$ (20 mM) with MeMgCl (4 equiv) in THF. The incorporated methoxide originates from traces of methanol as reported previously.[1,2]

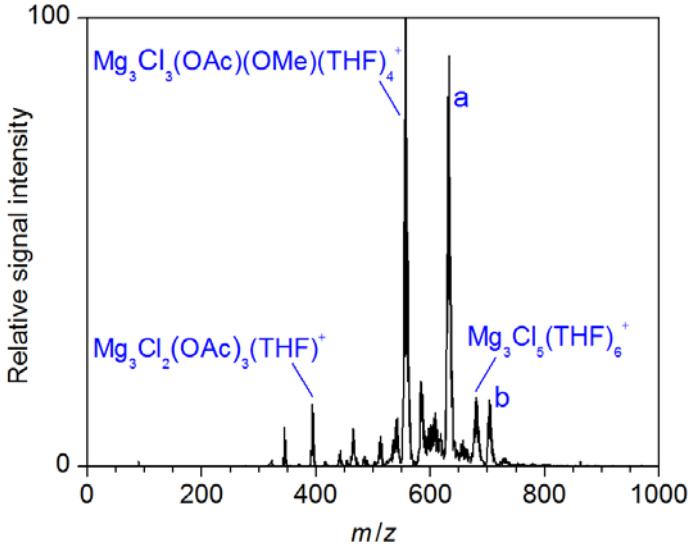

Figure S6. Positive-ion mode ESI mass spectrum of a solution of the products formed in the reaction of $Fe(OAc)_2$ (20 mM) with MeMgCl (4 equiv) in THF; a = $Mg_4Cl_4(OAc)(OH)(OMe)(THF)_4^+$, b = $Mg_4Cl_4(OAc)(OH)(OMe)(THF)_5^+$. The incorporated methoxide originates from traces of methanol as reported previously.[1,2]

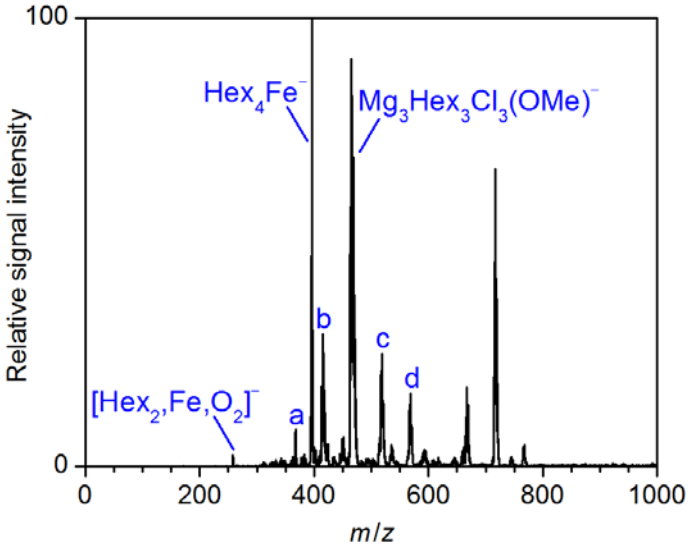

Figure S7. Negative-ion mode ESI mass spectrum of a solution of the products formed in the reaction of $Fe(acac)_3$ (20 mM) with HexMgCl (4 equiv) in THF; a = Hex_4Al^-, b = $Mg_3Hex_2Cl_4(OMe)^-$, c = $Mg_3Hex_4Cl_3^-$, d = $Mg_3Hex_5Cl_2^-$.

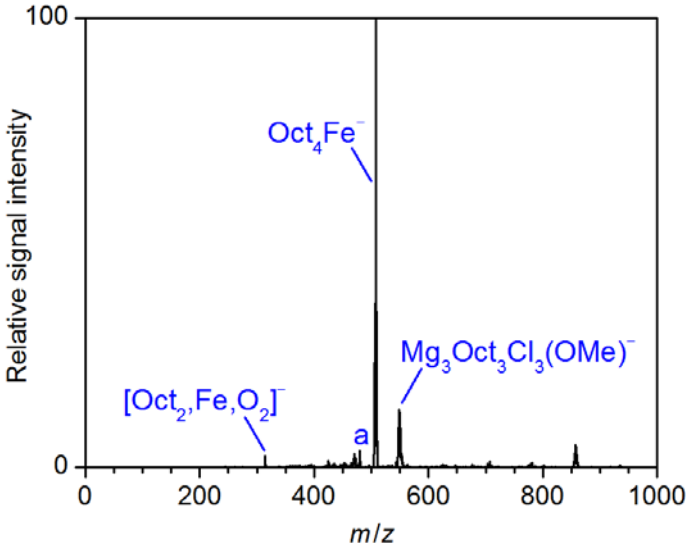

Figure S8. Negative-ion mode ESI mass spectrum of a solution of the products formed in the reaction of $Fe(acac)_3$ (20 mM) with OctMgCl (4 equiv) in THF; a = Oct_4Al^-.

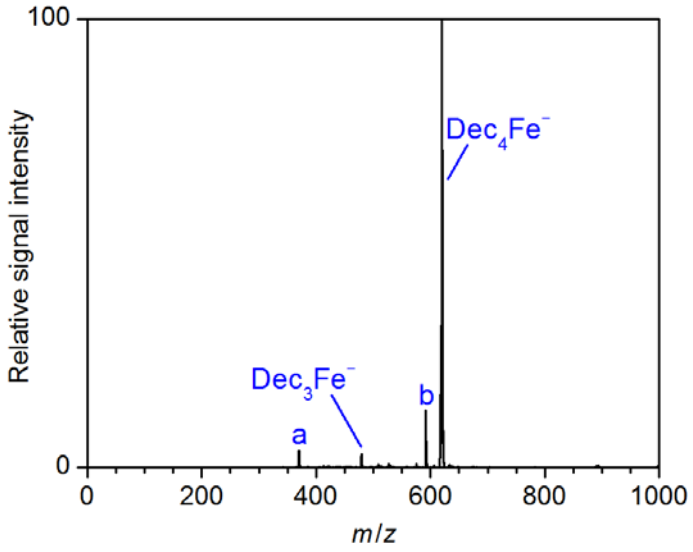

Figure S9. Negative-ion mode ESI mass spectrum of a solution of the products formed in the reaction of $Fe(acac)_3$ (20 mM) with DecMgCl (4 equiv) in THF; a = $[Dec_2,Fe,O_2]^-$, b = Dec_4Al^-.

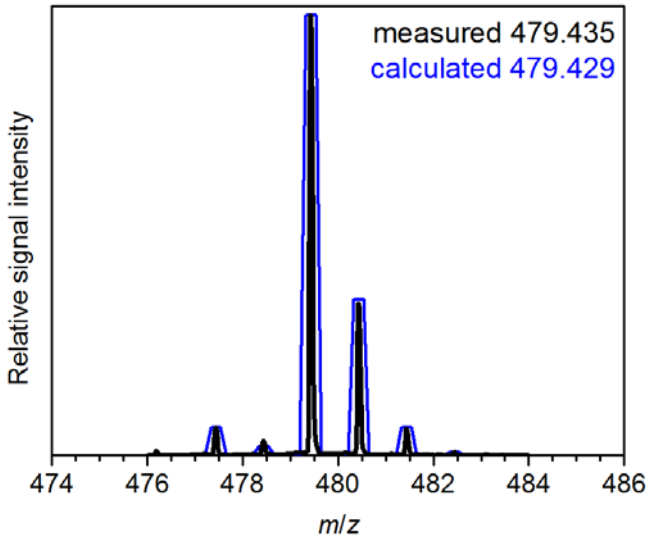

Figure S10. Comparison of the observed (black, measured with the micrOTOF-Q II instrument) and simulated (blue) isotope pattern of Dec_3Fe^-.

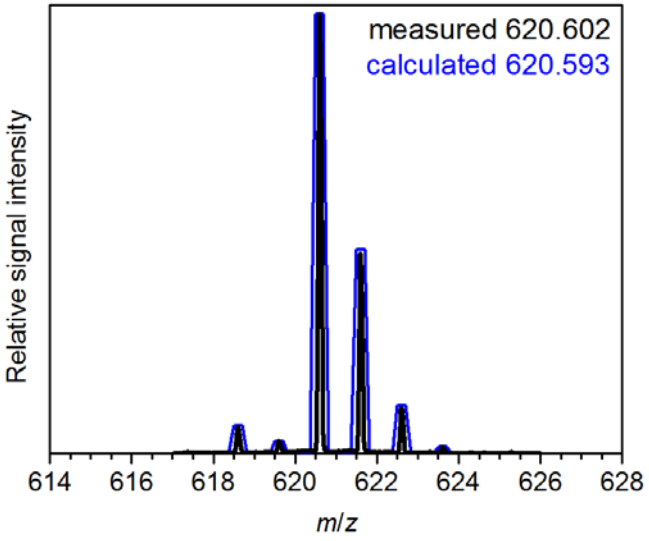

Figure S11. Comparison of the observed (black, measured with the micrOTOF-Q II instrument) and simulated (blue) isotope pattern of Dec_4Fe^-.

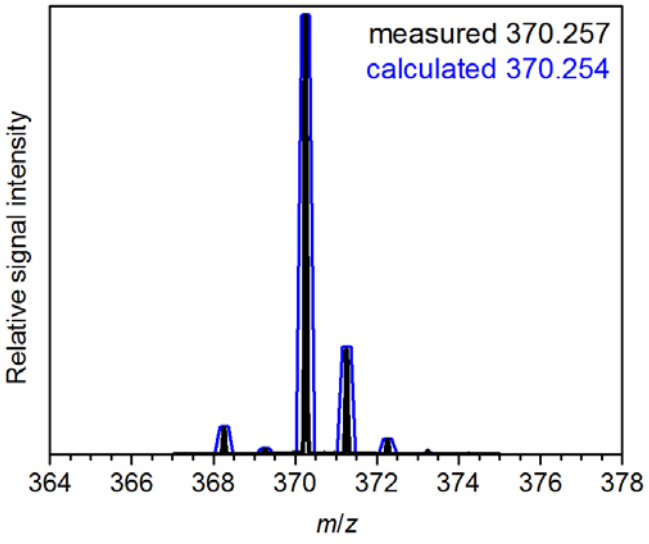

Figure S12. Comparison of the observed (black, measured with the micrOTOF-Q II instrument) and simulated (blue) isotope pattern of $[Dec_2Fe,O_2]^-$.

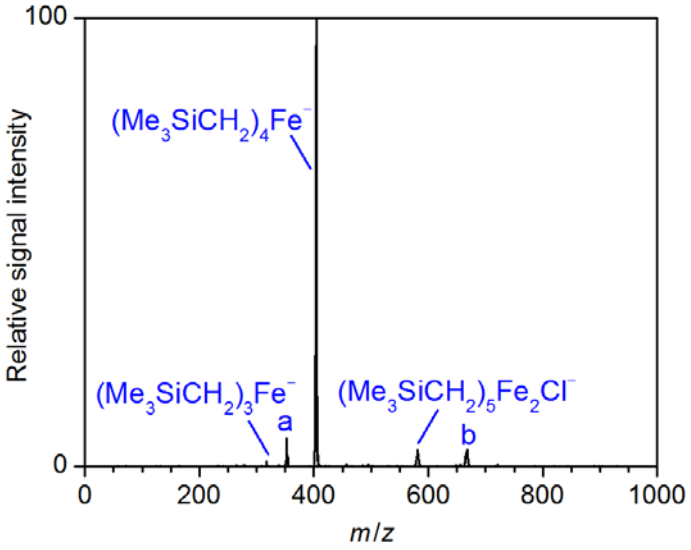

Figure S13. Negative-ion mode ESI mass spectrum of a solution of the products formed in the reaction of $Fe(acac)_3$ (20 mM) with Me_3SiCH_2MgCl (4 equiv) in THF; a = $(Me_3SiCH_2)_3FeCl^-$, b = $(Me_3SiCH_2)_6Fe_2Cl^-$.

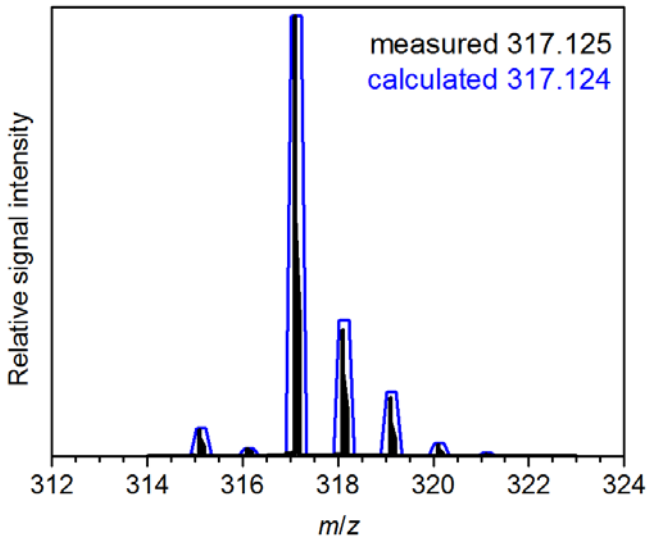

Figure S14. Comparison of the observed (black, measured with the micrOTOF-Q II instrument) and simulated (blue) isotope pattern of $(Me_3SiCH_2)_3Fe^-$.

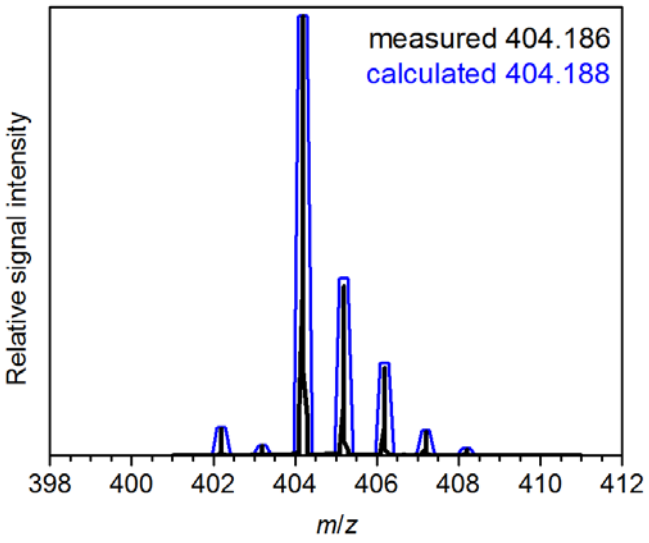

Figure S15. Comparison of the observed (black, measured with the micrOTOF-Q II instrument) and simulated (blue) isotope pattern of $(Me_3SiCH_2)_4Fe^-$.

Table S1. Specific electrical conductivity κ / (μS cm^{-1}) of organoferrates produced by transmetallation of $Fe(acac)_3$ (50 mM) with 4 equiv of RMgX (R = Me_3SiCH_2, Bn, Ph, Mes, Ar_F; X = Cl or Br) in THF (T = 273 K); Ar_F = 3,5-$(CF_3)_2$-C_6H_3.

sample solution in THF	**κ / μS cm^{-1}**
$Fe(acac)_3$ + 4 Me_3SiCH_2MgCl	319 ± 24
$Fe(acac)_3$ + 4 BnMgCl	201 ± 10
$Fe(acac)_3$ + 4 PhMgCl	99 ± 16
$Fe(acac)_3$ + 4 MesMgBr	339 ± 6
$Fe(acac)_3$ + 4 Ar_FMgCl	450 ± 6

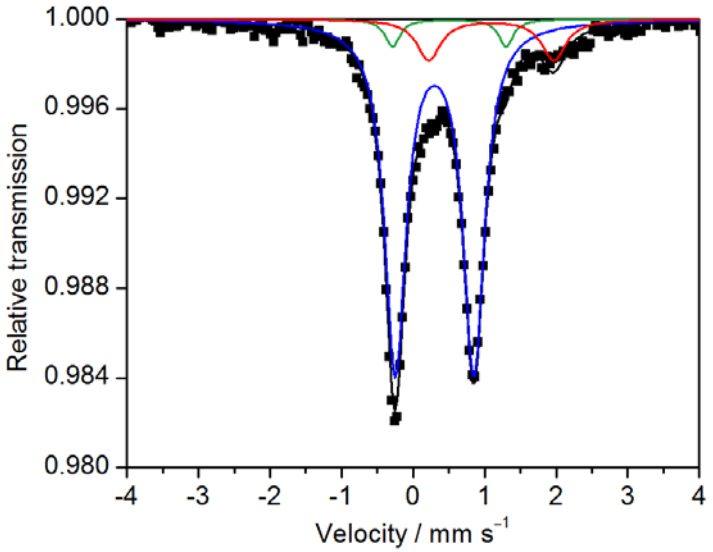

Figure S16. Mössbauer spectrum of a frozen solution (T = 80 K) of the products formed in the reaction of $^{57}FeCl_2$ (5 mM) with Me_3SiCH_2MgCl (4 equiv) in THF together with overall fit (black); components of the fit: δ(blue) = 0.30 mm s^{-1}, ΔE_Q(blue) = 1.10 mm s^{-1}, rel. int. (blue) = 84%; ; δ(red) = 1.09 mm s^{-1}, ΔE_Q(red) = 1.75 mm s^{-1}, rel. int. (red) = 11%; δ(green) = 0.50 mm s^{-1}, ΔE_Q(green) = 1.59 mm s^{-1}, rel. int. (green) = 5%.

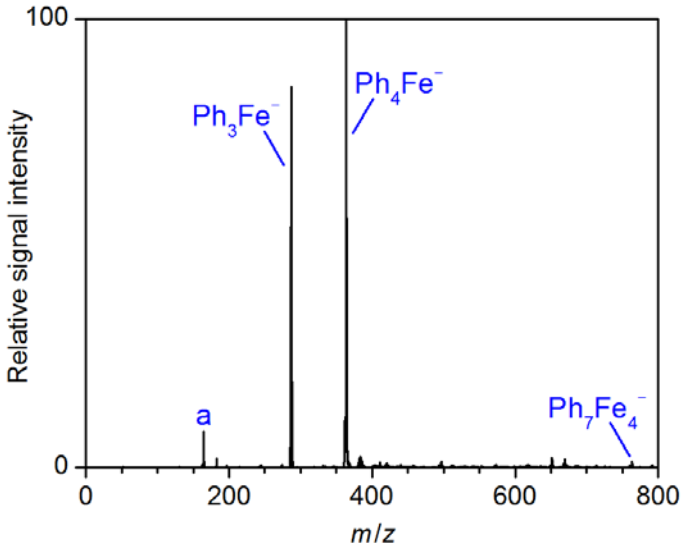

Figure S17. Negative-ion mode ESI mass spectrum of a solution of the products formed in the reaction of $Fe(acac)_3$ (20 mM) with PhMgCl (4 equiv) in THF; a = $[Ph,Fe,O_2]^-$.

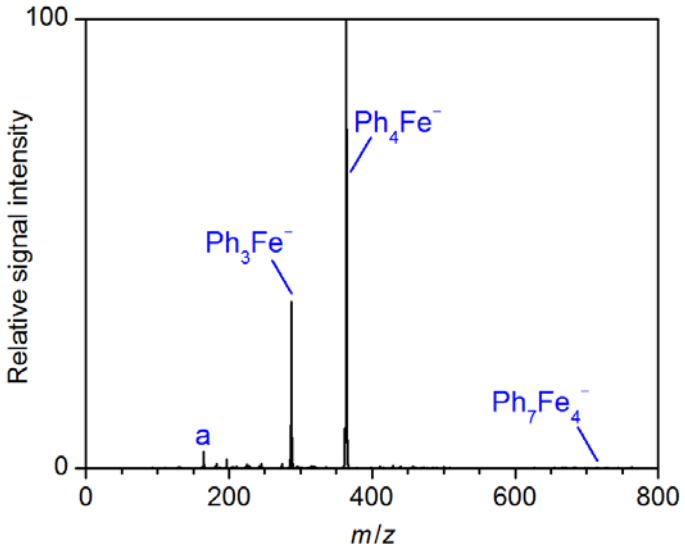

Figure S18. Negative-ion mode ESI mass spectrum of a solution of the products formed in the reaction of $FeCl_3$ (20 mM) with PhMgCl (4 equiv) in THF; a = $[Ph,Fe,O_2]^-$.

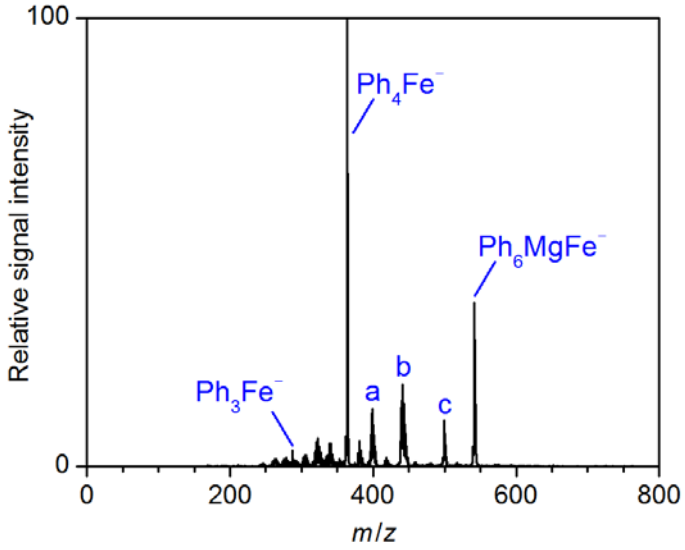

Figure S19. Negative-ion mode ESI mass spectrum of a solution of the products formed in the reaction of $FeCl_2$ (20 mM) with PhMgCl (4 equiv) in THF; a = $Ph_2Mg_3Cl_4(OMe)^-$, b = $Ph_3Mg_3Cl_3(OMe)^-$, c = $Ph_5MgFeCl^-$.

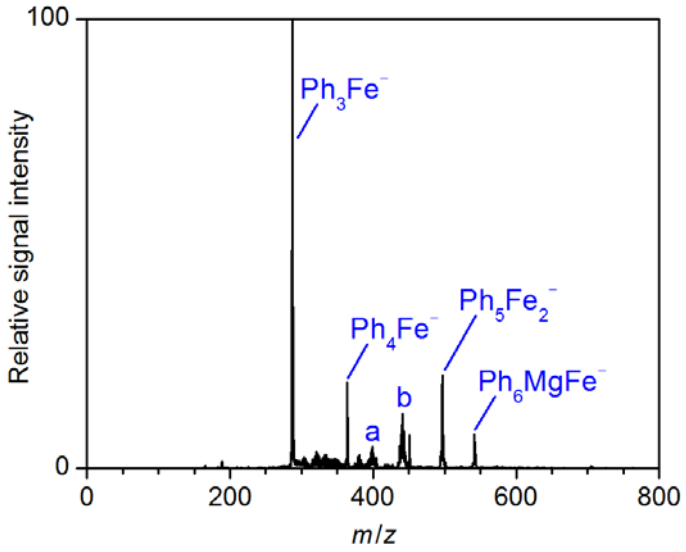

Figure S20. Negative-ion mode ESI mass spectrum of a solution of the products formed in the reaction of $Fe(OAc)_2$ (20 mM) with PhMgCl (4 equiv) in THF; a = $Ph_2Mg_3Cl_4(OMe)^-$, b = $Ph_3Mg_3Cl_3(OMe)^-$.

Table S2. Specific electrical conductivity κ / (μS cm^{-1}) of organoferrates produced by transmetallation of an iron precursor (50 mM) with 4 equiv of PhMgCl in THF (T = 273 K).

sample solution in THF	**κ / μS cm^{-1}**
$Fe(acac)_3$ + 4 PhMgCl	99 ± 16
$FeCl_3$ + 4 PhMgCl	59 ± 1
$FeCl_2$ + 4 PhMgCl	57 ± 3
$Fe(OAc)_2$ + 4 PhMgCl	98 ± 6

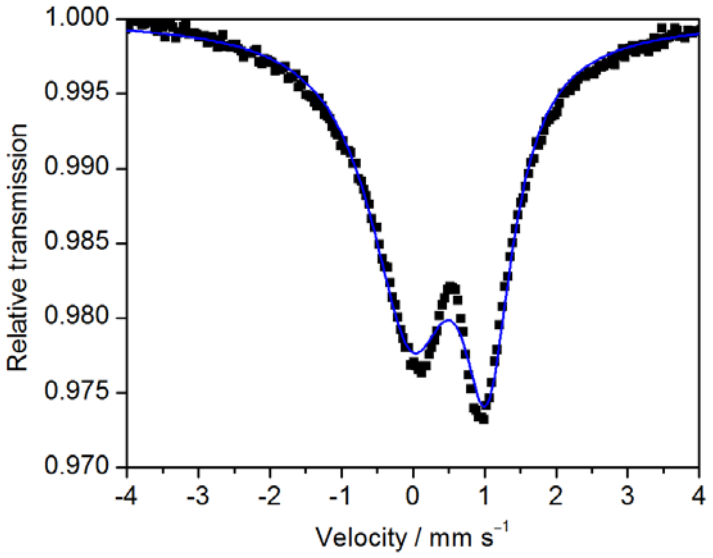

Figure S21. Mössbauer spectrum of a frozen solution (T = 80 K) of the products formed in the reaction of $^{57}FeCl_2$ (5 mM) with PhMgCl (4 equiv) in THF together with fit (blue); fit parameters: δ = 0.50 mm s^{-1}, ΔE_Q = 1.06 mm s^{-1}.

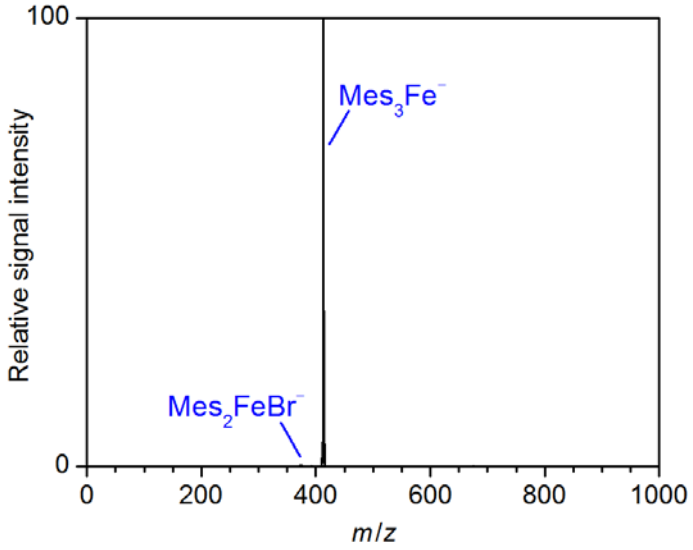

Figure S22. Negative-ion mode ESI mass spectrum of a solution of the products formed in the reaction of $Fe(acac)_3$ (20 mM) with MesMgBr (4 equiv) in THF.

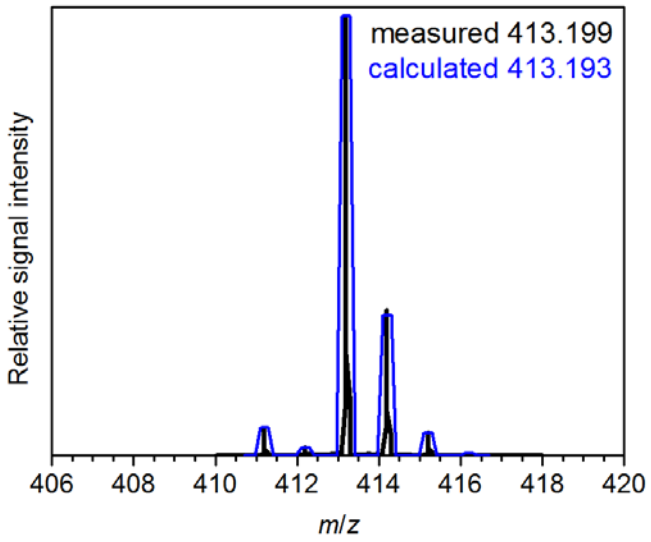

Figure S23. Comparison of the observed (black, measured with the micrOTOF-Q II instrument) and simulated (blue) isotope pattern of Mes_3Fe^-.

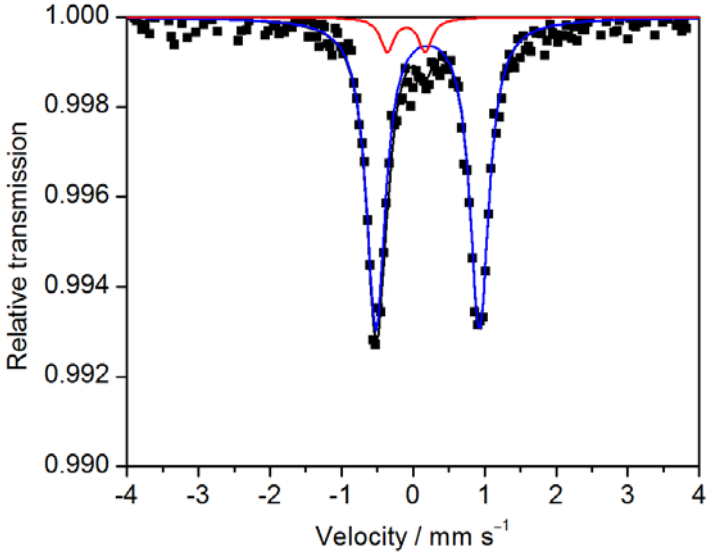

Figure S24. Mössbauer spectrum of a frozen solution (T = 80 K) of the products formed in the reaction of $^{57}FeCl_2$ (5 mM) with MesMgBr (4 equiv) in THF together with overall fit (black); components of the fit: δ(blue) = 0.20 mm s^{-1}, ΔE_Q(blue) = 1.45 mm s^{-1}, rel. int. (blue) = 93%; δ(red) = –0.10 mm s^{-1}, ΔE_Q(red) = 0.53 mm s^{-1}, rel. int. (red) = 7%.

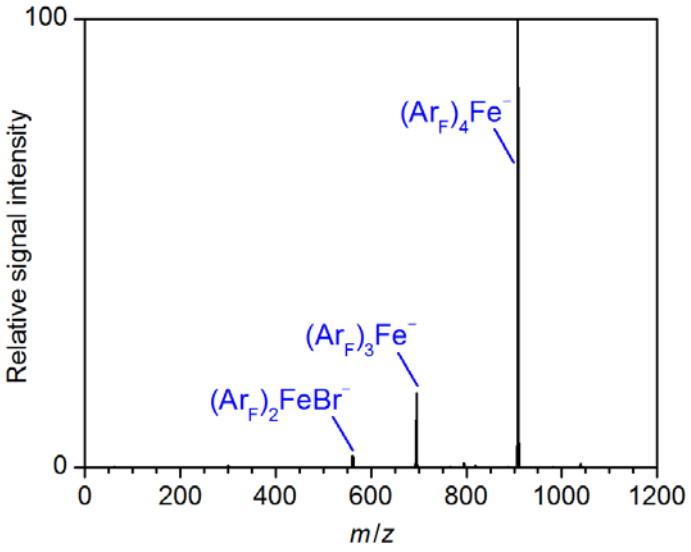

Figure S25. Negative-ion mode ESI mass spectrum of a solution of the products formed in the reaction of $Fe(acac)_3$ (20 mM) with $(Ar_F)MgBr$ (4 equiv) in THF; Ar_F = 3,5-$(CF_3)_2$-C_6H_3.

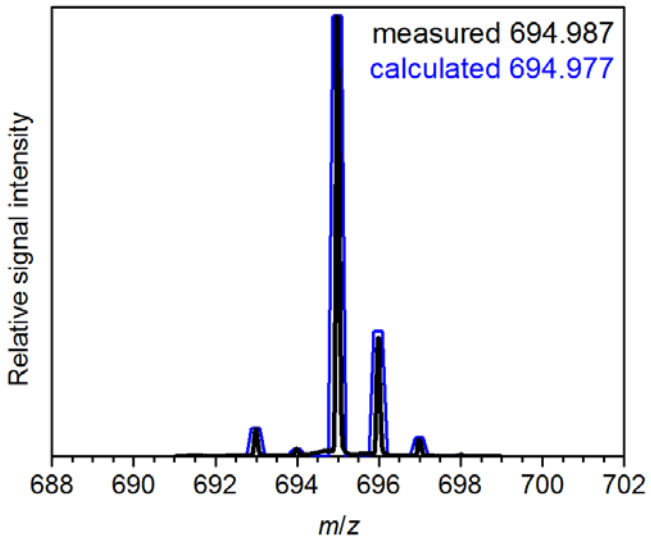

Figure S26. Comparison of the observed (black, measured with the micrOTOF-Q II instrument) and simulated (blue) isotope pattern of $(Ar_F)_3Fe^-$; Ar_F = 3,5-$(CF_3)_2$-C_6H_3.

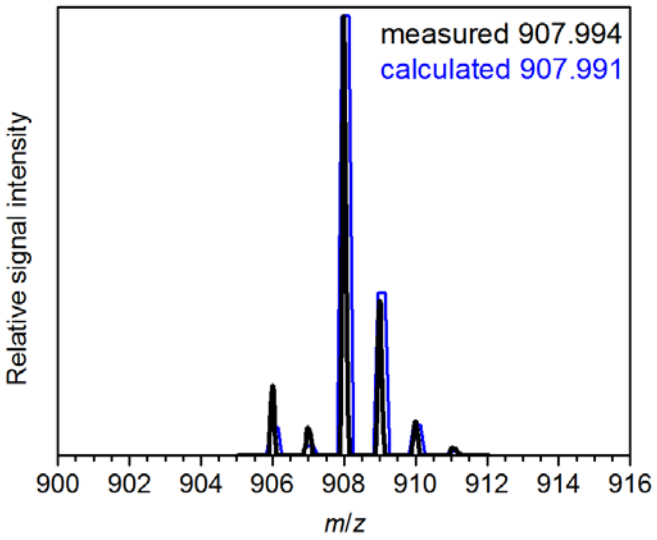

Figure S27. Comparison of the observed (black, measured with the micrOTOF-Q II instrument) and simulated (blue) isotope pattern of $(Ar_F)_4Fe^-$; Ar_F = 3,5-$(CF_3)_2$-C_6H_3.

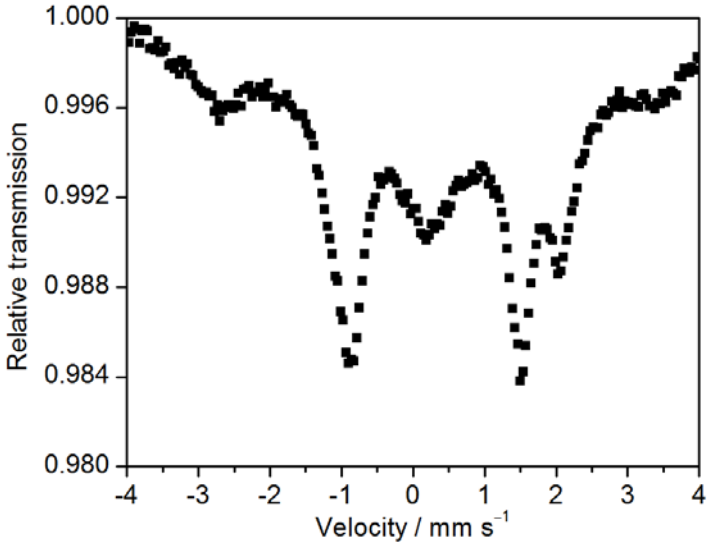

Figure S28. Mössbauer spectrum of a frozen solution (T = 80 K) of the products formed in the reaction of $^{57}FeCl_2$ (5 mM) with $(Ar_F)MgBr$ (4 equiv) in THF; Ar_F = 3,5-$(CF_3)_2$-C_6H_3.

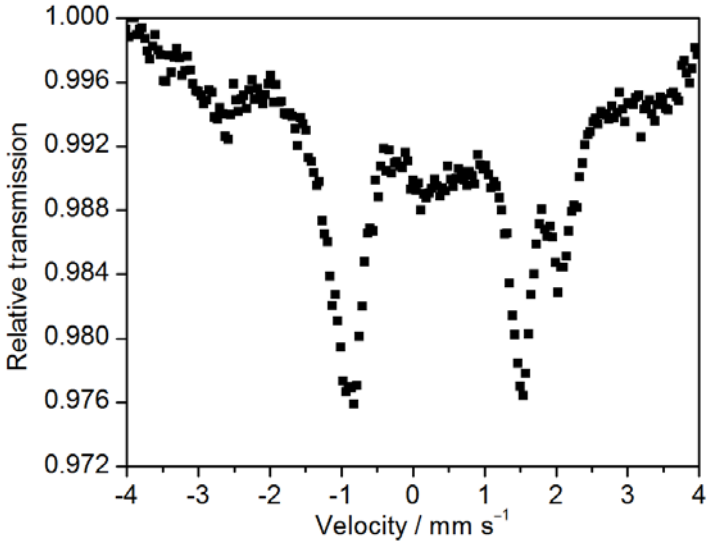

Figure S29. Mössbauer spectrum of a frozen solution (T = 7 K) of the products formed in the reaction of $^{57}FeCl_2$ (5 mM) with $(Ar_F)MgBr$ (4 equiv) in THF; Ar_F = 3,5-$(CF_3)_2$-C_6H_3.

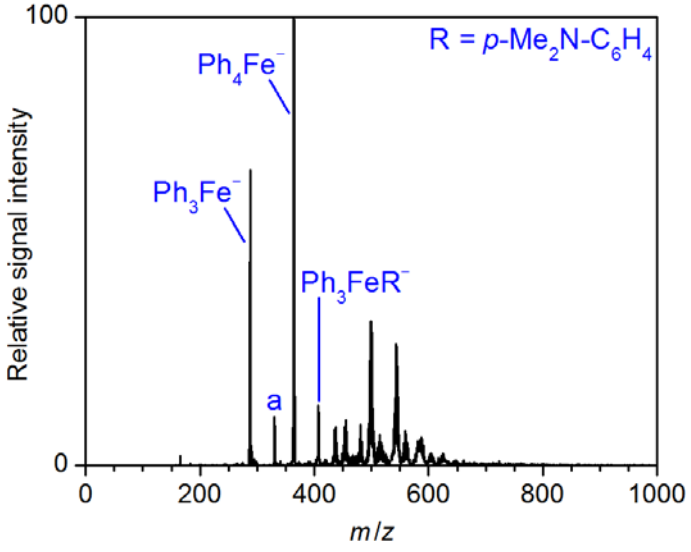

Figure S30. Negative-ion mode ESI mass spectrum of a solution of the products formed in the reaction of $Fe(acac)_3$ (20 mM) with PhMgCl (2 equiv) and RMgBr (2 equiv) in THF; a = Ph_2FeR^-; R = *p*-Me_2N-C_6H_4.

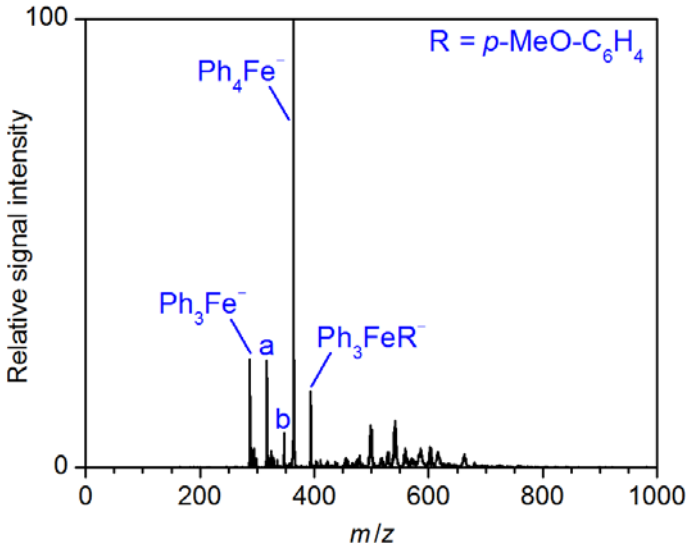

Figure S31. Negative-ion mode ESI mass spectrum of a solution of the products formed in the reaction of $Fe(acac)_3$ (20 mM) with PhMgCl (2 equiv) and RMgBr (2 equiv) in THF; a = Ph_2FeR^-, b = $PhFeR_2^-$; R = *p*-MeO-C_6H_4.

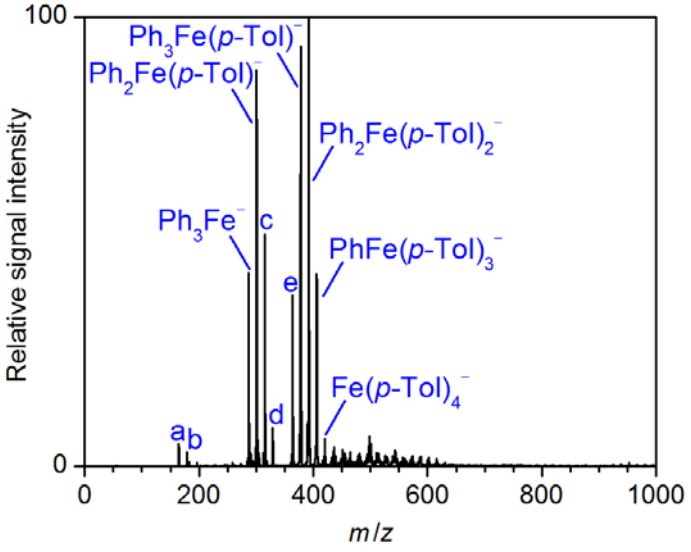

Figure S32. Negative-ion mode ESI mass spectrum of a solution of the products formed in the reaction of $Fe(acac)_3$ (20 mM) with PhMgCl (2 equiv) and (*p*-Tol)MgBr (2 equiv) in THF; a = $[Fe,Ph,O_2]^-$, b = $[(p\text{-Tol}),Fe,O_2]^-$, c = $PhFe(p\text{-Tol})_2^-$, d = $Fe(p\text{-Tol})_3^-$, e = Ph_4Fe^-.

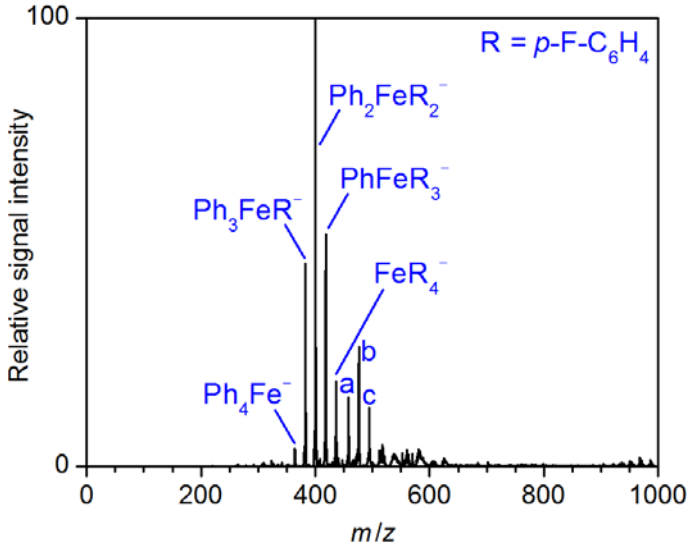

Figure S33. Negative-ion mode ESI mass spectrum of a solution of the products formed in the reaction of $Fe(acac)_3$ (20 mM) with PhMgCl (2 equiv) and RMgBr (2 equiv) in THF; a = $Ph_3Fe(C_6H_4C_6H_4F)^-$, b = $Ph_2FeR(C_6H_4C_6H_4F)^-$, c = $PhFeR_2(C_6H_4C_6H_4F)^-$; R = *p*-F-C_6H_4.

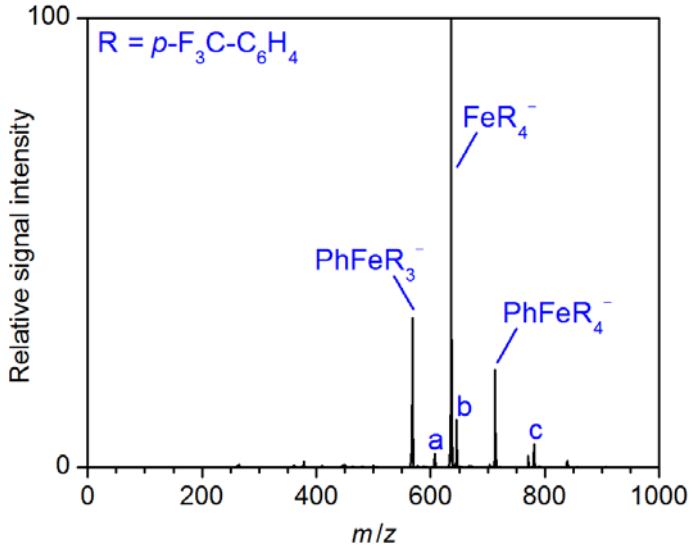

Figure S34. Negative-ion mode ESI mass spectrum of a solution of the products formed in the reaction of $Fe(acac)_3$ (20 mM) with PhMgCl (2 equiv) and RMgBr (2 equiv) in THF; a = AlR_4^-, b = $Ph_2FeR_3^-$, c = FeR_5^-; R = *p*-F_3C-C_6H_4.

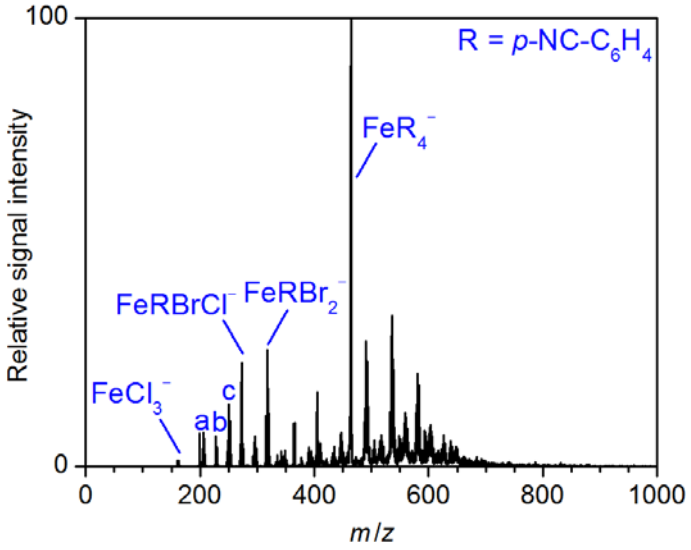

Figure S35. Negative-ion mode ESI mass spectrum of a solution of the products formed in the reaction of $Fe(acac)_3$ (20 mM) with PhMgCl (2 equiv) and RMgBr (2 equiv) in THF; a = $FeBrCl_2^-$, b = $FeRCl_2^-$, c = $FeBr_2Cl^-$; R = *p*-NC-C_6H_4.

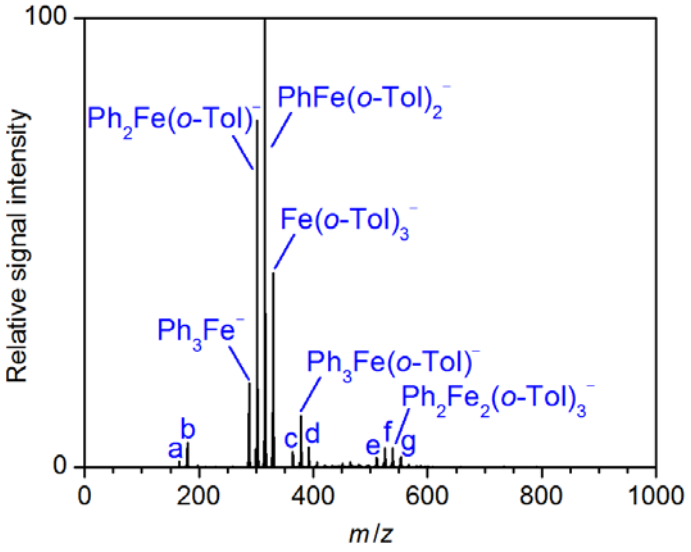

Figure S36. Negative-ion mode ESI mass spectrum of a solution of the products formed in the reaction of $Fe(acac)_3$ (20 mM) with PhMgCl (2 equiv) and (*o*-Tol)MgBr (2 equiv) in THF; a = $[Fe,Ph,O_2]^-$, b = $[(o\text{-Tol}),Fe,O_2]^-$, c = Ph_4Fe^-, d = $Ph_2Fe(o\text{-Tol})_2^-$, e = $Ph_4Fe_2(o\text{-Tol})^-$, f = $Ph_3Fe_2(o\text{-Tol})_2^-$; g = $PhFe_2(o\text{-Tol})_4^-$.

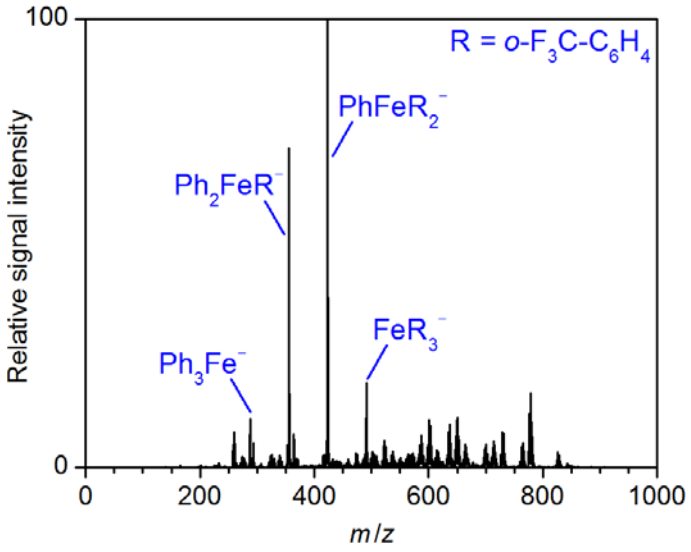

Figure S37. Negative-ion mode ESI mass spectrum of a solution of the products formed in the reaction of $Fe(acac)_3$ (20 mM) with PhMgCl (2 equiv) and RMgBr (2 equiv) in THF; R = *o*-F_3C-C_6H_4.

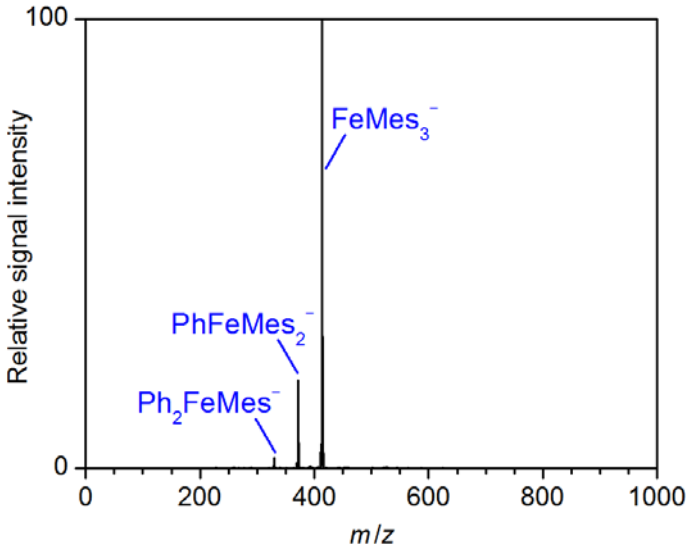

Figure S38. Negative-ion mode ESI mass spectrum of a solution of the products formed in the reaction of $Fe(acac)_3$ (20 mM) with PhMgCl (2 equiv) and MesMgBr (2 equiv) in THF.

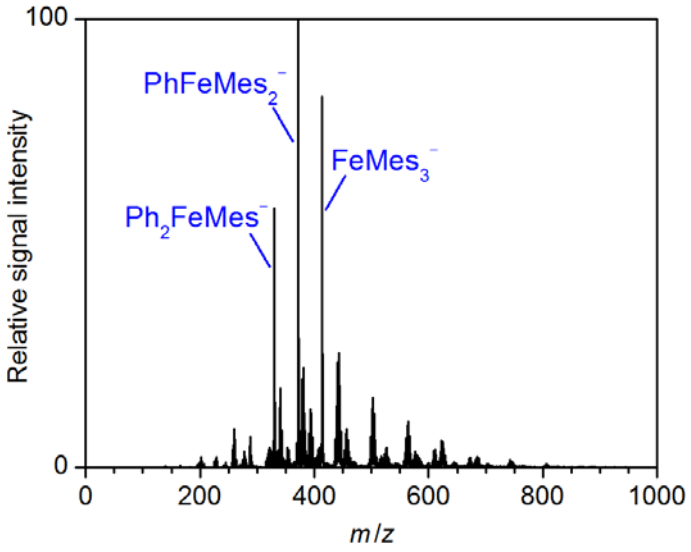

Figure S39. Negative-ion mode ESI mass spectrum of a solution of the products formed in the reaction of $Fe(acac)_3$ (20 mM) with PhMgCl (10 equiv) and MesMgBr (1 equiv) in THF.

2.) Effect of Added TMEDA

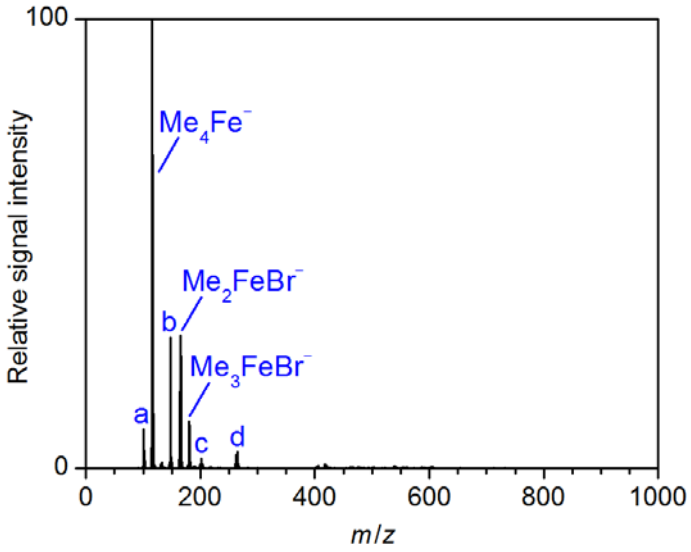

Figure S40. Negative-ion mode ESI mass spectrum of a solution of the products formed in the reaction of $Fe(acac)_3$ (20 mM) with TMEDA (4 equiv) and MeMgBr (4 equiv) in THF; a = Me_3Fe^-, b = $[Me_4,Fe,O_2]^-$, c = $Me_6Fe_2^-$, d = $MgBr_3^-$.

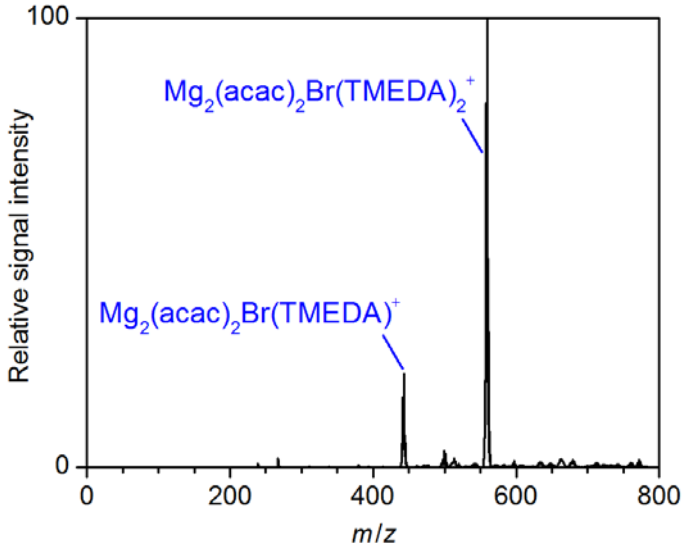

Figure S41. Positive-ion mode ESI mass spectrum of a solution of the products formed in the reaction of $Fe(acac)_3$ (10 mM) and TMEDA (4 equiv) with MeMgBr (4 equiv) in THF.

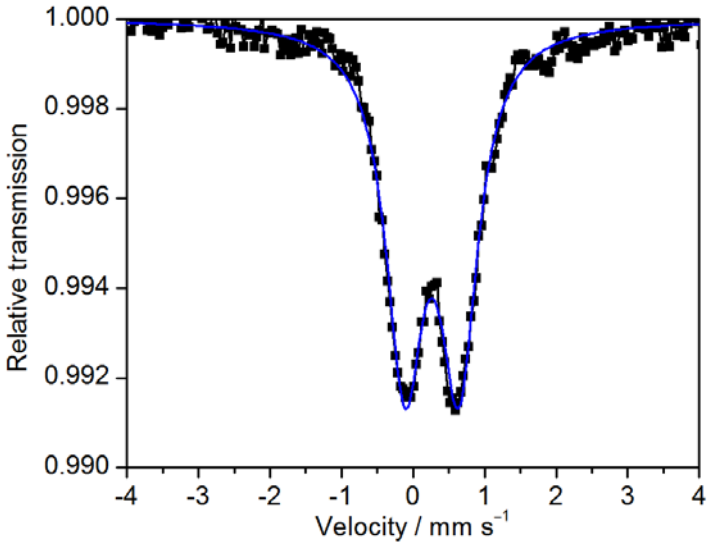

Figure S42. Mössbauer spectrum (T = 80 K) of the solid precipitated in the reaction of $^{57}FeCl_2$ (5 mM) with TMEDA (degassed, 4 equiv) and MeMgCl (4 equiv) in THF under inert atmosphere together with fit (blue); fit parameters: δ = 0.23 mm s^{-1}, ΔE_Q = 0.82 mm s^{-1}.

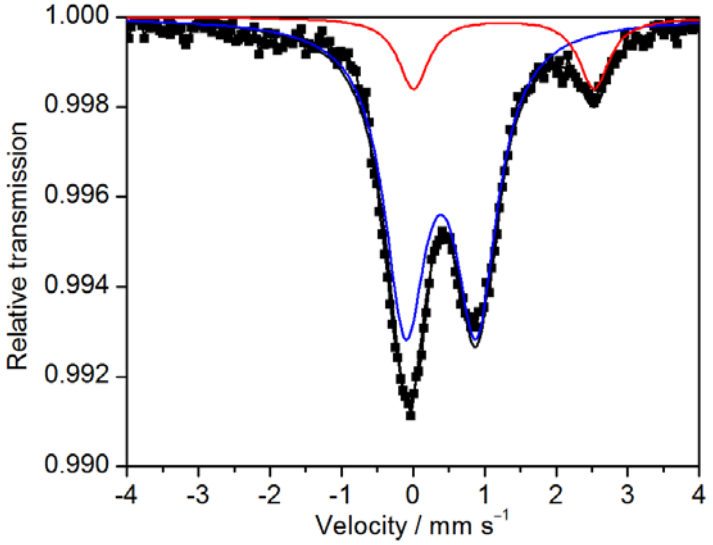

Figure S43. Mössbauer spectrum (T = 80 K) of the solid precipitated in the reaction of $^{57}FeCl_2$ (5 mM) with TMEDA (degassed, 4 equiv) and MeMgCl (4 equiv) in THF exposed to air for t = 30 min together with overall fit (black); components of the fit: δ(blue) = 0.39 mm s^{-1}, ΔE_Q(blue) = 0.99 mm s^{-1}, rel. int. (blue) = 85%; δ(red) = 1.27 mm s^{-1}, ΔE_Q(red) = 2.53 mm s^{-1}, rel. int. (red) = 15%.

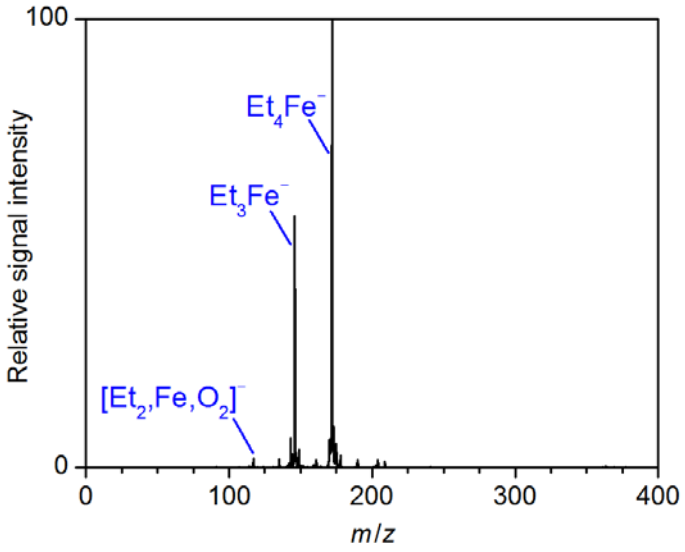

Figure S44. Negative-ion mode ESI mass spectrum of a solution of the products formed in the reaction of $Fe(acac)_3$ (20 mM) with TMEDA (4 equiv) and EtMgCl (4 equiv) in THF.

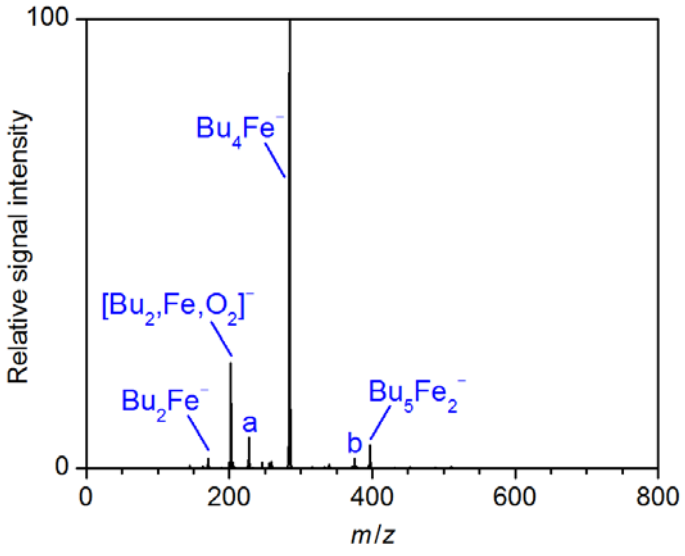

Figure S45. Negative-ion mode ESI mass spectrum of a solution of the products formed in the reaction of $Fe(acac)_3$ (20 mM) with TMEDA (4 equiv) and BuMgCl (4 equiv) in THF; a = Bu_3Fe^-, $Bu_4Fe_2Cl^-$.

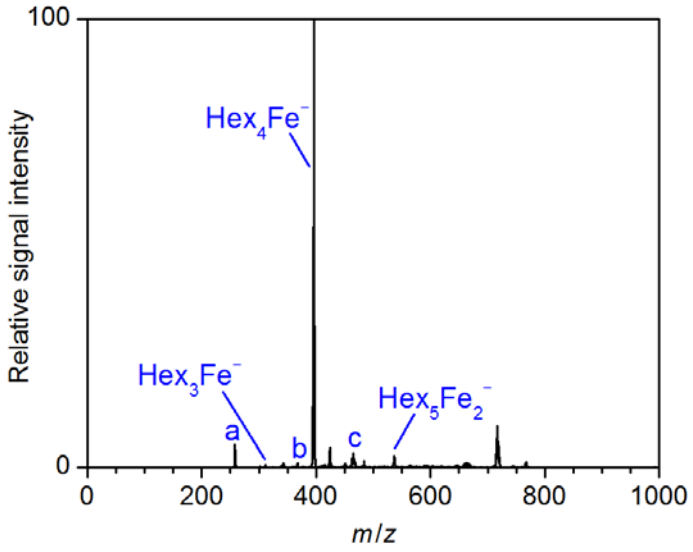

Figure S46. Negative-ion mode ESI mass spectrum of a solution of the products formed in the reaction of $Fe(acac)_3$ (20 mM) with TMEDA (4 equiv) and HexMgCl (4 equiv) in THF; a = $[Hex,Fe,O_2]^-$, b = Hex_4Al^-, c = $Mg_3Hex_3Cl_3(OMe)^-$.

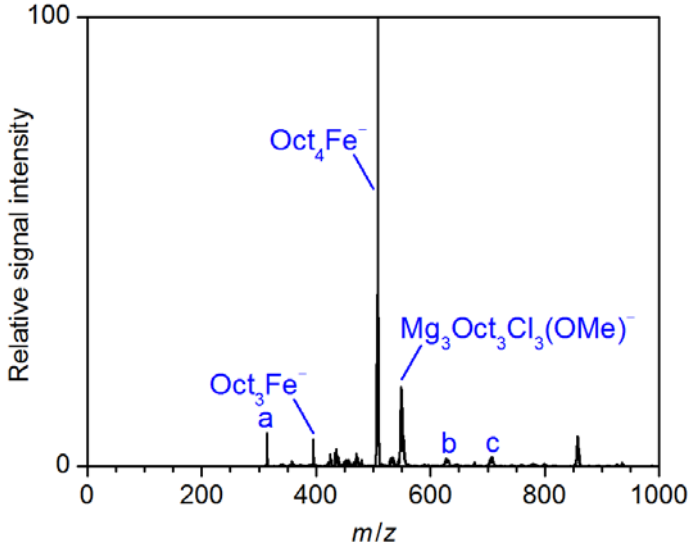

Figure S47. Negative-ion mode ESI mass spectrum of a solution of the products formed in the reaction of $Fe(acac)_3$ (20 mM) with TMEDA (4 equiv) and OctMgCl (4 equiv) in THF; a = $[Oct,Fe,O_2]^-$, b = $Mg_4Oct_3Cl_5(OMe)^-$, c = $Mg_4Oct_4Cl_4(OH)^-$.

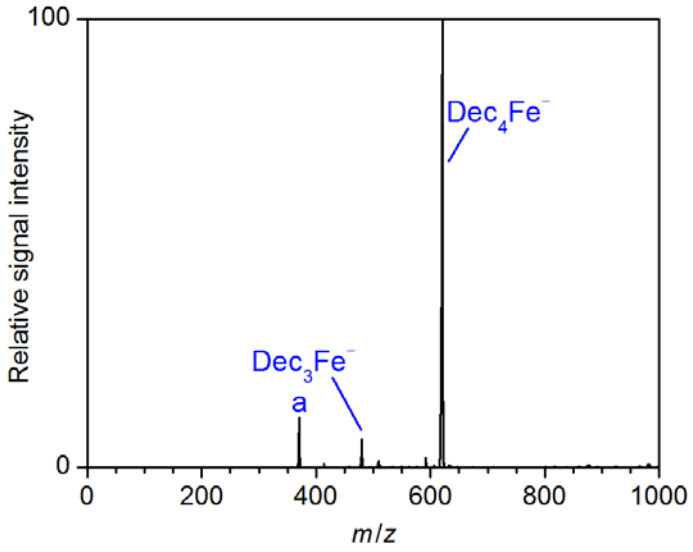

Figure S48. Negative-ion mode ESI mass spectrum of a solution of the products formed in the reaction of $Fe(acac)_3$ (20 mM) with TMEDA (4 equiv) and DecMgCl (4 equiv) in THF; a = $[Dec,Fe,O_2]^-$.

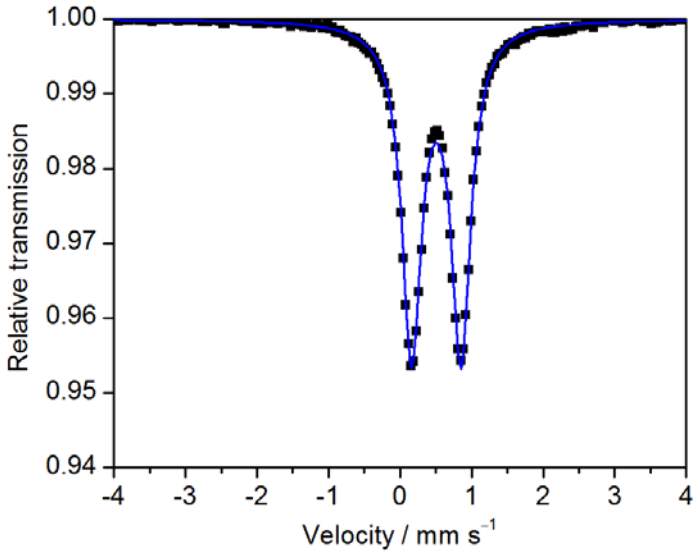

Figure S49. Mössbauer spectrum of a frozen solution (T = 80 K) of the products formed in the reaction of $^{57}FeCl_2$ (5 mM) with TMEDA (4 equiv) and DecMgCl (4 equiv) in THF together with fit (blue); fit parameters: δ = 0.51 mm s^{-1}, ΔE_Q = 0.69 mm s^{-1}.

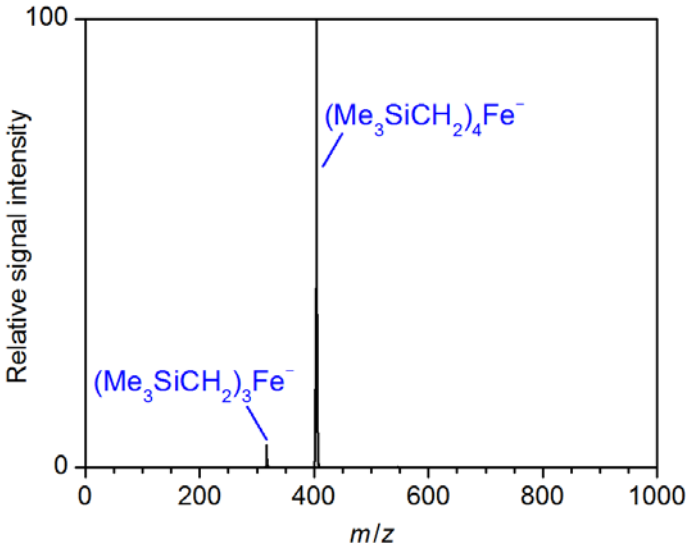

Figure S50. Negative-ion mode ESI mass spectrum of a solution of the products formed in the reaction of $Fe(acac)_3$ (20 mM) with TMEDA (4 equiv) and Me_3SiCH_2MgCl (4 equiv) in THF.

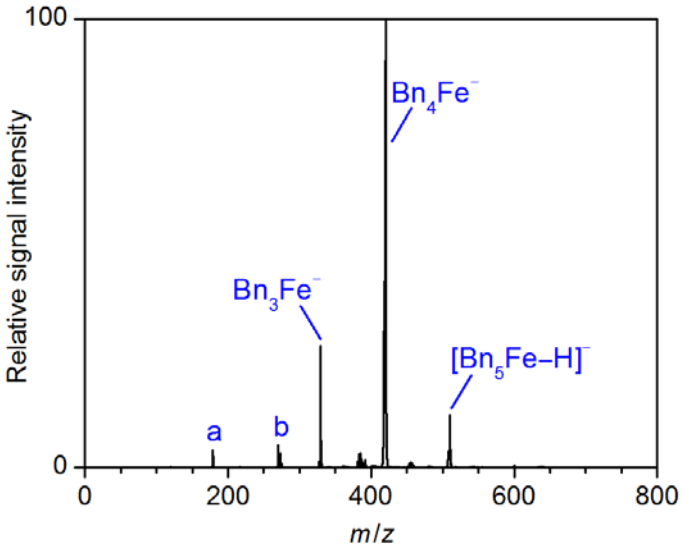

Figure S51. Negative-ion mode ESI mass spectrum of a solution of the products formed in the reaction of $Fe(acac)_3$ (20 mM) with TMEDA (4 equiv) and BnMgCl (4 equiv) in THF; a = $[Bn,Fe,O_2]^-$, b = $[Bn_2,Fe,O_2]^-$.

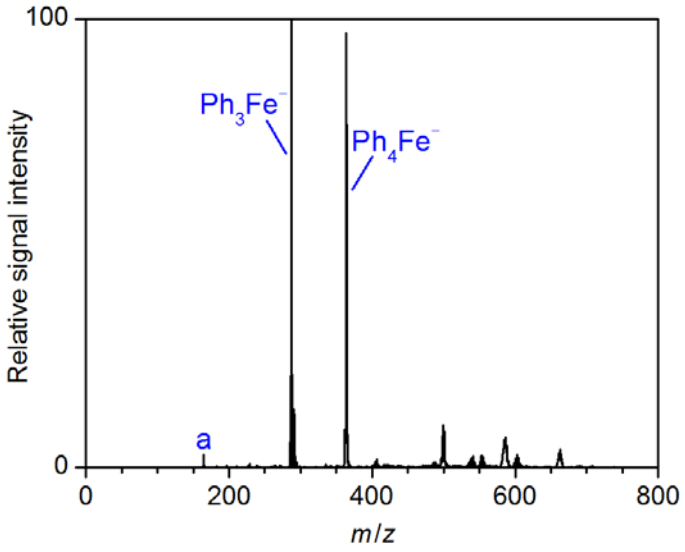

Figure S52. Negative-ion mode ESI mass spectrum of a solution of the products formed in the reaction of $Fe(acac)_3$ (20 mM) with TMEDA (4 equiv) and PhMgCl (4 equiv) in THF; a = $[Ph,Fe,O_2]^-$.

Table S3. Specific electrical conductivity κ / (μS cm^{-1}) of organoferrates produced by transmetallation of $Fe(acac)_3$ (50 mM) with 4 equiv of TMEDA and 4 equiv of RMgCl (R = Bn, Ph) in THF (T = 273 K).

sample solution in THF	**κ / μS cm^{-1}**
$Fe(acac)_3$ + 4 TMEDA + 4 BnMgCl	20 ± 4
$Fe(acac)_3$ + 4 TMEDA + 4 PhMgCl	83 ± 5

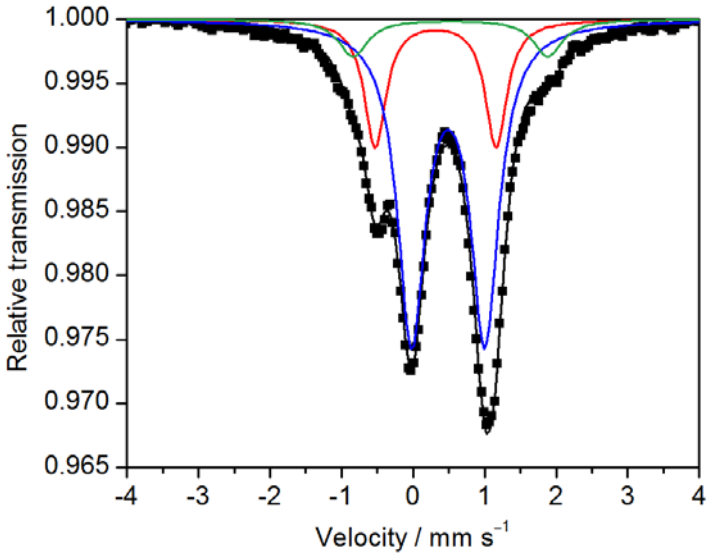

Figure S53. Mössbauer spectrum of a frozen solution (T = 80 K) of the products formed in the reaction of $^{57}FeCl_2$ (5 mM) with TMEDA (4 equiv) and PhMgCl (4 equiv) in THF together with overall fit (black); components of the fit: δ(blue) = 0.49 mm s^{-1}, ΔE_Q(blue) = 1.03 mm s^{-1}, rel. int. (blue) = 78%; δ(red) = 0.32 mm s^{-1}, ΔE_Q(red) = 1.69 mm s^{-1}, rel. int. (red) = 14%; δ(green) = 0.52 mm s^{-1}, ΔE_Q(green) = 2.72 mm s^{-1}, rel. int. (green) = 8%.

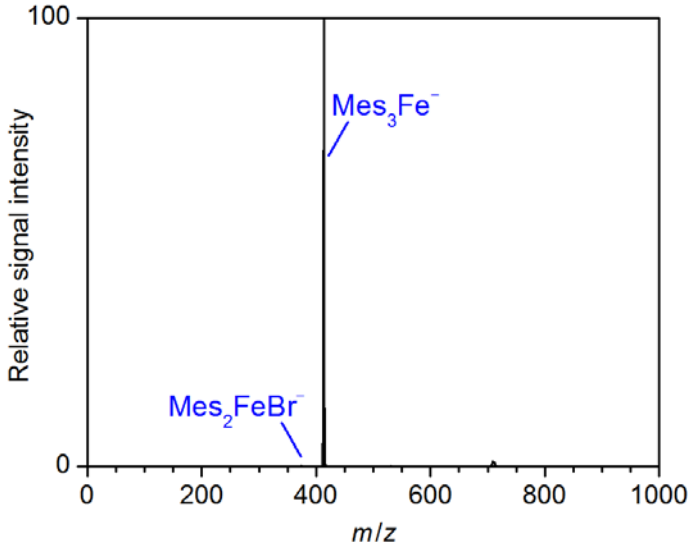

Figure S54. Negative-ion mode ESI mass spectrum of a solution of the products formed in the reaction of $Fe(acac)_3$ (20 mM) with TMEDA (4 equiv) and MesMgBr (4 equiv) in THF.

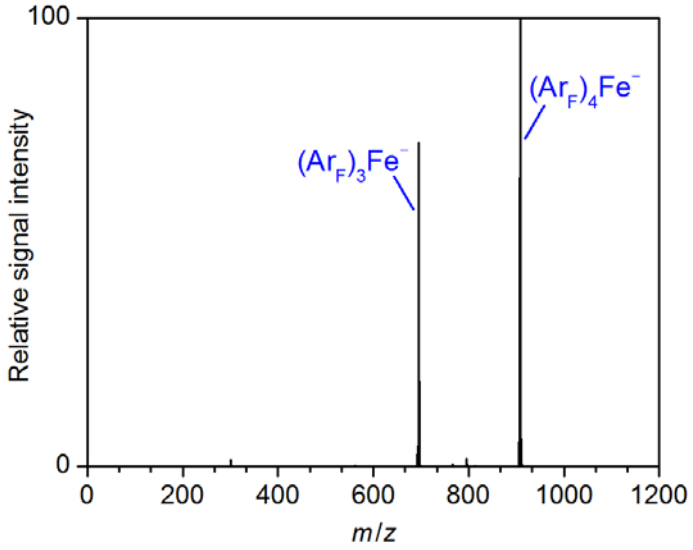

Figure S55. Negative-ion mode ESI mass spectrum of a solution of the products formed in the reaction of $Fe(acac)_3$ (20 mM) with TMEDA (4 equiv) and Ar_FMgBr (4 equiv) in THF; Ar_F = 3,5-$(CF_3)_2$-C_6H_3.

3.) Effect of Added dppbz

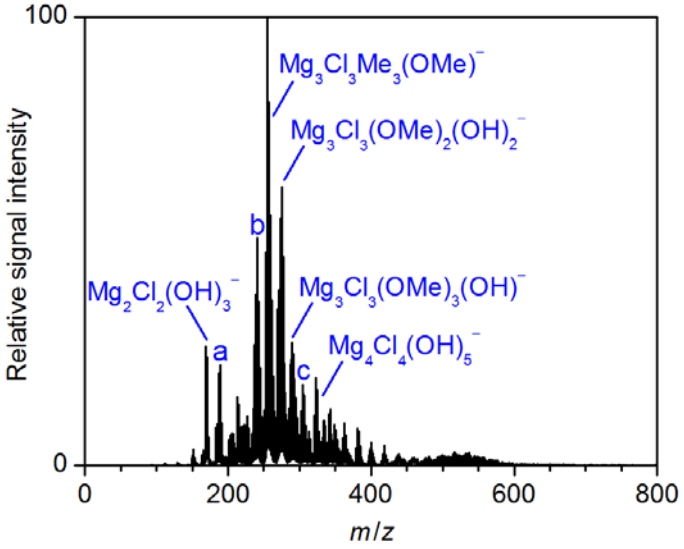

Figure S56. Negative-ion mode ESI mass spectrum of a solution of the products formed in the reaction of $FeCl_2(dppbz)_2$ (10 mM) and MeMgCl (4 equiv) in THF; a = $Mg_2Cl_3(OH)_2^-$, b = $Mg_3Cl_3Me_3(OH)^-$, c = $Mg_3Cl_3(OH)(OMe)_3^-$. Unwanted hydrolysis reactions with traces of water present in the vacuum system resulted in numerous further, species (not labeled) resulting from the successive exchange of all Me groups by OH. The incorporated methoxide originates from traces of methanol as reported previously.[1,2]

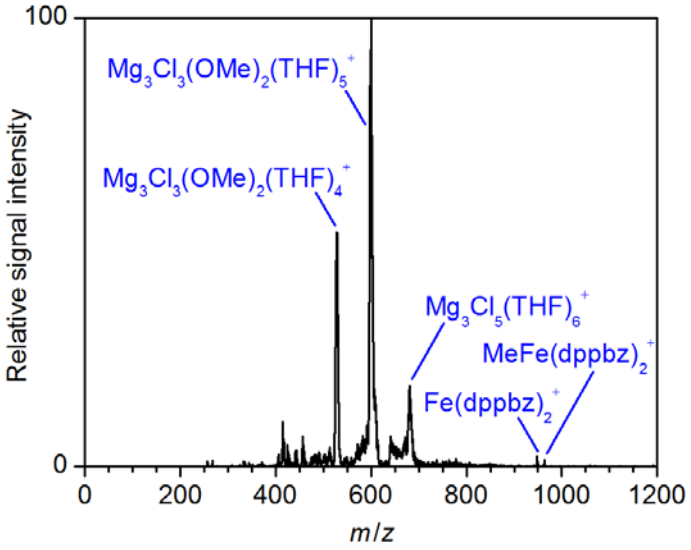

Figure S57. Positive-ion mode ESI mass spectrum of a solution of the products formed in the reaction of $FeCl_2(dppbz)_2$ (10 mM) and MeMgCl (4 equiv) in THF.

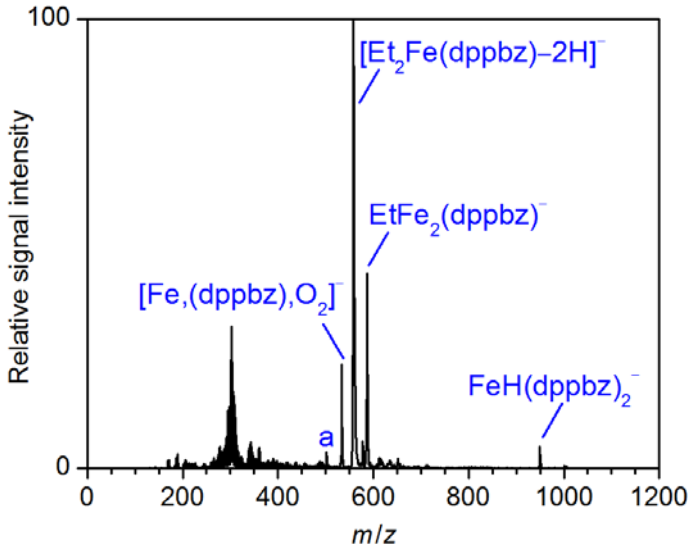

Figure S58. Negative-ion mode ESI mass spectrum of a solution of the products formed in the reaction of $FeCl_2(dppbz)_2$ (10 mM) and EtMgCl (4 equiv) in THF; a = $Fe(dppbz)^-$.

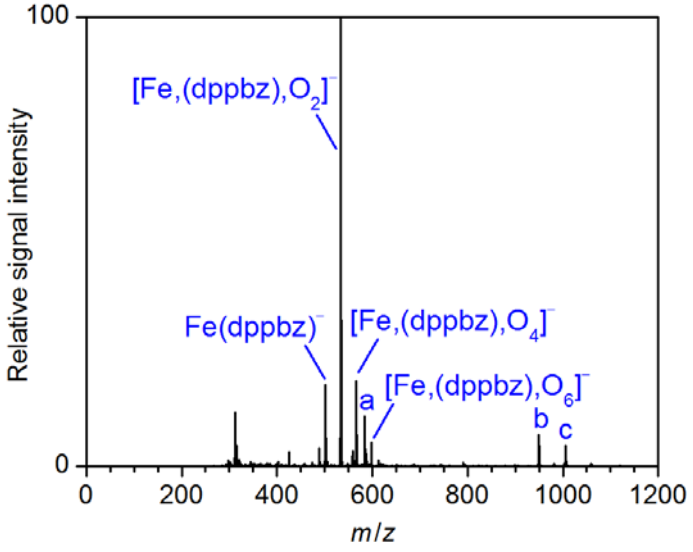

Figure S59. Negative-ion mode ESI mass spectrum of a solution of the products formed in the reaction of $FeCl_2(dppbz)_2$ (10 mM) and EtMgCl (4 equiv) in THF measured with the microQ-TOF II instrument; a = $[Fe,(dppbz),O_5,2H]^-$, b = $FeH(dppbz)_2^-]^-$, c = $Fe_2H(dppbz)_2^-$.

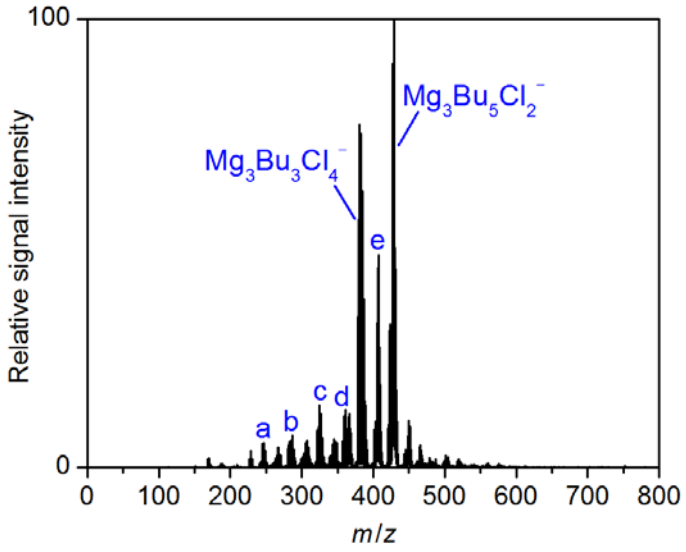

Figure S60. Negative-ion mode ESI mass spectrum of a solution of the products formed in the reaction of $FeCl_2(dppbz)_2$ (10 mM) and BuMgCl (4 equiv) in THF; a = $Mg_3Cl_3(OH)_4^-$, b = $Mg_3Cl_5(OH)_2^-$, c = $Mg_3Bu_2Cl_3(OH)_2^-$ + $Mg_3BuCl_5(OH)^-$, d = $Mg_3Bu_3Cl_3(OH)^-$, e = $Mg_3Bu_4Cl_3^-$.

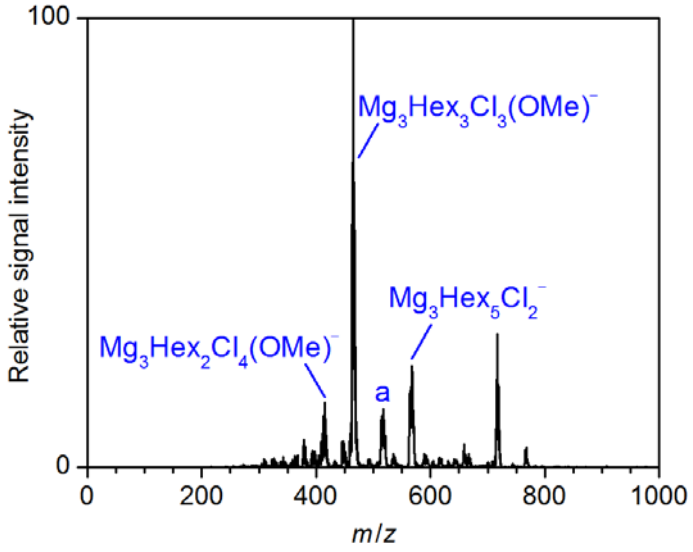

Figure S61. Negative-ion mode ESI mass spectrum of a solution of the products formed in the reaction of $FeCl_2(dppbz)_2$ (10 mM) and HexMgCl (4 equiv) in THF; a = $Mg_3Hex_4Cl_3^-$. The incorporated methoxide originates from traces of methanol as reported previously.[1,2]

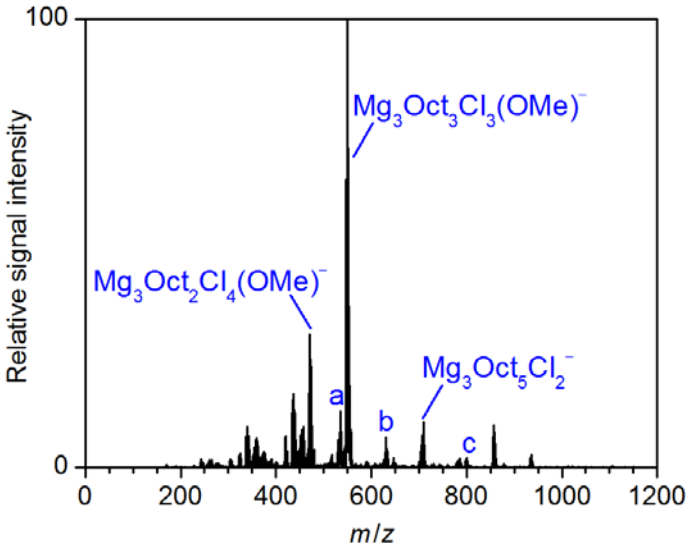

Figure S62. Negative-ion mode ESI mass spectrum of a solution of the products formed in the reaction of $FeCl_2(dppbz)_2$ (10 mM) and OctMgCl (4 equiv) in THF; a = $Mg_3Oct_3Cl_3(OH)^-$, b = $Mg_3Oct_4Cl_3^-$, c = $Mg_4Oct_5Cl_3(OMe)^-$. The incorporated methoxide originates from traces of methanol as reported previously.[1,2]

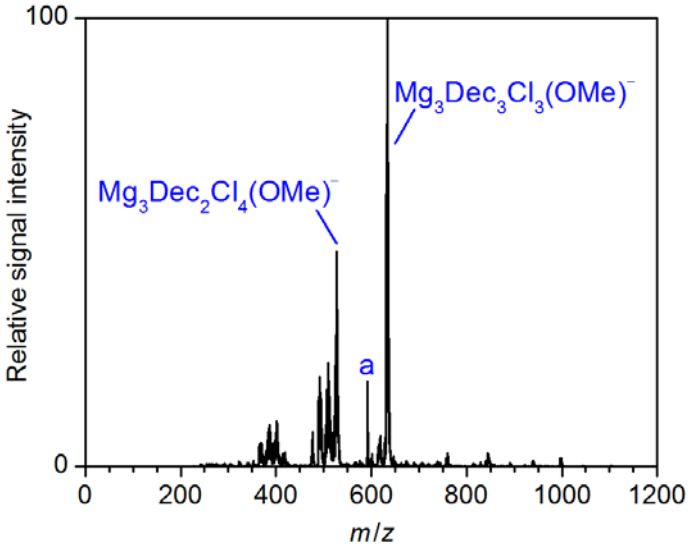

Figure S63. Negative-ion mode ESI mass spectrum of a solution of the products formed in the reaction of $FeCl_2(dppbz)_2$ (10 mM) and DecMgCl (4 equiv) in THF; a = Dec_4Al^-. The incorporated methoxide originates from traces of methanol as reported previously.[1,2]

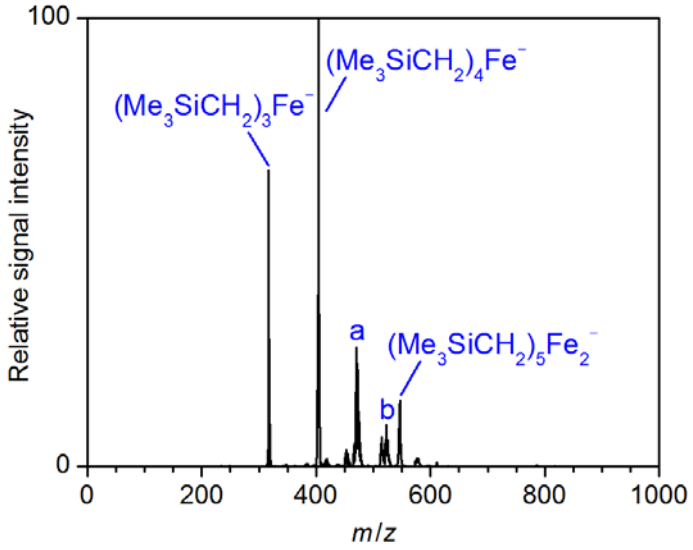

Figure S64. Negative-ion mode ESI mass spectrum of a solution of the products formed in the reaction of $FeCl_2(dppbz)_2$ (10 mM) and Me_3SiCH_2MgCl (4 equiv) in THF; a = $Mg_3(Me_3SiCH_2)_3Cl_3(OMe)^-$, b = $Mg_3(Me_3SiCH_2)_4Cl_2(OMe)^-$.

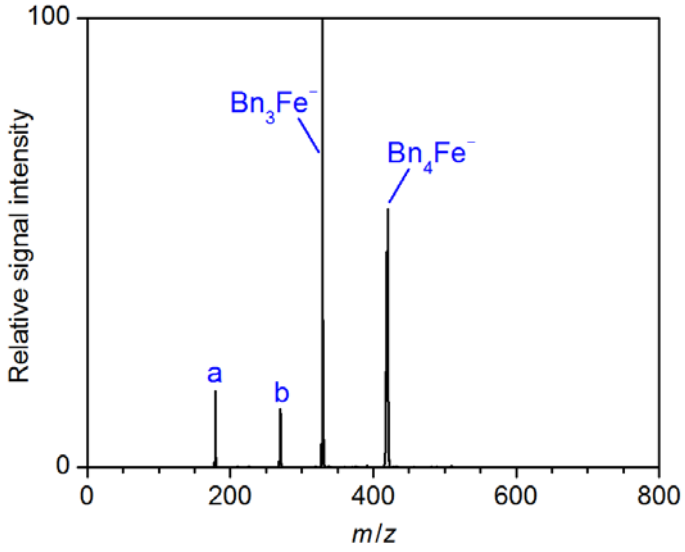

Figure S65. Negative-ion mode ESI mass spectrum of a solution of the products formed in the reaction of $FeCl_2(dppbz)_2$ (10 mM) and BnMgCl (4 equiv) in THF; a = $[Bn,Fe,O_2]^-$, b = $[Bn_2,Fe,O_2]^-$.

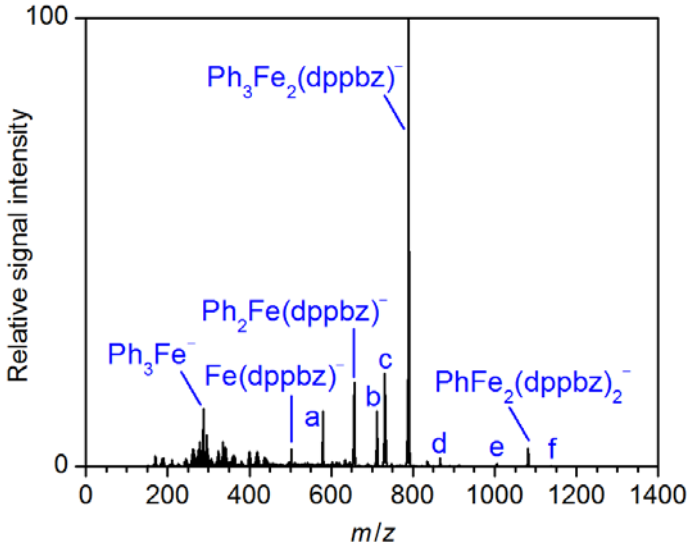

Figure S66. Negative-ion mode ESI mass spectrum of a solution of the products formed in the reaction of $FeCl_2(dppbz)_2$ (10 mM) and PhMgCl (4 equiv) in THF; a = $PhFe(dppbz)^-$, b = $Ph_2Fe_2(dppbz)^-$, c = $[Ph_3Fe(dppbz)–2H]^-$ + $Ph_3Fe(dppbz)^-$, d = $Ph_4Fe_2(dppbz)^-$, e = $Fe_2H(dppbz)_2^-$, f = $PhFe_3(dppbz)_2^-$.

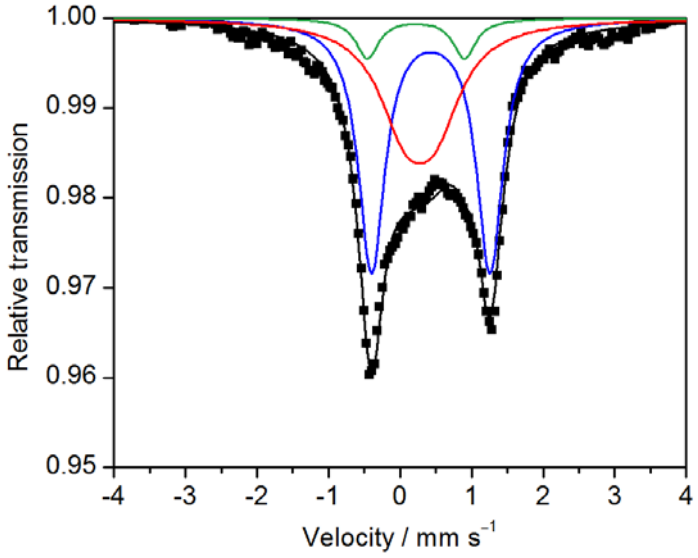

Figure S67. Mössbauer spectrum of a frozen solution (T = 80 K) of the products formed in the reaction of $^{57}FeCl_2$ (5 mM) with dppbz (2 equiv) and PhMgCl (4 equiv) in THF together with overall fit (black); components of the fit: δ(blue) = 0.43 mm s^{-1}, ΔE_Q(blue) = 1.65 mm s^{-1}, rel. int. (blue) = 61%; δ(red) = 0.28 mm s^{-1}, ΔE_Q(red) 0.42 mm s^{-1}, rel. int. (red) = 35%; δ(green) = 0.22 mm s^{-1}, ΔE_Q(green) 1.36 mm s^{-1}, rel. int. (green) = 4%.

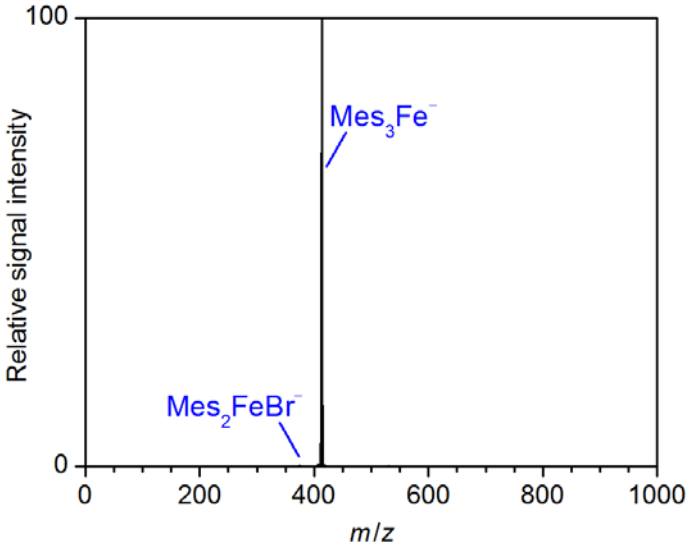

Figure S68. Negative-ion mode ESI mass spectrum of a solution of the products formed in the reaction of $FeCl_2(dppbz)_2$ (10 mM) and MesMgBr (4 equiv) in THF.

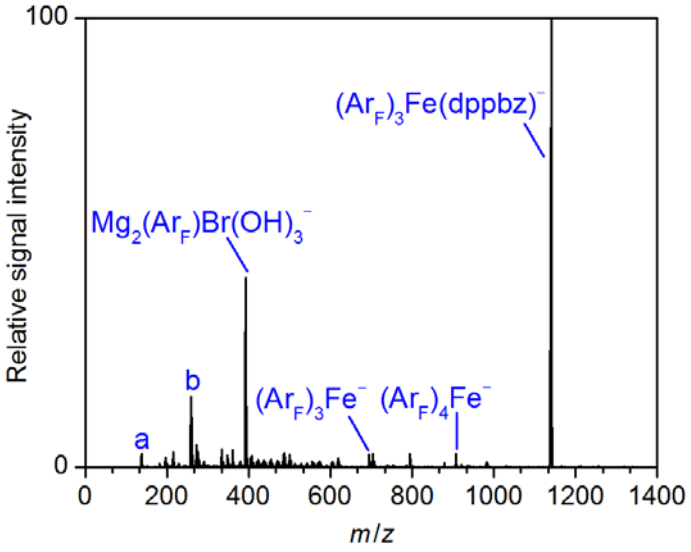

Figure S69. Negative-ion mode ESI mass spectrum of a solution of the products formed in the reaction of $FeCl_2(dppbz)_2$ (10 mM) and Ar_FMgBr (4 equiv) in THF; a = $MgBr(OH)_2^-$, b = $Mg_2Br_2(OH)_3^-$; Ar_F = 3,5-$(CF_3)_2$-C_6H_3.

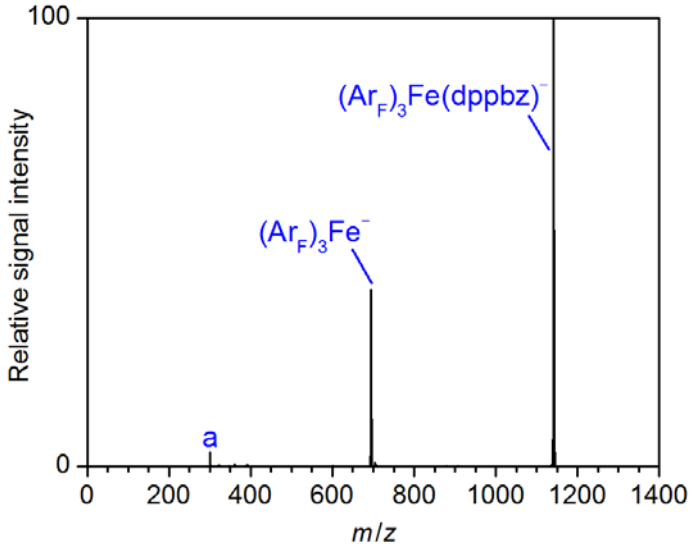

Figure S70. Negative-ion mode ESI mass spectrum of a solution of the products formed in the reaction of $FeCl_2(dppbz)_2$ (10 mM) and Ar_FMgBr (4 equiv) in THF measured with the microQ-TOF II instrument; a = $[Ar_F,Fe,O_2]^-$; Ar_F = 3,5-$(CF_3)_2$-C_6H_3.

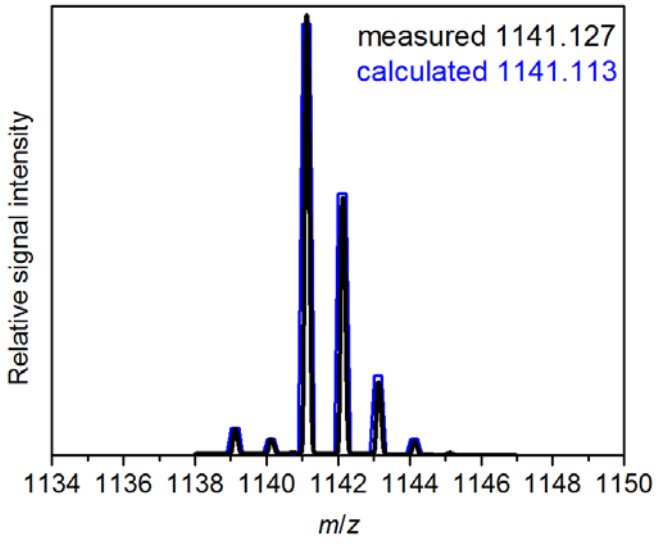

Figure S71. Comparison of the observed (black, measured with the micrOTOF-Q II instrument) and simulated (blue) isotope pattern of $(Ar_F)_3Fe(dppbz)^-$; Ar_F = 3,5-$(CF_3)_2$-C_6H_3.

4.) Intermolecular Exchange Reactions

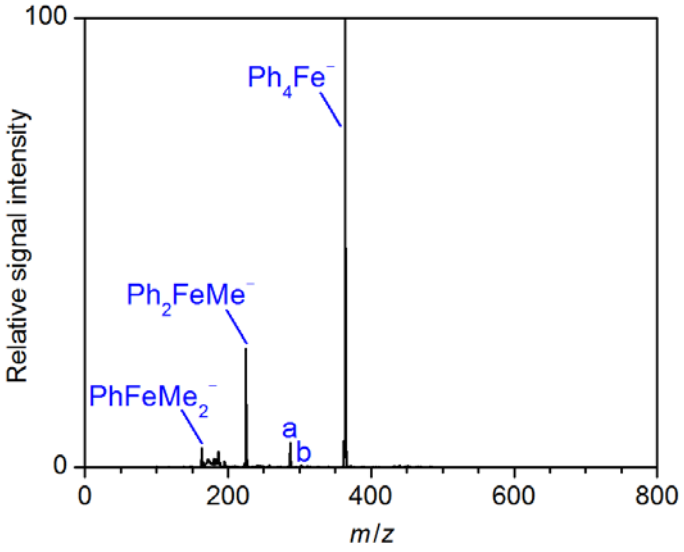

Figure S72. Negative-ion mode ESI mass spectrum of a solution of the products formed in the exchange reaction of $Fe(acac)_3$ (10 mM)/PhMgCl (4 equiv) with $Fe(acac)_3$ (10 mM)/TMEDA (4 equiv)/MeMgCl (4 equiv) in THF; trap drive 30; a = Ph_3Fe^-, b = Ph_3FeMe^-.

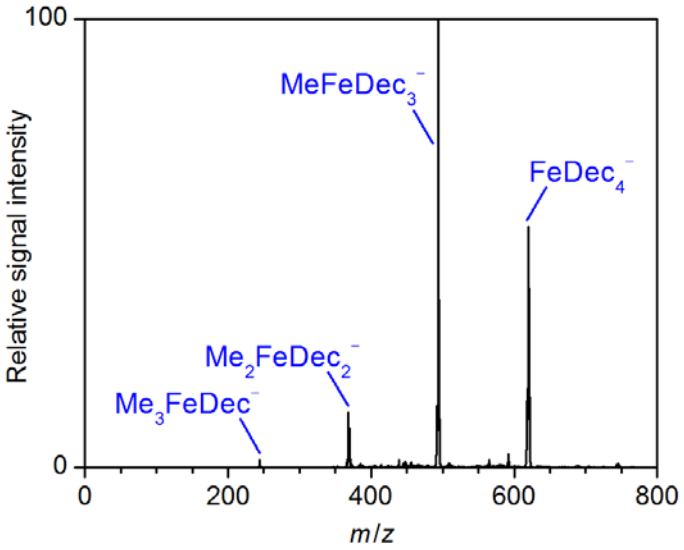

Figure S73. Negative-ion mode ESI mass spectrum of a solution of the products formed in the exchange reaction of $Fe(acac)_3$ (10 mM)/MeMgCl (4 equiv) with $Fe(acac)_3$ (10 mM)/TMEDA (4 equiv)/DecMgCl (4 equiv) in THF.

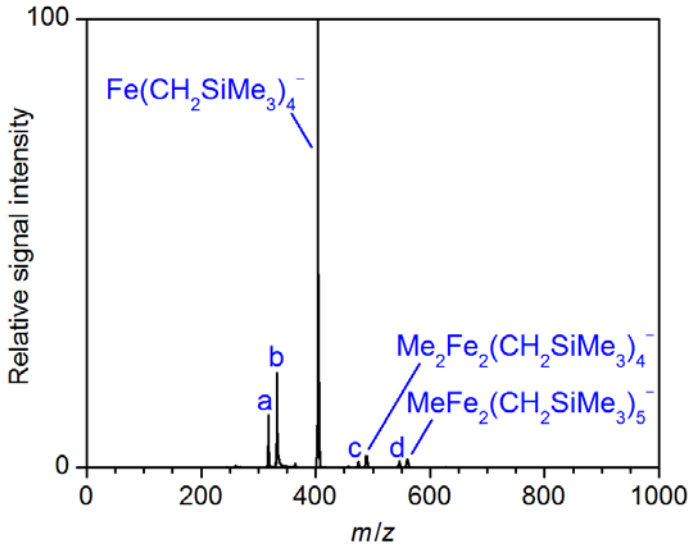

Figure S74. Negative-ion mode ESI mass spectrum of a solution of the products formed in the exchange reaction of $Fe(acac)_3$ (10 mM)/MeMgCl (4 equiv) with $Fe(acac)_3$ (10 mM)/Me_3SiCH_2MgCl (4 equiv) in THF; trap drive 40; a = $Fe(CH_2SiMe_3)_3^-$, b = $MeFe(CH_2SiMe_3)_3^-$, c = $MeFe_2(CH_2SiMe_3)_4^-$, d = $Fe_2(CH_2SiMe_3)_5^-$.

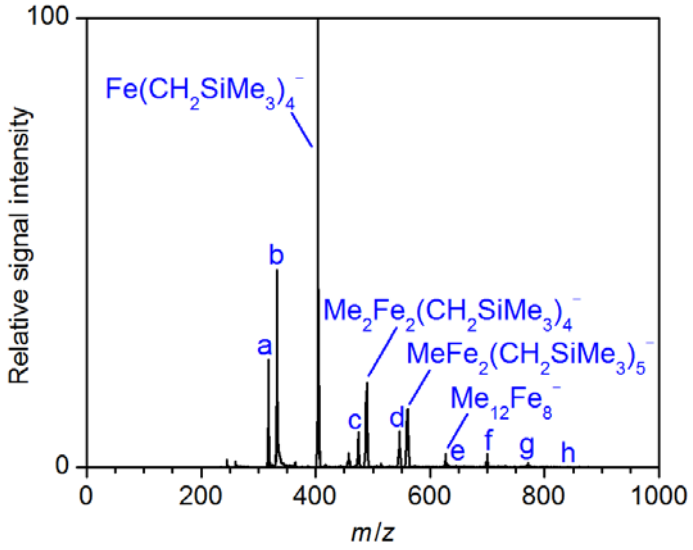

Figure S75. Negative-ion mode ESI mass spectrum of a solution of the products formed in the exchange reaction of $Fe(acac)_3$ (10 mM)/MeMgCl (4 equiv) with $Fe(acac)_3$ (10 mM)/Me_3SiCH_2MgCl (4 equiv) in THF; trap drive 60; a = $Fe(CH_2SiMe_3)_3^-$, b = $MeFe(CH_2SiMe_3)_3^-$, c = $MeFe_2(CH_2SiMe_3)_4^-$, d = $Fe_2(CH_2SiMe_3)_5^-$, e = $Me_2Fe_3(CH_2SiMe_3)_5^-$, f = $Me_{11}Fe_8(CH_2SiMe_3)^-$, g = $Me_{10}Fe_8(CH_2SiMe_3)_2^-$, h = $Me_9Fe_8(CH_2SiMe_3)_3^-$.

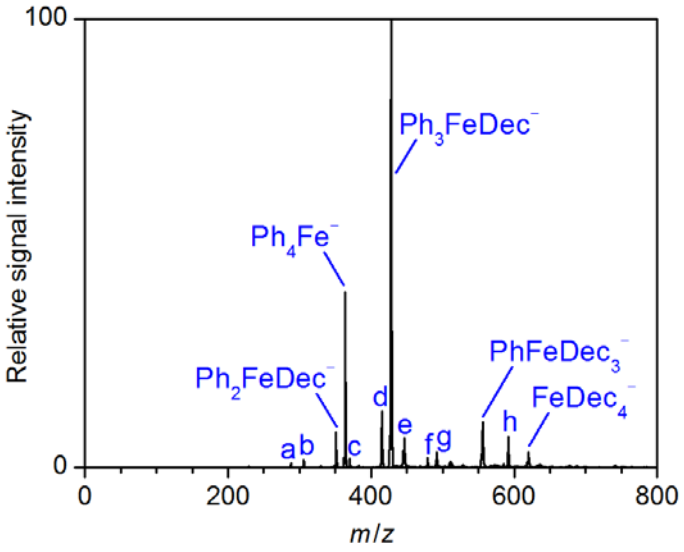

Figure S76. Negative-ion mode ESI mass spectrum of a solution of the products formed in the exchange reaction of $Fe(acac)_3$ (10 mM)/PhMgCl (4 equiv) with $Fe(acac)_3$ (10 mM)/TMEDA (4 equiv)/DecMgCl (4 equiv) in THF; a = Ph_3Fe^-, b = $[Ph_3Fe,Dec,O_2]^-$, c = $[Fe,Dec_2,O_2]^-$, d = $PhFeDec_2^-$, e = $[Ph_3Fe,Dec_2,O_2]^-$, f = Dec_3Fe^-, g = $Ph_2FeDec_2^-$, h = Dec_4Al^-.

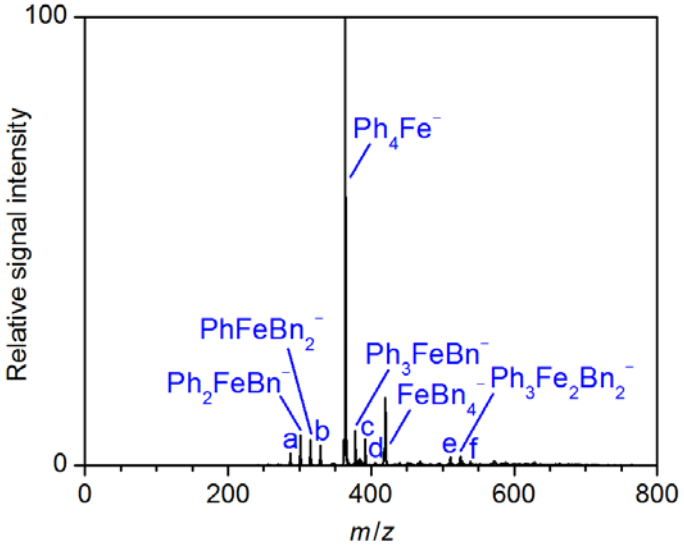

Figure S77. Negative-ion mode ESI mass spectrum of a solution of the products formed in the exchange reaction of $Fe(acac)_3$ (10 mM)/PhMgCl (4 equiv) with $Fe(acac)_3$ (10 mM)/BnMgCl (4 equiv) in THF; a = Ph_3Fe^-, b = $FeBn_3^-$, c = $Ph_2FeBn_2^-$, d = $PhFeBn_3^-$, e = $Ph_4Fe_2Bn^-$, f = $Ph_2Fe_2Bn_3^-$.

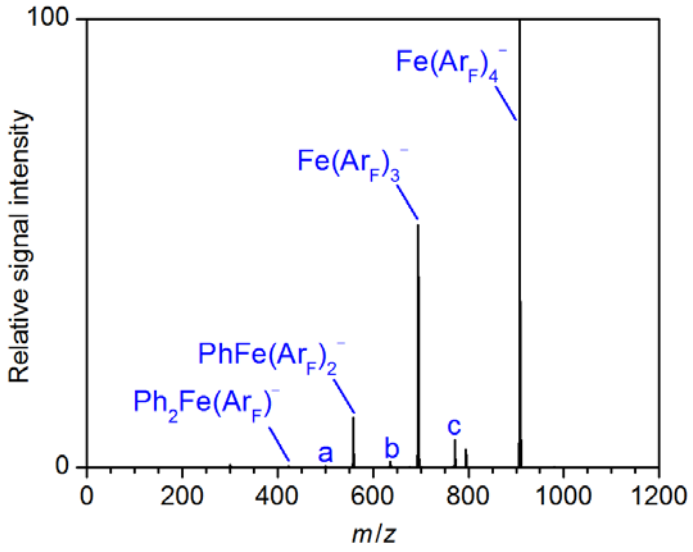

Figure S78. Negative-ion mode ESI mass spectrum of a solution of the products formed in the exchange reaction of $Fe(acac)_3$ (10 mM)/PhMgCl (4 equiv) with $Fe(acac)_3$ (10 mM)/(Ar_F)MgBr (4 equiv) in THF; a = $Ph_3Fe(Ar_F)^-$, b = $Ph_2Fe(Ar_F)_2^-$, c = $PhFe(ArF)_3^-$; Ar_F = 3,5-$(CF_3)_2$-C_6H_3.

5.) Reactivity of Organoferrates toward Organyl (Pseudo-)Halides

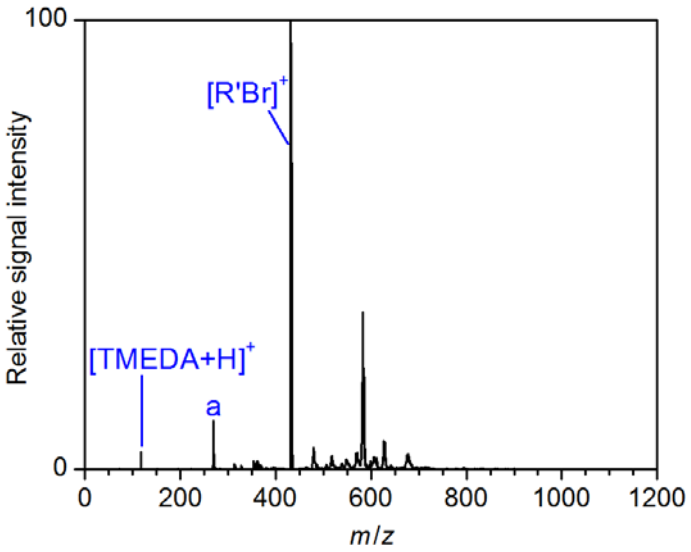

Figure S79. Positive-ion mode ESI mass spectrum of the products formed in the reaction of the soluble methyliron species resulting from the transmetallation of $FeCl_2$ (20 mM) with TMEDA (4 equiv) and MeMgCl (4 equiv) (separated from the concomitantly formed precipitate) with (*p*-bromobenzyl)triphenylphosphonium bromide ($[R'Br]^+$ Br^-, 0.5 equiv) in THF; a = $[TMEDA+HCl+H]^+$.

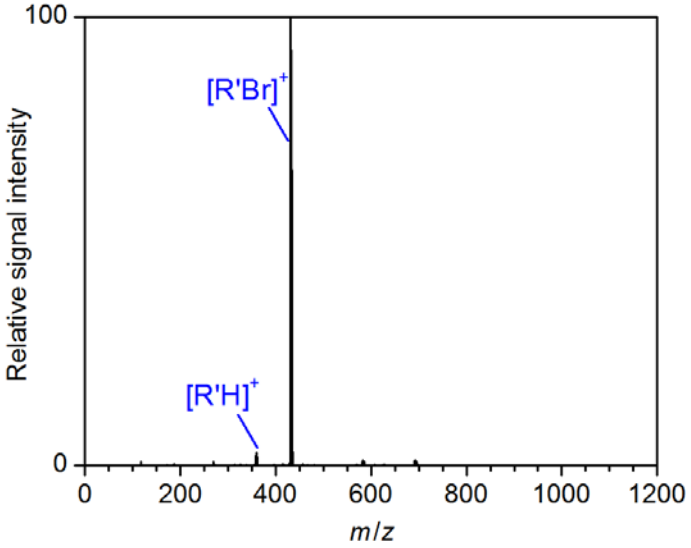

Figure S80. Positive-ion mode ESI mass spectrum of the products formed in the reaction of the insoluble methyloiron species resulting from the transmetallation of $FeCl_2$ (20 mM) with TMEDA (4 equiv) and MeMgCl (4 equiv) (separated from the supernatant solution) with (*p*-bromobenzyl)triphenylphosphonium bromide ($[R'Br]^+$ Br^-, 0.5 equiv) in THF.

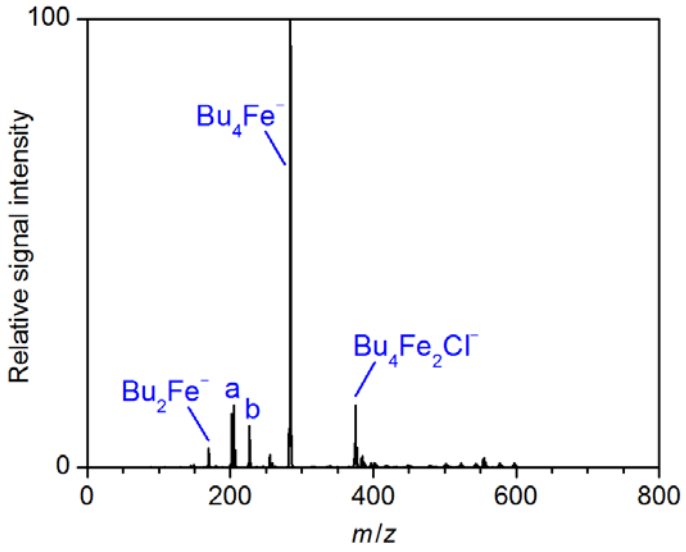

Figure S81. Negative-ion mode ESI mass spectrum of a solution of the products formed in the reaction of $Fe(acac)_3$ (20 mM) with TMEDA (4 equiv), BuMgCl (4 equiv), and PhCl (0.5 equiv) in THF; a = $[Bu_2,Fe,O_2]^-$ + Bu_2FeCl^-, b = Bu_3Fe^-.

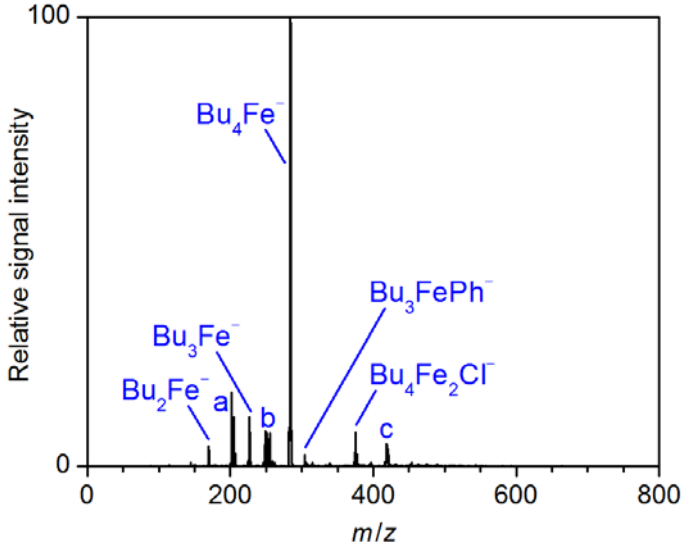

Figure S82. Negative-ion mode ESI mass spectrum of a solution of the products formed in the reaction of $Fe(acac)_3$ (20 mM) with TMEDA (4 equiv), BuMgCl (4 equiv), and PhBr (0.5 equiv) in THF; a = $[Bu_2,Fe,O_2]^-$ + Bu_2FeCl^-, b = Bu_2FeBr^-, c = $Bu_4Fe_2Br^-$.

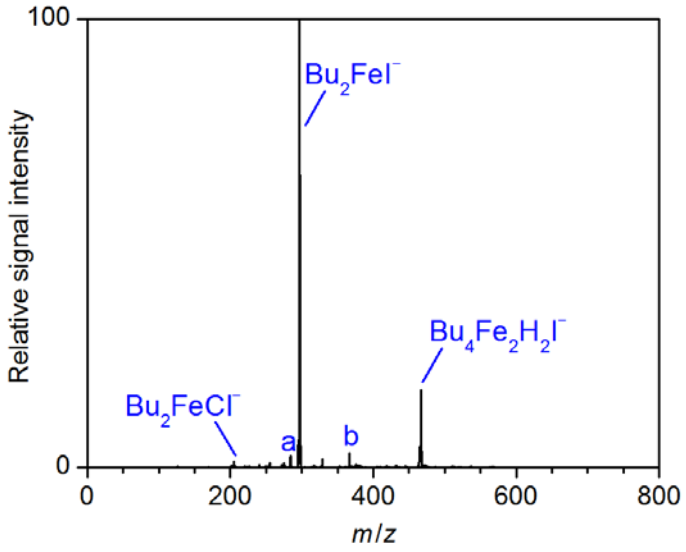

Figure S83. Negative-ion mode ESI mass spectrum of a solution of the products formed in the reaction of $Fe(acac)_3$ (20 mM) with TMEDA (4 equiv), BuMgCl (4 equiv), and PhI (0.5 equiv) in THF; a = $[Bu_2,Fe,O_2]^-$ + Bu_2FeCl^-, b = $BuFeI_2^-$.

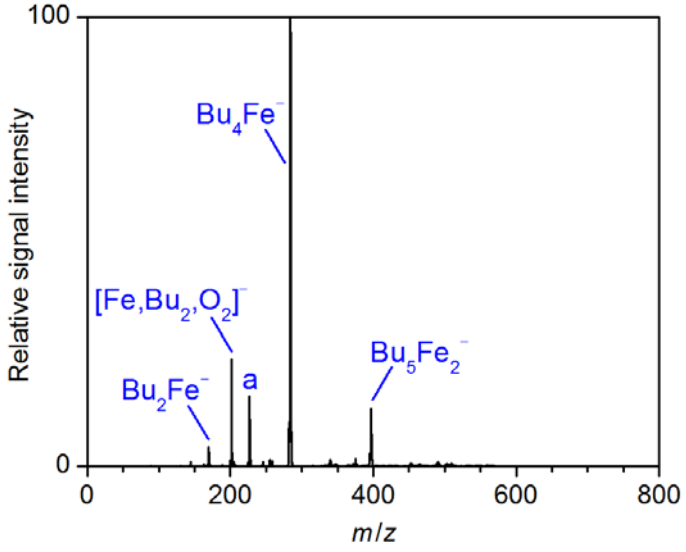

Figure S84. Negative-ion mode ESI mass spectrum of a solution of the products formed in the reaction of $Fe(acac)_3$ (20 mM) with TMEDA (4 equiv), BuMgCl (4 equiv) and *p*-TolCl (0.5 equiv) in THF; a = Bu_3Fe^-.

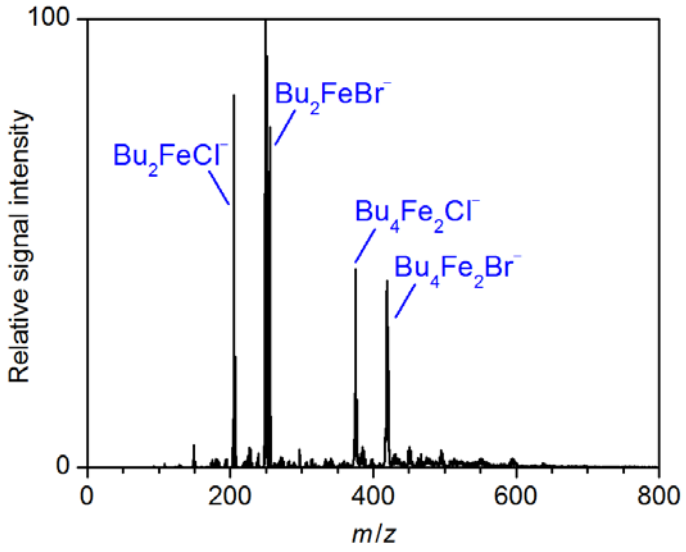

Figure S85. Negative-ion mode ESI mass spectrum of a solution of the products formed in the reaction of $Fe(acac)_3$ (20 mM) with TMEDA (4 equiv), BuMgCl (4 equiv), and *p*-TolBr (0.5 equiv) in THF.

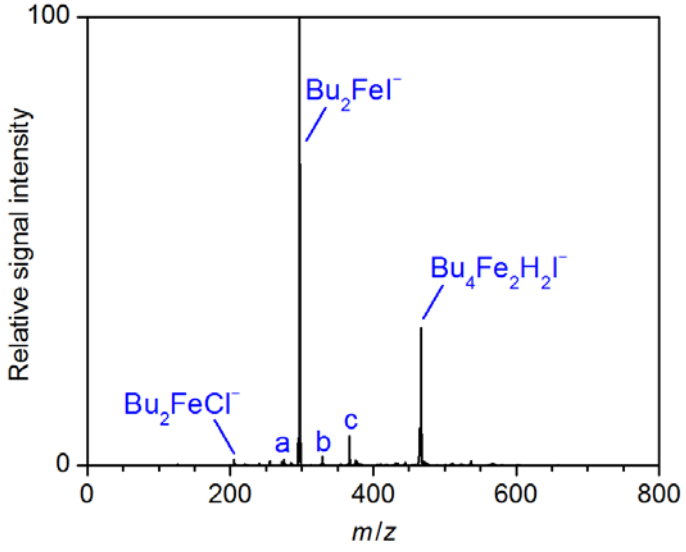

Figure S86. Negative-ion mode ESI mass spectrum of a solution of the products formed in the reaction of $Fe(acac)_3$ (20 mM) with TMEDA (4 equiv), BuMgCl (4 equiv) and *p*-TolI (0.5 equiv) in THF; a = $BuFeClI^-$, b = $[Bu_2,Fe,I,O_2]^-$, c = $BuFeI_2^-$.

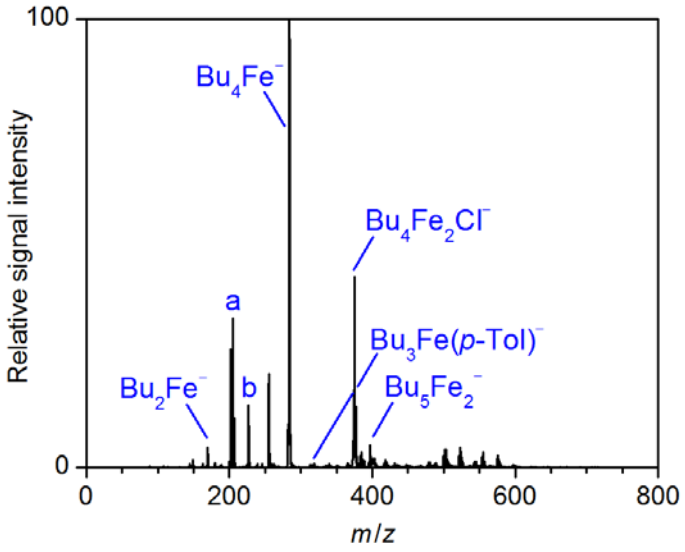

Figure S87. Negative-ion mode ESI mass spectrum of a solution of the products formed in the reaction of $Fe(acac)_3$ (20 mM) with TMEDA (4 equiv), BuMgCl (4 equiv) and *p*-TolOTf (0.5 equiv) in THF; a = $[Bu_2,Fe,O_2]^-$ + Bu_2FeCl^-, b = Bu_3Fe^-.

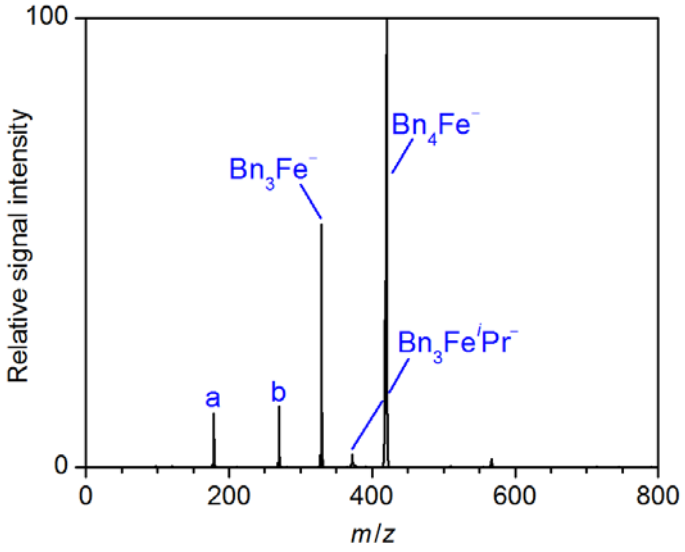

Figure S88. Negative-ion mode ESI mass spectrum of a solution of the products formed in the reaction of $Fe(acac)_3$ (20 mM) with BnMgCl (4 equiv) and ^{i}PrCl (1 equiv) in THF; a = $[Bn,Fe,O_2]^-$, b = $[Bn_2,Fe,O_2]^-$.

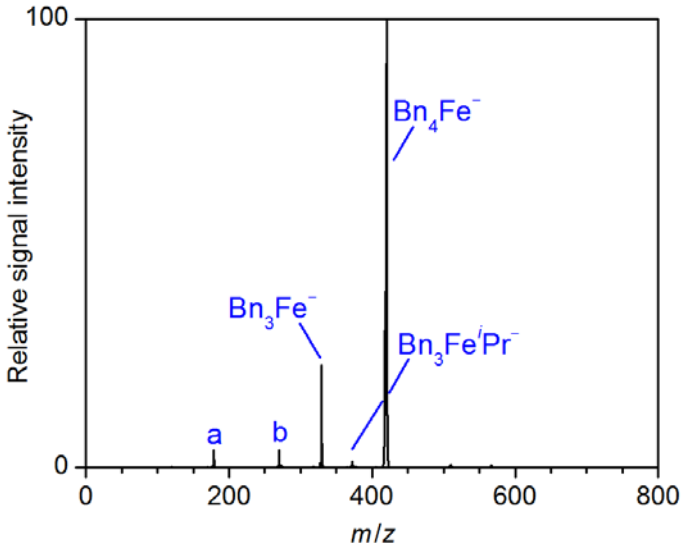

Figure S89. Negative-ion mode ESI mass spectrum of a solution of the products formed in the reaction of $Fe(acac)_3$ (20 mM) with BnMgCl (4 equiv) and ^{i}PrBr (1 equiv) in THF; a = $[Bn,Fe,O_2]^-$, b = $[Bn_2,Fe,O_2]^-$.

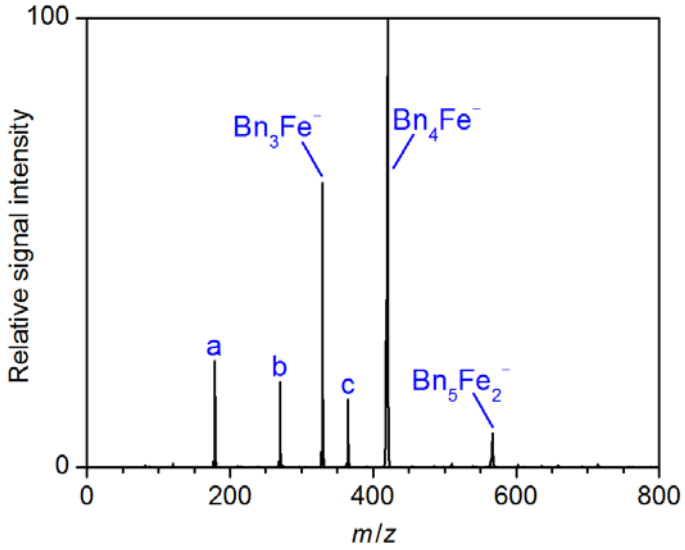

Figure S90. Negative-ion mode ESI mass spectrum of a solution of the products formed in the reaction of $Fe(acac)_3$ (20 mM) with BnMgCl (4 equiv) and ^{i}PrI (0.5 equiv) in THF; a = $[Bn,Fe,O_2]^-$, b = $[Bn_2,Fe,O_2]^-$, c = Bn_2FeI^-.

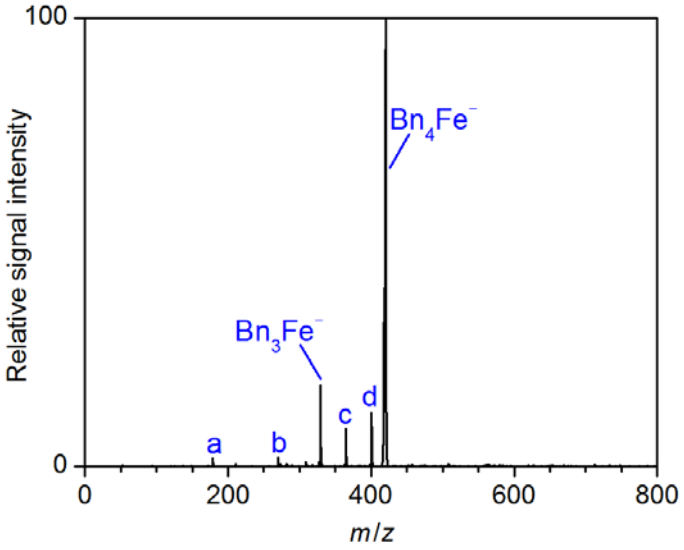

Figure S91. Negative-ion mode ESI mass spectrum of a solution of the products formed in the reaction of $Fe(acac)_3$ (20 mM) with BnMgCl (4 equiv) and ^{i}PrI (1.0 equiv) in THF; a = $[Bn,Fe,O_2]^-$, b = $[Bn_2,Fe,O_2]^-$, c = Bn_2FeI^-, d = $BnFeI_2^-$.

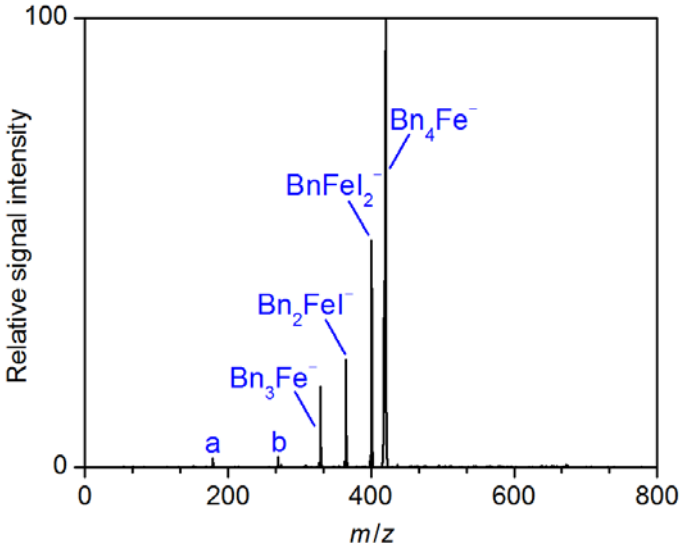

Figure S92. Negative-ion mode ESI mass spectrum of a solution of the products formed in the reaction of $Fe(acac)_3$ (20 mM) with BnMgCl (4 equiv) and ^{i}PrI (2.0 equiv) in THF; a = $[Bn,Fe,O_2]^-$, b = $[Bn_2,Fe,O_2]^-$.

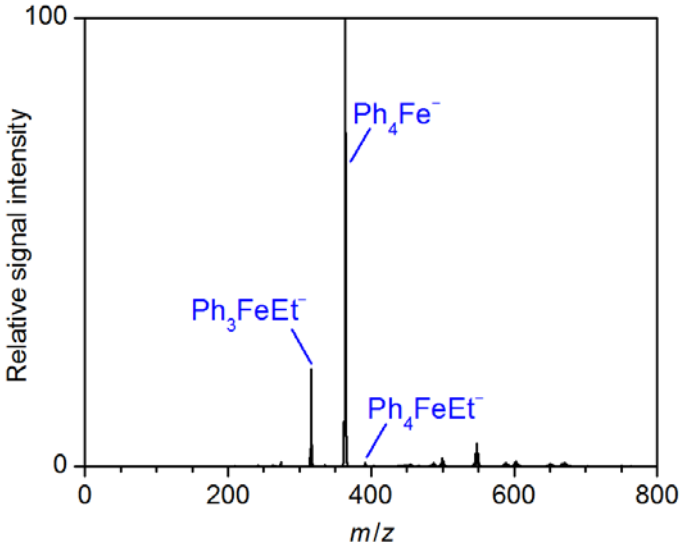

Figure S93. Negative-ion mode ESI mass spectrum of a solution of the products formed in the reaction of $Fe(acac)_3$ (20 mM) with PhMgBr (4 equiv) and EtBr (0.5 equiv) in THF.

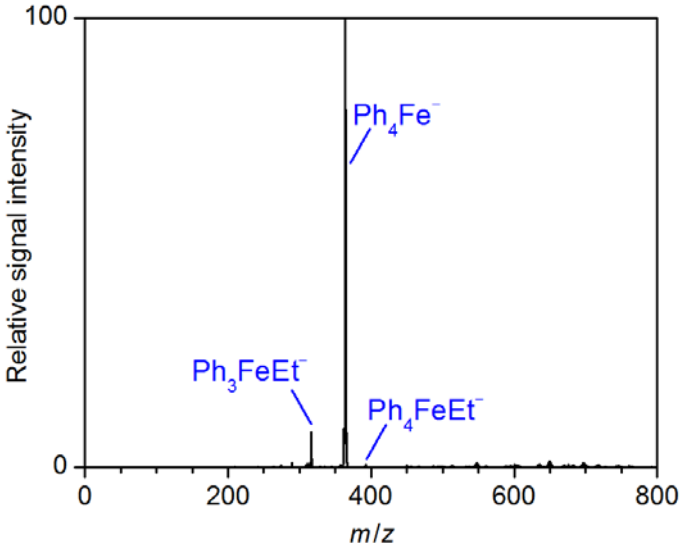

Figure S94. Negative-ion mode ESI mass spectrum of a solution of the products formed in the reaction of $Fe(acac)_3$ (20 mM) with PhMgBr (4 equiv) and EtI (0.5 equiv) in THF.

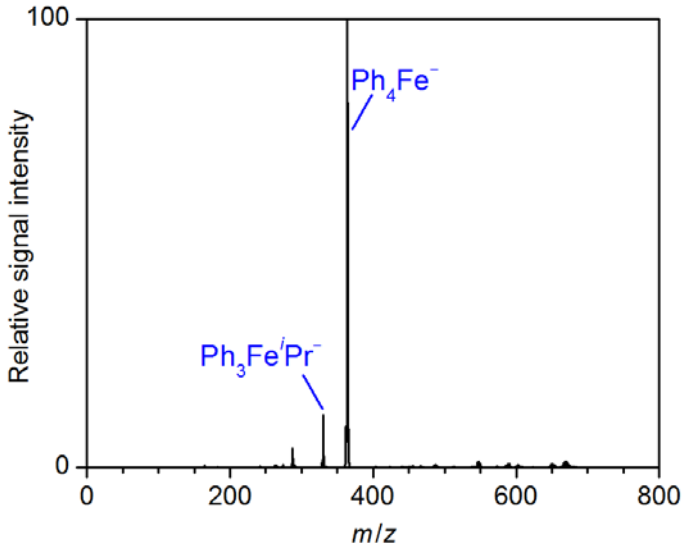

Figure S95. Negative-ion mode ESI mass spectrum of a solution of the products formed in the reaction of $Fe(acac)_3$ (20 mM) with PhMgBr (4 equiv) and ^{i}PrBr (0.5 equiv) in THF.

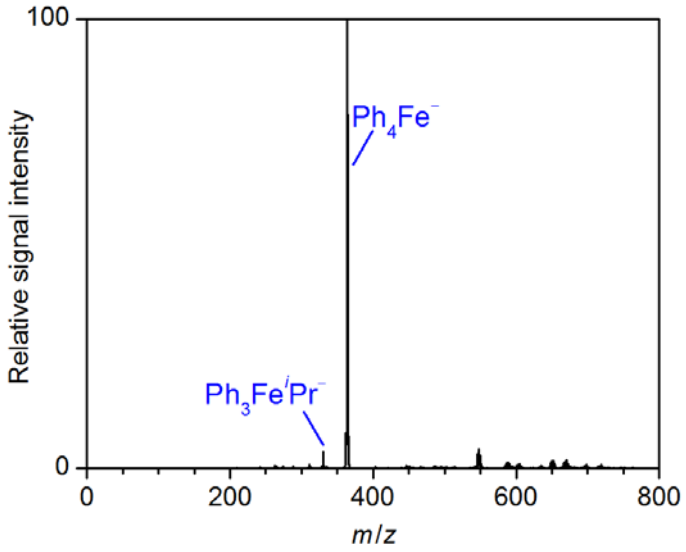

Figure S96. Negative-ion mode ESI mass spectrum of a solution of the products formed in the reaction of $Fe(acac)_3$ (20 mM) with PhMgBr (4 equiv) and ^{i}PrI (0.5 equiv) in THF.

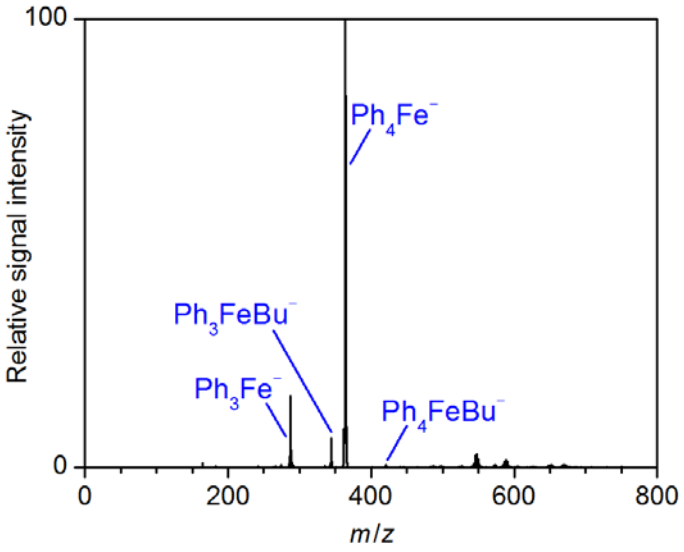

Figure S97. Negative-ion mode ESI mass spectrum of a solution of the products formed in the reaction of $Fe(acac)_3$ (20 mM) with PhMgBr (4 equiv) and BuCl (0.5 equiv) in THF.

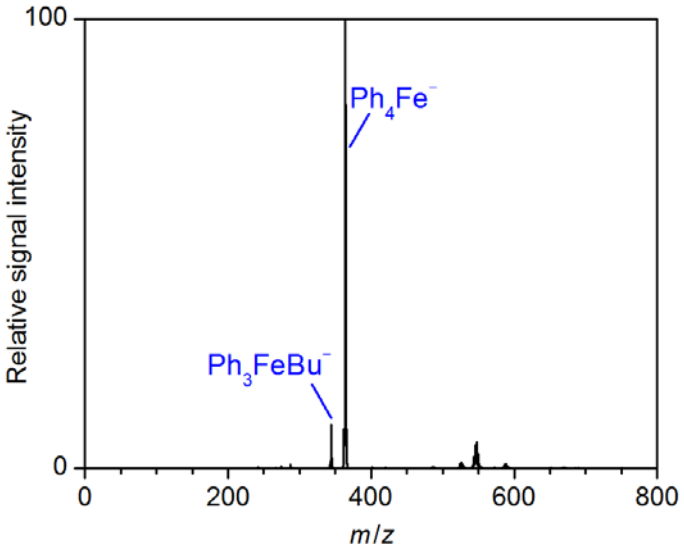

Figure S98. Negative-ion mode ESI mass spectrum of a solution of the products formed in the reaction of $Fe(acac)_3$ (20 mM) with PhMgBr (4 equiv) and BuBr (0.5 equiv) in THF.

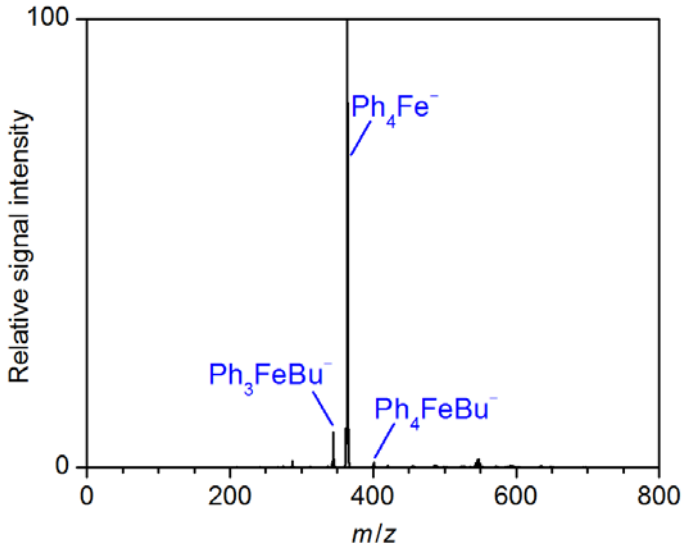

Figure S99. Negative-ion mode ESI mass spectrum of a solution of the products formed in the reaction of $Fe(acac)_3$ (20 mM) with PhMgBr (4 equiv) and BuI (0.5 equiv) in THF.

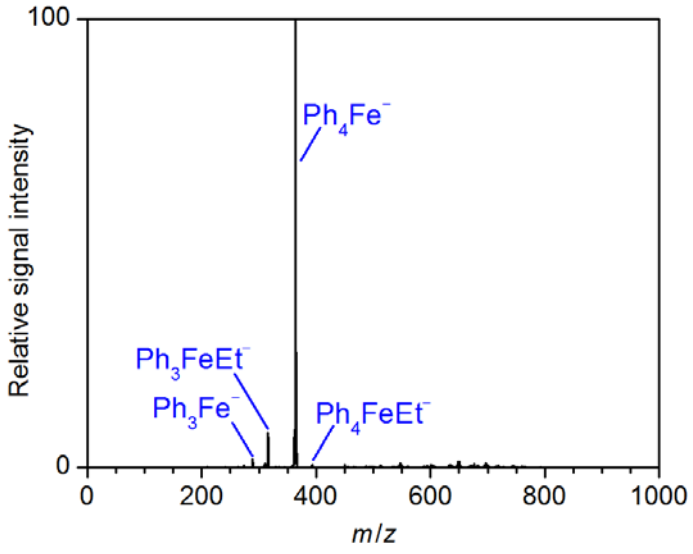

Figure S100. Negative-ion mode ESI mass spectrum of a solution of the products formed in the reaction of $Fe(acac)_3$ (20 mM) with PhMgBr (4 equiv), EtBr (0.5 equiv), and 4,4'-dimethylbiphenyl (0.5 equiv) in THF.

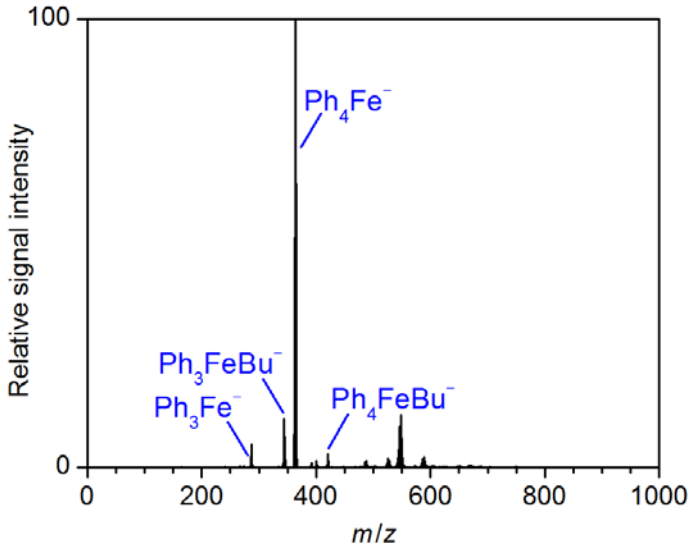

Figure S101. Negative-ion mode ESI mass spectrum of a solution of the products formed in the reaction of $Fe(acac)_3$ (20 mM) with PhMgBr (4 equiv), BuI (0.5 equiv) and 4,4'-dimethylbiphenyl (0.5 equiv) in THF.

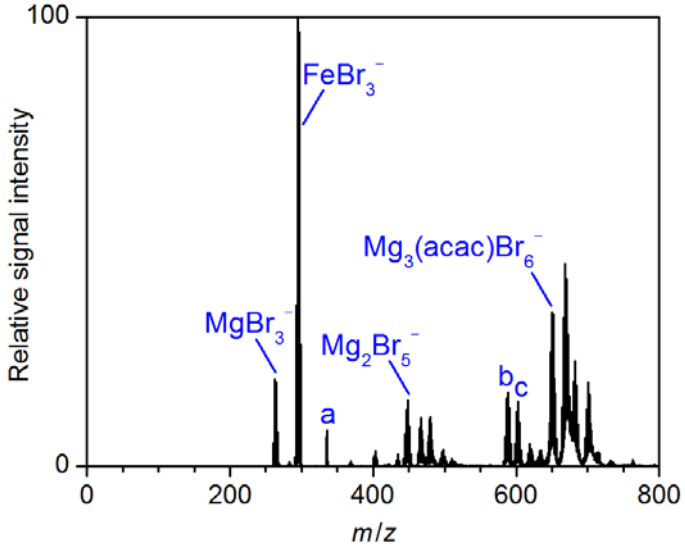

Figure S102. Negative-ion mode ESI mass spectrum of a solution of the products formed in the reaction of $Fe(acac)_3$ (20 mM) with PhMgBr (4 equiv) and EtBr (1 equiv) in THF; a = Ph_4Al^-, b = $Mg_3(acac)Br_5(OH)^-$, c = $Mg_3(acac)Br_5(OMe)^-$.

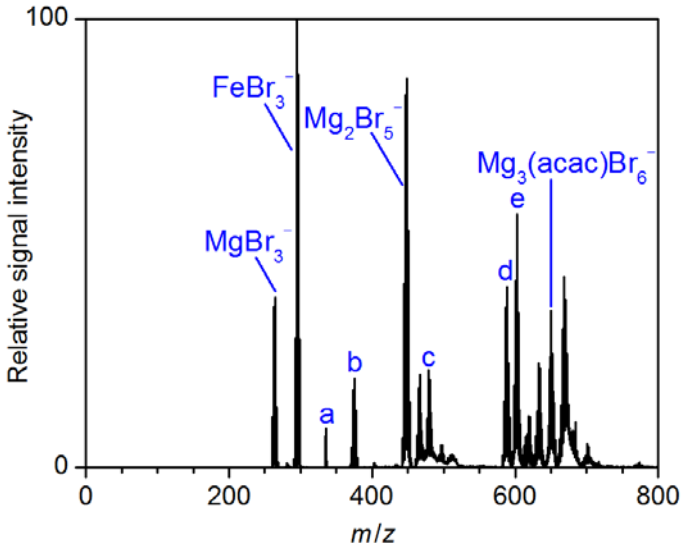

Figure S103. Negative-ion mode ESI mass spectrum of a solution of the products formed in the reaction of $Fe(acac)_3$ (5 mM) with PhMgBr (10 equiv) and EtBr (10 equiv) in THF; a = Ph_4Al^-, b = $FeBr_4^-$, c = $MgFeBr_5^-$, d = $Mg_3(acac)Br_5(OH)^-$, e = $Mg_3(acac)Br_5(OMe)^-$.

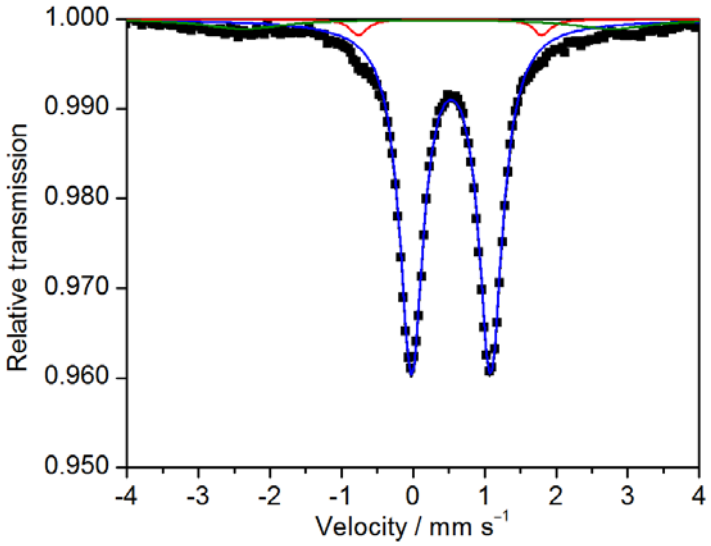

Figure S104. Mössbauer spectrum of a frozen solution (T = 80 K) of the products formed in the reaction of $^{57}FeCl_2$ (5 mM) with TMEDA (4 equiv), PhMgCl (4 equiv) and ^{i}PrCl (0.5 equiv) in THF together with overall fit (black); components of the fit: δ(blue) = 0.53 mm s^{-1}, ΔE_Q(blue) = 1.10 mm s^{-1}, rel. int. (blue) = 90%; δ(red) = 0.26 mm s^{-1}, ΔE_Q(red) = 2.03 mm s^{-1}, rel. int. (red) = 7%; δ(green) = 0.21 mm s^{-1}, ΔE_Q(green) = 5.14 mm s^{-1}, rel. int. (green) = 3%.

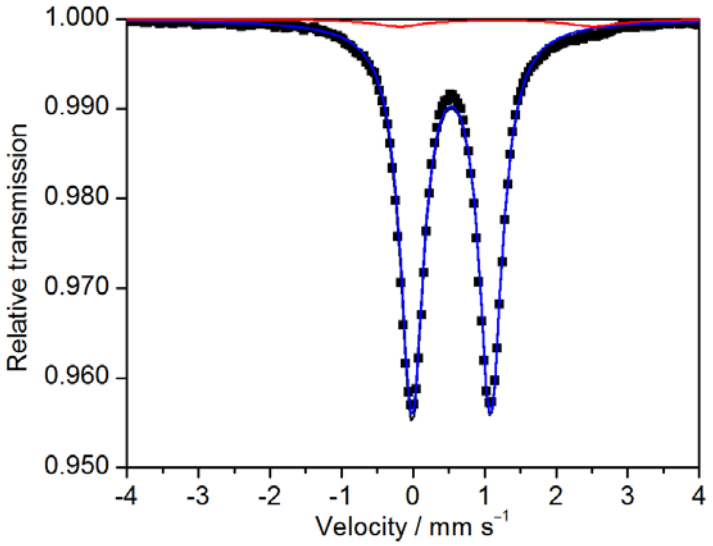

Figure S105. Mössbauer spectrum of a frozen solution (T = 80 K) of the products formed in the reaction of $^{57}FeCl_2$ (5 mM) with TMEDA (4 equiv) and PhMgCl (4 equiv) in THF together with overall fit (black); components of the fit: δ(blue) = 0.53 mm s^{-1}, ΔE_Q(blue) = 1.11 mm s^{-1}, rel. int. (blue) = 96%; δ(red) = 1.16 mm s^{-1}, ΔE_Q(red) = 2.72 mm s^{-1}, rel. int. (red) = 4%; The spectrum was used for quantitative comparison of the species formed in the experiment above.

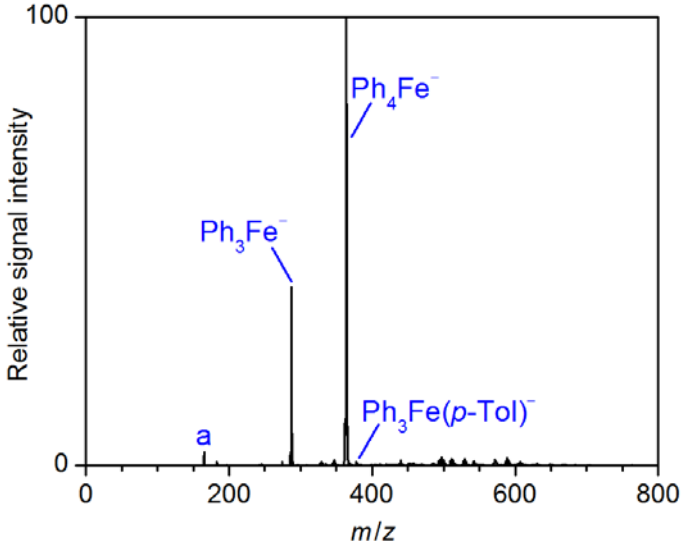

Figure S106. Negative-ion mode ESI mass spectrum of a solution of the products formed in the reaction of $Fe(acac)_3$ (20 mM) with PhMgBr (4 equiv) and *p*-TolCl (0.5 equiv) in THF.

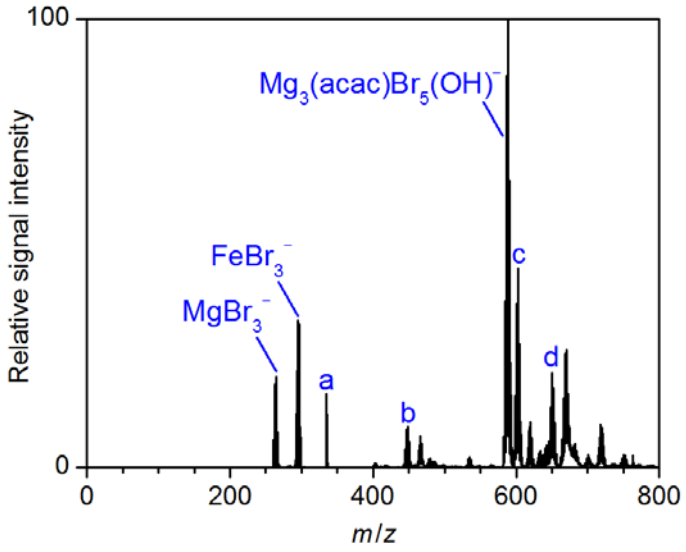

Figure S107. Negative-ion mode ESI mass spectrum of a solution of the products formed in the reaction of $Fe(acac)_3$ (20 mM) with PhMgBr (4 equiv) and *p*-TolBr (0.5 equiv) in THF; a = Ph_4Al^-, b = $Mg_2Br_5^-$, c = $Mg_4(acac)_2Br_3(OH)_4^-$, d = $Mg_3(acac)Br_6^-$.

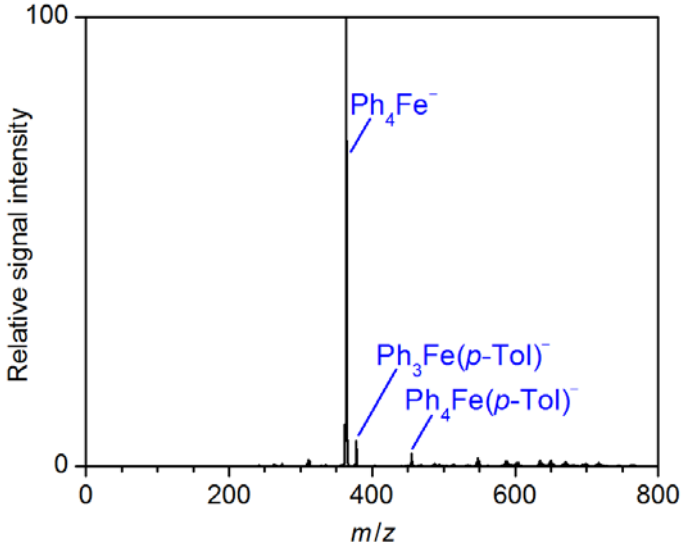

Figure S108. Negative-ion mode ESI mass spectrum of a solution of the products formed in the reaction of $Fe(acac)_3$ (20 mM) with PhMgBr (4 equiv) and *p*-TolI (0.5 equiv) in THF.

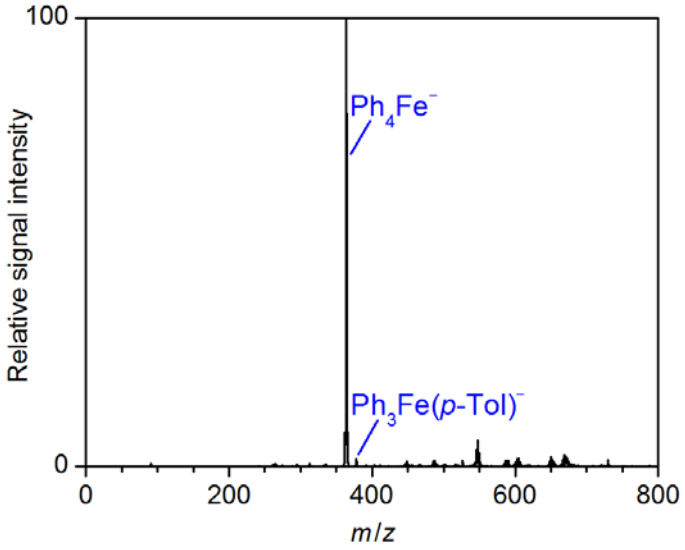

Figure S109. Negative-ion mode ESI mass spectrum of a solution of the products formed in the reaction of $Fe(acac)_3$ (20 mM) with PhMgBr (4 equiv) and *p*-TolOTf (0.5 equiv) in THF.

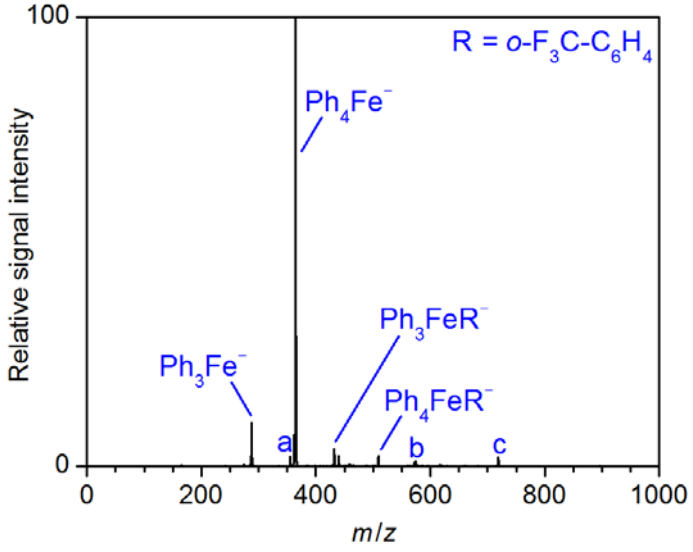

Figure S110. Negative-ion mode ESI mass spectrum of a solution of the products formed in the reaction of $Fe(acac)_3$ (20 mM) with PhMgBr (4 equiv) and RBr (0.5 equiv) in THF; a = Ph_2FeR^-, b = $Ph_6Fe_2^-$, c = $Ph_6Fe_2R^-$; R = *o*-F_3C-C_6H_4.

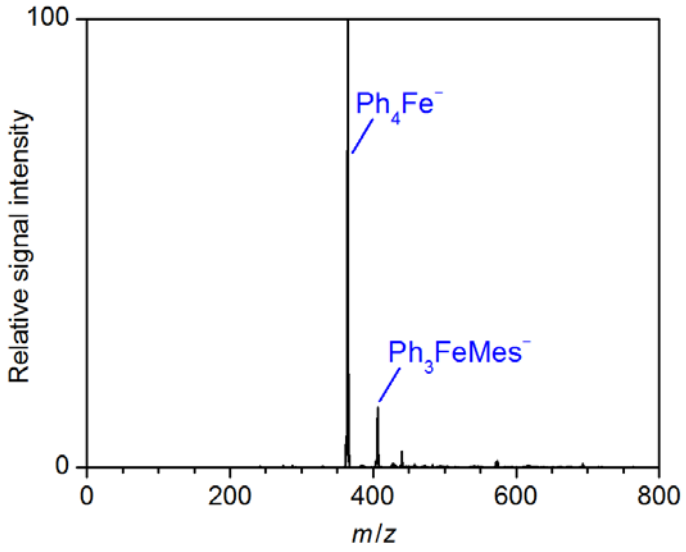

Figure S111. Negative-ion mode ESI mass spectrum of a solution of the products formed in the reaction of $Fe(acac)_3$ (20 mM) with PhMgBr (4 equiv) and MesBr (0.5 equiv) in THF.

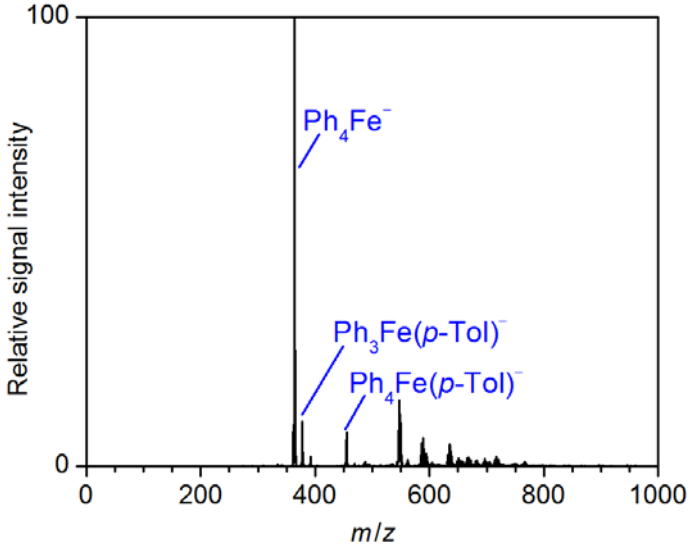

Figure S112. Negative-ion mode ESI mass spectrum of a solution of the products formed in the reaction of $Fe(acac)_3$ (20 mM) with PhMgBr (4 equiv), *p*-TolI (0.5 equiv) and 4,4'-dimethylbiphenyl (0.5 equiv) in THF.

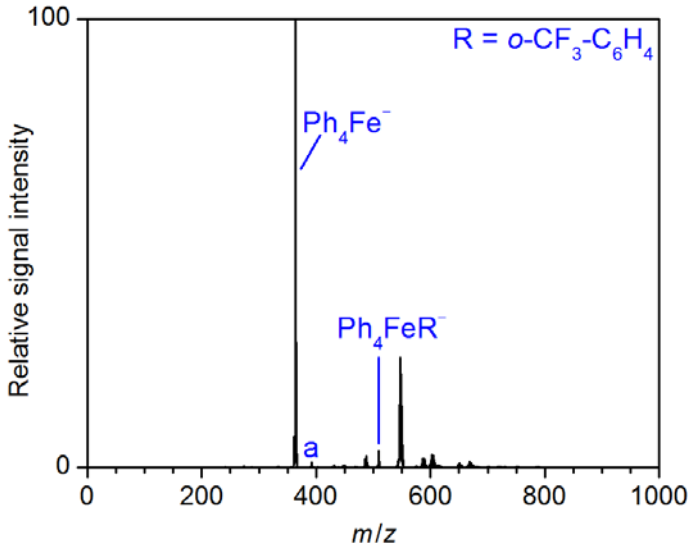

Figure S113. Negative-ion mode ESI mass spectrum of a solution of the products formed in the reaction of $Fe(acac)_3$ (20 mM) with PhMgBr (4 equiv), RBr (0.5 equiv), and 4,4'-dimethylbiphenyl (0.5 equiv) in THF; a = Ph_3FeR^-; R = o-CF_3-C_6H_4.

6.) Gas-Phase Fragmentation Reactions of Mass-Selected Organoiron Ions

Table S4. Overview of gas-phase fragmentation reactions of mass-selected organoiron ions.

Entry	Parent ion		Fragment ion		Neutral fragment(s)		Figure
	m/*z*	assignment	*m*/*z*	assignment	Δ*m*	assignment	
1a	558	$[Et_2Fe(dppbz)-2H]^-$	502	$Fe(dppbz)^-$	56	C_4H_8	S114
1b			531	$EtFe(dppbz)^-$	27	$[C_2H_3]$	
2	588	$EtFe_2(dppbz)^-$	560	$Fe_2H(dppbz)^-$	28	C_2H_4	S115
3a	763	$Ph_7Fe_4^-$	531	$[Ph_7Fe_4-C_{18}H_{16}]^-$	232	$Ph_2 + C_6H_6$	S116
3b			609	$Ph_5Fe_4^-$	154	Ph_2	
4a	896	$Ph_8Fe_5^-$	586	$[Fe_5,C_{24},H_{18}]^-$	310	$Ph_2 + 2\ C_6H_6$	S117
4b			664	$[Fe_5,C_{30},H_{24}]^-$	232	$Ph_2 + C_6H_6$	
4c			742	$Ph_6Fe_5^-$	154	Ph_2	
5a	948	$Fe(dppbz)_2^+$	424	$[Fe,C_{24},H_{18},P_2]^+$	524	$dppbz + C_6H_6$	S118
5b			502	$Fe(dppbz)^+$	446	dppbz	
5c			578	$[Fe,C_{36},H_{28},P_2]^+$	370	$2\ PPh_2$	
5d			685	$[Fe,C_{42},H_{32},P_3]^+$	263	$PPh_2 + C_6H_6$	
5e			763	$[Fe,C_{48},H_{38},P_3]^+$	185	PPh_2	
5f			893	$[Fe,C_{56},H_{41},P_4]^+$	55	C_4H_7	
6a	633	$Me_2Fe_3(CH_2SiMe_3)_5^-$	317	$Fe(CH_2SiMe_3)_3^-$	316	$2\ MeFe(CH_2SiMe_3)$	S119
6b			475	$MeFe_2(CH_2SiMe_3)_4^-$	158	$MeFe(CH_2SiMe_3)$	
7a	227	Bu_3Fe^-	115	$BuFeH_2^-$	112	$2\ C_4H_8$	S120
7b			171	Bu_2FeH^-	56	C_4H_8	
8a	205	Bu_2FeCl^-	93	$FeClH_2^-$	112	$2\ C_4H_8$	S121
8b			149	$BuFeClH^-$	56	C_4H_8	
9a	249	Bu_2FeBr^-	137	$FeBrH_2^-$	112	$2\ C_4H_8$	S122
9b			193	$BuFeBrH^-$	56	C_4H_8	
10a	297	Bu_2FeI^-	127	I^-	170	Bu_2Fe	S123
10b			185	$FeIH_2^-$	112	$2\ C_4H_8$	
10c			241	$BuFeIH^-$	56	C_4H_8	
11a	275	$BuFeClI^-$	127	I^-	148	BuFeCl	S124
11b			219	$FeClIH^-$	56	C_4H_8	
12	367	$BuFeI_2^-$	311	FeI_2H^-	56	C_4H_8	S125
13a	311	Hex_3Fe^-	143	$HexFeH_2^-$	168	$2\ C_6H_{12}$	S126
13b			227	Hex_2FeH^-	84	C_6H_{12}	
14a	537	$Hex_5Fe_2^-$	283	$Hex_2Fe_2H_3^-$	254	$3\ C_6H_{12}$	S127
14b			369	$Hex_3Fe_2H_2^-$	168	$2\ C_6H_{12}$	
14c			453	$Hex_4Fe_2H^-$	84	C_6H_{12}	
15a	395	Oct_3Fe^-	171	$OctFeH_2^-$	224	$2\ C_8H_{16}$	S128
15b			283	Oct_2FeH^-	112	C_8H_{16}	
16a	479	Dec_3Fe^-	199	$DecFeH_2^-$	280	$2\ C_{10}H_{20}$	7
16b			339	Dec_2FeH^-	140	$C_{10}H_{20}$	

Table S4, continued. Overview of gas-phase fragmentation reactions of mass-selected organoiron ions.

Entry	Parent ion		Fragment ion		Neutral fragment(s)		Figure
	m/*z*	assignment	*m*/*z*	assignment	Δ*m*	assignment	
17	547	$(Me_3SiCH_2)_5Fe_2^-$	317	$(Me_3SiCH_2)_3Fe^-$	230	$(Me_3SiCH_2)_2Fe$	S129
18	329	Bn_3Fe^-	238	Bn_2Fe^-	91	$Bn^•$	S130
19a	365	Bn_2FeI^-	127	I^-	238	Bn_2Fe	S131
19b			274	$BnFeI^-$	91	$Bn^•$	
20	401	$BnFeI_2^-$	310	FeI_2^-	91	$Bn^•$	S132
21	567	$Bn_5Fe_2^-$	329	Bn_3Fe^-	238	Bn_2Fe	S133
22a	287	Ph_3Fe^-	209	$[Ph_3Fe–C_6H_6]^-$	78	C_6H_6	S134
22b			133	$FePh^-$	154	Ph_2	
23	497	$Ph_5Fe_2^-$	343	$Ph_3Fe_2^-$	154	Ph_2	S135
24	225	Ph_2FeMe^-	210	Ph_2Fe^-	15	$Me^•$	S136
25a	351	Ph_2FeDec^-	273	$[Ph_2FeDec–C_6H_6]^-$	78	C_6H_6	S137
25b			211	Ph_2FeH^-	140	$C_{10}H_{20}$	
26	415	$PhFeDec_2^-$	275	$PhFeDecH^-$	140	$C_{10}H_{20}$	S138
27	301	Ph_2FeBn^-	210	Ph_2Fe^-	91	$Bn^•$	S139
28	315	$PhFeBn_2^-$	224	$PhFeBn^-$	91	$Bn^•$	S140
29a	329	Ph_2FeMes^-	196	$[Fe,C_{11},H_8]^-$	133	$[C_{10},H_{13}]$	S141
29b			209	$[Fe,C_{12},H_9]^-$	120	C_9H_{12}	
29c			251	$[Fe,C_{15},H_{15}]^-$	78	C_6H_6	
30a	371	$PhFeMes_2^-$	196	$[Fe,C_{11},H_8]^-$	175	$[C_{13},H_{19}]$	S142
30b			251	$[Fe,C_{15},H_{15}]^-$	120	MesH	
30c			293	$[Fe,C_{18},H_{21}]^-$	78	C_6H_6	
31a	301	$Ph_2Fe(o\text{-Tol})^-$	209	$[Ph_2Fe(o\text{-Tol})–C_7H_8]^-$	92	C_7H_8	S143
31b			223	$[Ph_2Fe(o\text{-Tol})–C_6H_6]^-$	78	C_6H_6	
32a	355	$Ph_2Fe(o\text{-}CF_3\text{-}C_6H_4)^-$	114	$[C_6,H_4,F_2]^-$	241	$[Fe,C_{13},H_{10},F]$	S144
32b			171	$[Fe,C_6,H_4,F_2]^-$	184	$[C_{13},H_{10},F]$	
32c			184	$[Fe,C_7,H_6,F_2]^-$	171	$[C_{12},H_8,F]$	
32d			227	$[Fe,C_{12},H_8,F]^-$	128	$[C_7,H_6,F_2]$	
32e			229	$[Fe,C_{12},H_{10},F]^-$	126	$[C_7,H_4,F_2]$	
32f			241	$[Fe,C_{13},H_{10},F]^-$	114	$[C_6,H_4,F_2]$	
33	413	Mes_3Fe^-	293	$[Mes_3Fe–C_9H_{12}]^-$	120	C_9H_{12}	S145
34	373	Mes_2FeBr^-	253	$[Mes_2FeBr–C_9H_{12}]^-$	120	C_9H_{12}	S146
35	695	$(Ar_F)_3Fe^-$	482	$(Ar_F)_2Fe^-$	213	$(Ar_F)^•$	S147
36	1141	$(Ar_F)_3Fe(dppbz)^-$	695	$(Ar_F)_3Fe^-$	446	(dppbz)	S148
37	329	$(o\text{-Tol})_3Fe^-$	237	$[(o\text{-Tol})_3Fe–(C_7H_8)]^-$	92	C_7H_8	S149
38a	491	$(o\text{-}CF_3\text{-}C_6H_4)_3Fe^-$	239	$[Fe,C_7,H_4,F_5]^-$	252	$[C_{14},H_8,F_4]$	S150
38b			377	$[Fe,C_{15},H_8,F_7]^-$	114	$[C_6,H_4,F_2]$	
39	963	$MeFe(dppbz)_2^+$	948	$Fe(dppbz)_2^+$	15	$Me^•$	S151

Table S4, continued. Overview of gas-phase fragmentation reactions of mass-selected organoiron ions.

Entry	Parent ion		Fragment ion		Neutral fragment(s)		Figure
	m/*z*	assignment	*m*/*z*	assignment	Δ*m*	assignment	
40	116	Me_4Fe^-	101	Me_3Fe^-	15	$Me^{\bullet}$	S152
41	368	$Me_2FeDec_2^-$	227	Me_2FeDec^-	141	$Dec^{\bullet}$	S153
42a	494	$MeFeDec_3^-$	212	$MeFeDec^-$	282	Dec_2	S154
42b			338	$FeDec_2^-$	156	Me-Dec	
42c			353	$MeFeDec_2^-$	141	$Dec^{\bullet}$	
43a	332	$MeFe(CH_2SiMe_3)_3^-$	245	$MeFe(CH_2SiMe_3)_2^-$	87	$Me_3SiCH_2^{\bullet}$	S155
43b			317	$Fe(CH_2SiMe_3)_3^-$	15	$Me^{\bullet}$	
44	490	$Me_2Fe_2(CH_2SiMe_3)_4^-$	317	$Fe(CH_2SiMe_3)_3^-$	173	$[FeMe_2 + Me_3SiCH_2^{\bullet}]$	S156
45a	562	$MeFe_2(CH_2SiMe_3)_5^-$	317	$Fe(CH_2SiMe_3)_3^-$	245	$[MeFe(CH_2SiMe_3) + Me_3SiCH_2^{\bullet}]$	S157
45b			475	$MeFe_2(CH_2SiMe_3)_4^-$	87	$Me_3SiCH_2^{\bullet}$	
46a	284	Bu_4Fe^-	114	$BuFeH^-$	170	$Bu_2 + C_4H_8$	S158
46b			170	Bu_2Fe^-	114	Bu_2	
46c			227	Bu_3Fe^-	57	$Bu^{\bullet}$	
47a	469	$Bu_4Fe_2H_2I^-$	297	$BuFe_2I^-$	172	$2\ C_4H_{10} + C_4H_8$	S159
47b			353	$Bu_2Fe_2I^-$	116	$2\ C_4H_{10}$	
47c			411	$Bu_3Fe_2HI^-$	58	C_4H_{10}	
48a	318	$Bu_3Fe(p\text{-Tol})^-$	170	Bu_2Fe^-	148	Bu-(*p*-Tol)	S160
48b			204	$BuFe(p\text{-Tol})^-$	114	Bu_2	
48c			226	$[Bu_3Fe(p\text{-Tol})-C_7H_8]^-$	92	C_7H_8	
48d			261	$Bu_2Fe(p\text{-Tol})^-$	57	$Bu^{\bullet}$	
49a	396	Hex_4Fe^-	226	Hex_2Fe^-	170	Hex_2	S161
49b			311	Hex_3Fe^-	85	$Hex^{\bullet}$	
50a	508	Oct_4Fe^-	282	Oct_2Fe^-	226	Oct_2	S162
50b			395	Oct_3Fe^-	113	$Oct^{\bullet}$	
51a	536	Oct_3FeDec^-	282	Oct_2Fe^-	254	Oct-Dec	S163
51b			310	$OctFeDec^-$	226	Oct_2	
51c			395	Oct_3Fe^-	141	$Dec^{\bullet}$	
51d			423	Oct_2FeDec^-	113	$Oct^{\bullet}$	
52a	564	$Oct_2FeDec_2^-$	310	$OctFeDec^-$	254	Oct-Dec	S164
52b			338	$FeDec_2^-$	226	Oct_2	
52c			423	Oct_2FeDec^-	141	$Dec^{\bullet}$	
52d			451	$OctFeDec_2^-$	113	$Oct^{\bullet}$	
53a	592	$OctFeDec_3^-$	451	$OctFeDec_2^-$	141	$Dec^{\bullet}$	S165
53b			479	Dec_3Fe^-	113	$Oct^{\bullet}$	
54a	620	Dec_4Fe^-	338	Dec_2Fe^-	282	Dec_2	7
54b			479	Dec_3Fe^-	141	$Dec^{\bullet}$	
55	404	$(Me_3SiCH_2)_4Fe^-$	317	$(Me_3SiCH_2)_3Fe^-$	87	$Me_3SiCH_2^{\bullet}$	S166
56	420	Bn_4Fe^-	329	Bn_3Fe^-	91	$Bn^{\bullet}$	S167
57a	372	$Bn_3Fe^iPr^-$	281	$Bn_2Fe^iPr^-$	91	$Bn^{\bullet}$	S168
57b			329	Bn_3Fe^-	43	$^iPr^{\bullet}$	

Table S4, continued. Overview of gas-phase fragmentation reactions of mass-selected organoiron ions.

Entry	Parent ion		Fragment ion		Neutral fragment(s)		Figure
	m/*z*	assignment	*m*/*z*	assignment	Δ*m*	assignment	
58	302	Ph_3FeMe^-	210	Ph_2Fe^-	92	Ph-Me	S169
59	316	Ph_3FeEt^-	210	Ph_2Fe^-	106	Ph-Et	S170
60	330	$Ph_3Fe^{i}Pr^-$	210	Ph_2Fe^-	120	Ph-^{i}Pr	S171
61	344	Ph_3FeBu^-	210	Ph_2Fe^-	134	Ph-Bu	S172
62a	304	$PhFeBu_3^-$	170	$FeBu_2^-$	134	Ph-Bu	S173
62b			190	$PhFeBu^-$	114	Bu_2	
62c			226	$[PhFeBu_3–C_6H_6]^-$	78	C_6H_6	
63a	428	Ph_3FeDec^-	210	Ph_2Fe^-	218	Ph-Dec	S174
63b			274	$PhFeDec^-$	154	Ph_2	
64	492	$Ph_2FeDec_2^-$	274	$PhFeDec^-$	218	Ph-Dec	S175
65a	556	$PhFeDec_3^-$	338	$FeDec_2^-$	218	Ph-Dec	S176
65b			415	$PhFeDec_2^-$	141	Dec$^{\bullet}$	
65c			478	$[PhFeDec_3–C_6H_6]^-$	78	C_6H_6	
66a	378	Ph_3FeBn^-	224	$PhFeBn^-$	154	Ph_2	S177
66b			210	Ph_2Fe^-	168	Ph-Bn	
67	392	$Ph_2FeBn_2^-$	210	Ph_2Fe^-	182	Bn_2	S178
68	406	$PhFeBn_3^-$	315	$PhFeBn_2^-$	91	Bn$^{\bullet}$	S179
69	500	$Ph_3Fe(Ar_F)^-$	346	$PhFe(Ar_F)^-$	154	Ph_2	S180
70	636	$Ph_2Fe(Ar_F)_2^-$	482	$Fe(Ar_F)_2^-$	154	Ph_2	S181
71	772	$PhFe(Ar_F)_3^-$	482	$Fe(Ar_F)_2^-$	290	Ph-(Ar_F)	S182
72	908	$(Ar_F)_4Fe^-$	482	$Fe(Ar_F)_2^-$	426	$(Ar_F)_2$	S183
73a	421	Ph_4FeBu^-	211	Ph_2FeH^-	210	$Ph_2 + C_4H_8$	S184
73b			267	Ph_2FeBu^-	154	Ph_2	
73c			343	$[Ph_4FeBu–C_6H_6]^-$	78	C_6H_6	
73d			364	Ph_4Fe^-	57	Bu$^{\bullet}$	
73e			365	Ph_4FeH^-	56	C_4H_8	
74a	455	$Ph_4Fe(p\text{-Tol})^-$	211	$[Fe,C_{12},H_{11}]^-$	244	$Ph_2 + C_7H_6$	S185
74b			299	$[Ph_4Fe(p\text{-Tol})–2\ C_6H_6]^-$	156	$2\ C_6H_6$	
74c			377	$[Ph_4Fe(p\text{-Tol})–C_6H_6]^-$	78	C_6H_6	
75a	509	$Ph_4Fe(o\text{-}CF_3\text{-}C_6H_4)^-$	211	$[Fe,C_{12},H_{11}]^-$	298	$[C_{19},H_{13},F_3]$	S186
75b			353	$[Ph_4Fe(o\text{-}CF_3\text{-}C_6H_4)–2\ C_6H_6]^-$	156	$2\ C_6H_6$	
75c			431	$[Ph_4Fe(o\text{-}CF_3\text{-}C_6H_4)–C_6H_6]^-$	78	C_6H_6	

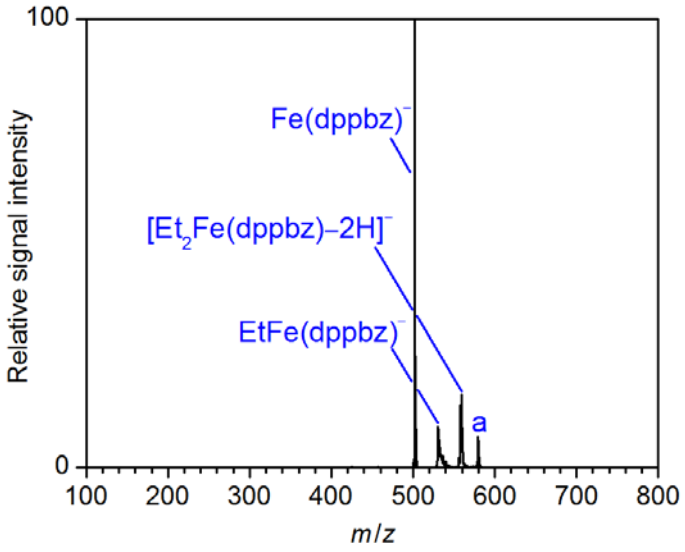

Figure S114. Mass spectrum of mass-selected $[Et_2Fe(dppbz)–2H]^-$ (m/z 558) and its fragment ions produced upon collision-induced dissociation (V_{exc} = 0.40 V); a = $Et_2Fe(dppbz)(H_2O)^-$.

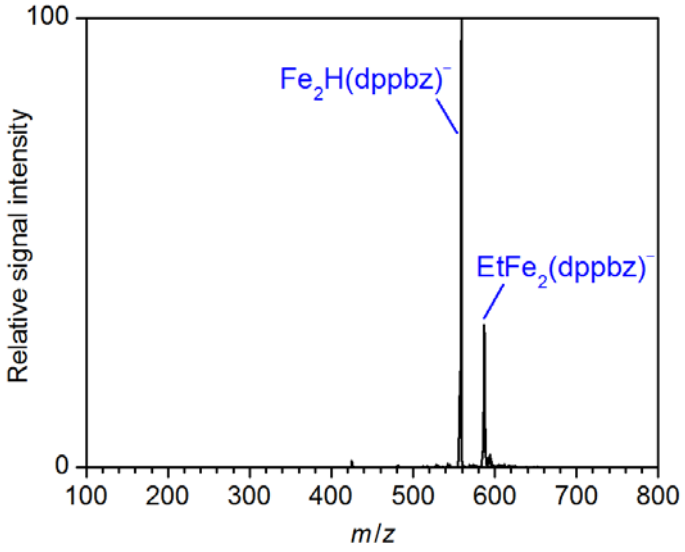

Figure S115. Mass spectrum of mass-selected $EtFe_2(dppbz)^-$ (m/z 588) and its fragment ions produced upon collision-induced dissociation (V_{exc} = 0.35 V).

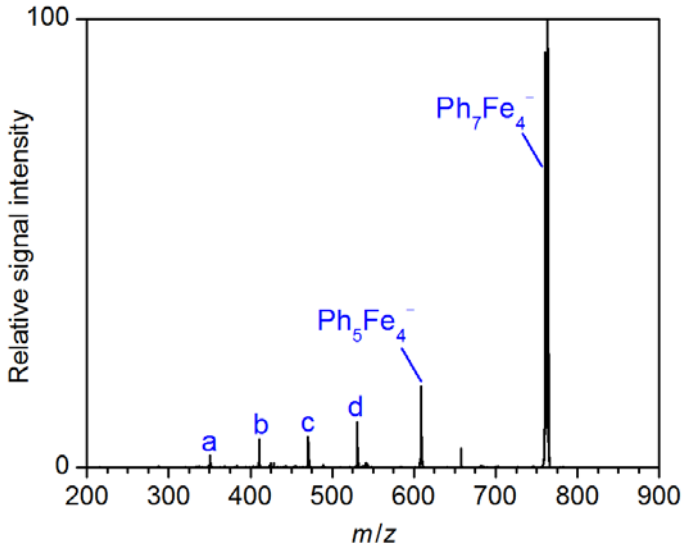

Figure S116. Mass spectrum of mass-selected $Ph_7Fe_4^-$ (*m*/*z* 764) and its fragment ions produced upon collision-induced dissociation (V_{exc} = 0.40 V); a = $[Fe_4,C_6,H_7,O_3]^-$, b = $[Fe_4,C_{12},H_{11},O_2]^-$, c = $[Fe_4,C_{18},H_{15},O]^-$, d = $[Fe_4,C_{24},H_{19}]^-$. The fragment ions a – d correspond to complexes of the type $[Ph_{4-n}Fe_4(OH)_n–H]^-$, *n* = 0 – 3. Species a – c result from the successive hydrolysis of phenyl substituents in ion-molecule reactions with traces of background water present in the vacuum system of the mass spectrometer.

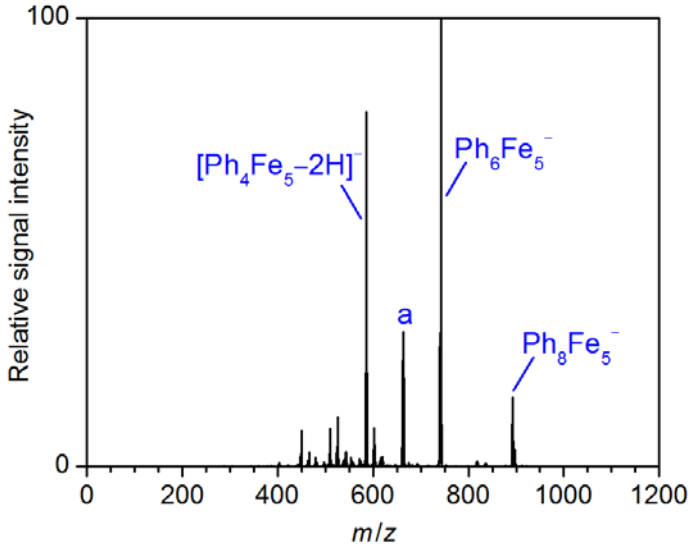

Figure S117. Mass spectrum of mass-selected $Ph_8Fe_5^-$ (*m*/*z* 896) and its fragment ions produced upon collision-induced dissociation (V_{exc} = 0.60 V); a = $[Ph_5Fe_5–H]^-$.

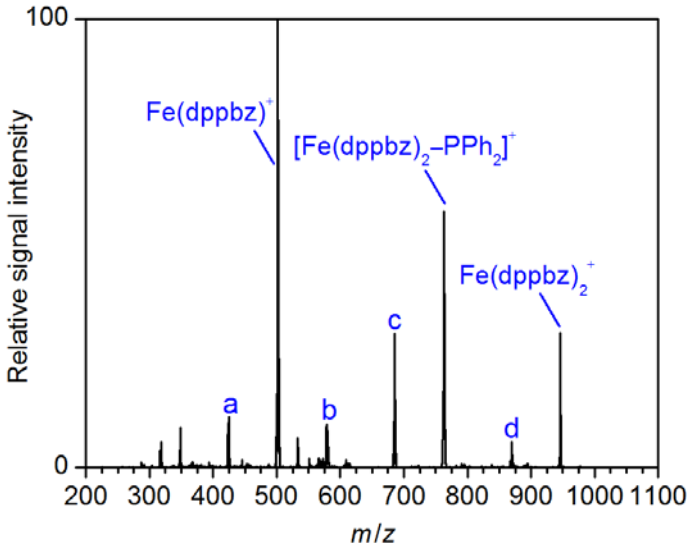

Figure S118. Mass spectrum of mass-selected $Fe(dppbz)_2^+$ (m/z 948) and its fragment ions produced upon collision-induced dissociation (V_{exc} = 0.80 V); a = $[Fe,C_{24},H_{18},P_2]^+$, b = $[Fe(dppbz)_2–2PPh_2]^+$ c = $[Fe,C_{42},H_{32},P_3]^+$, d = $[Fe,C_{56},H_{41},P_4]^+$.

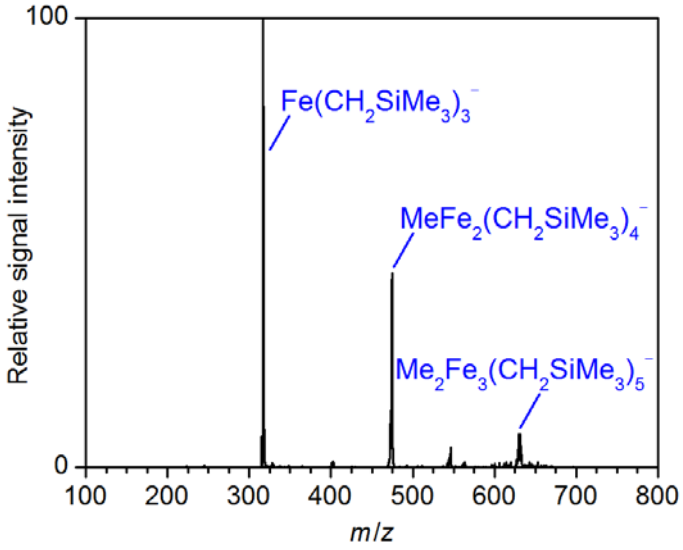

Figure S119. Mass spectrum of mass-selected $Me_2Fe_3(CH_2SiMe_3)_5^-$ (m/z 633) and its fragment ions produced upon collision-induced dissociation (V_{exc} = 0.50 V).

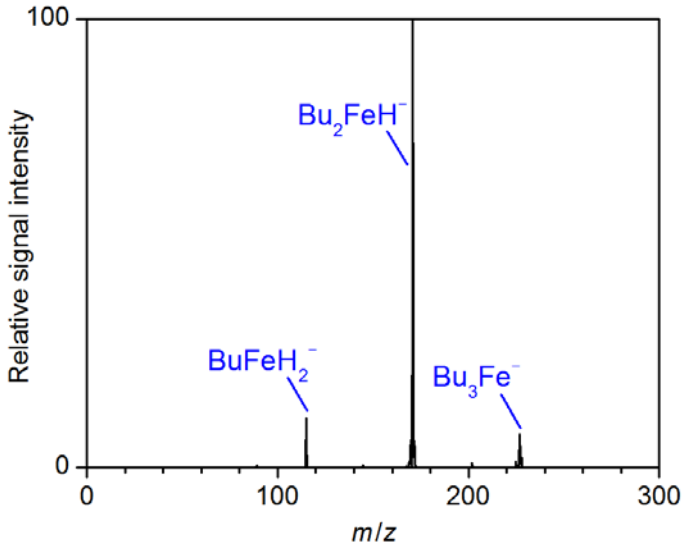

Figure S120. Mass spectrum of mass-selected Bu_3Fe^- (*m*/*z* 227) and its fragment ions produced upon collision-induced dissociation (V_{exc} = 0.40 V).

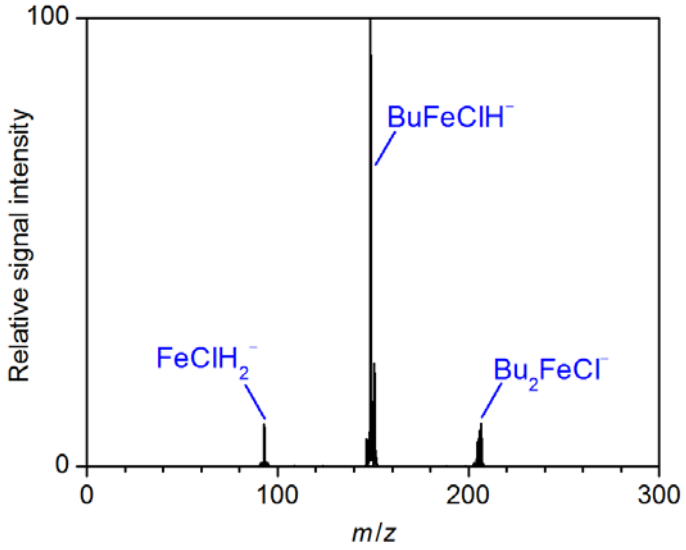

Figure S121. Mass spectrum of mass-selected Bu_2FeCl^- (*m*/*z* 205) and its fragment ions produced upon collision-induced dissociation (V_{exc} = 0.70 V).

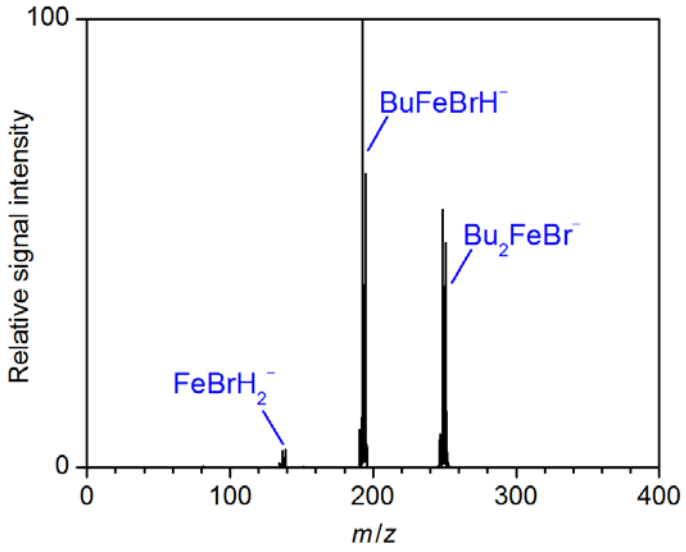

Figure S122. Mass spectrum of mass-selected Bu_2FeBr^- (*m*/*z* 249) and its fragment ions produced upon collision-induced dissociation (V_{exc} = 0.40 V).

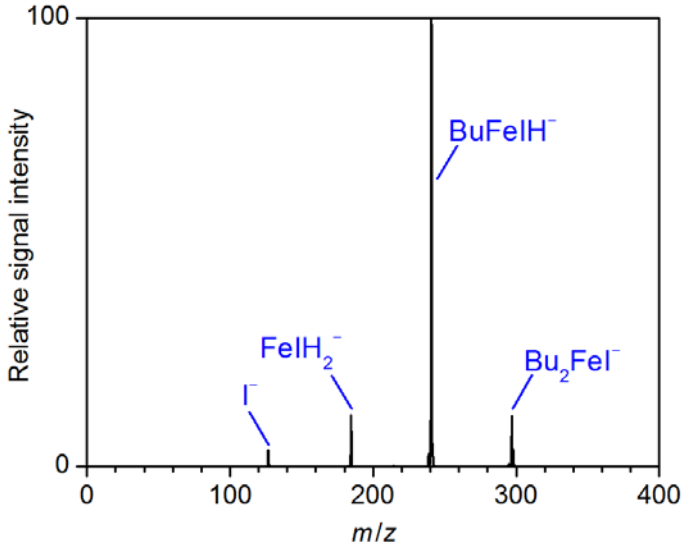

Figure S123. Mass spectrum of mass-selected Bu_2FeI^- (*m*/*z* 297) and its fragment ions produced upon collision-induced dissociation (V_{exc} = 0.50 V).

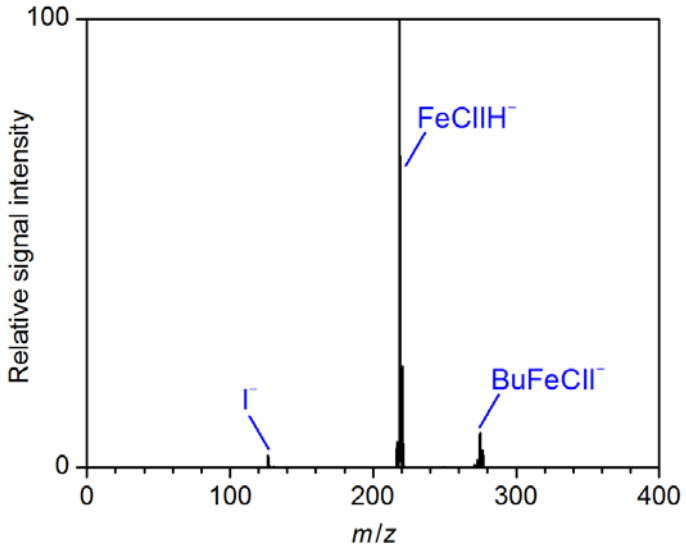

Figure S124. Mass spectrum of mass-selected Bu_2FeClI^- (*m*/*z* 275) and its fragment ions produced upon collision-induced dissociation (V_{exc} = 0.50 V).

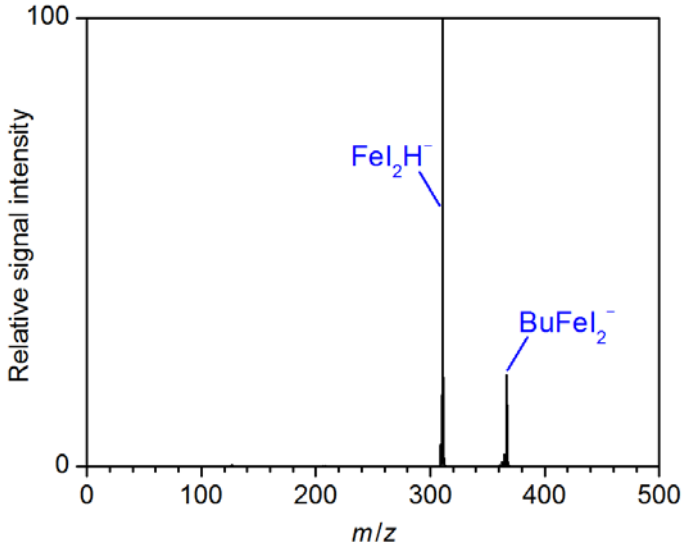

Figure S125. Mass spectrum of mass-selected $BuFeI_2^-$ (*m*/*z* 367) and its fragment ions produced upon collision-induced dissociation (V_{exc} = 0.50 V).

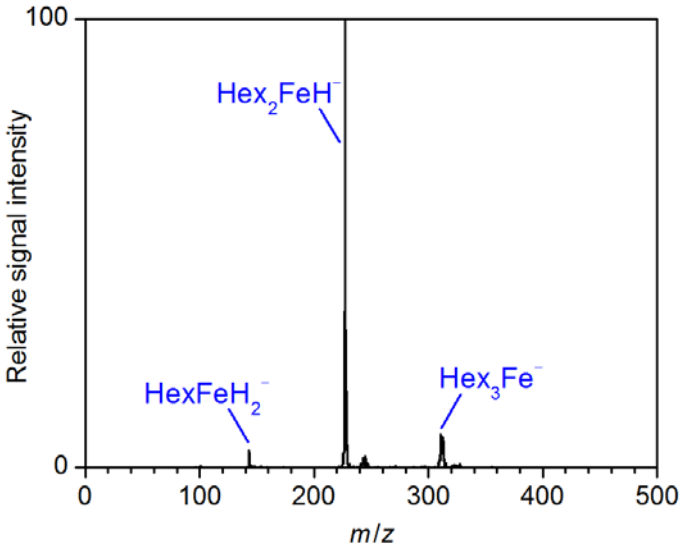

Figure S126. Mass spectrum of mass-selected Hex_3Fe^- (m/z 311) and its fragment ions produced upon collision-induced dissociation (V_{exc} = 0.65 V).

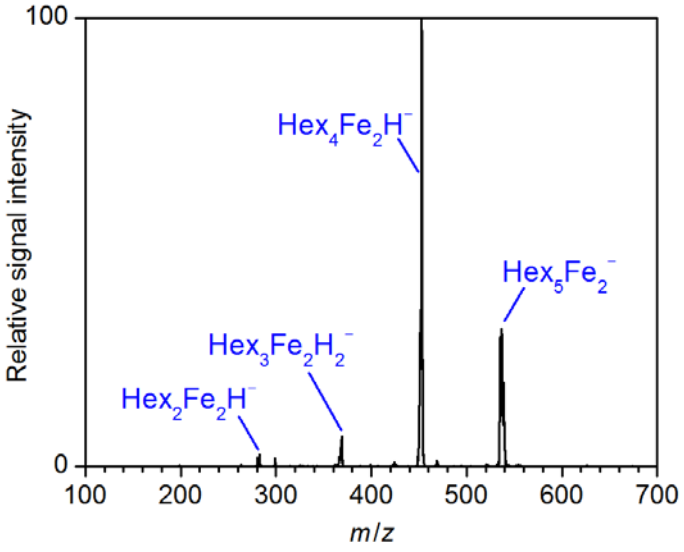

Figure S127. Mass spectrum of mass-selected $Hex_5Fe_2^-$ (m/z 537) and its fragment ions produced upon collision-induced dissociation (V_{exc} = 0.50 V).

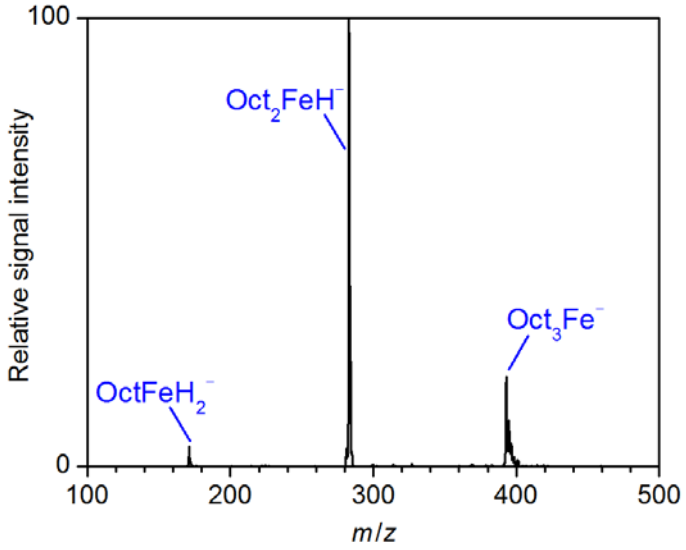

Figure S128. Mass spectrum of mass-selected Oct_3Fe^- (m/z 395) and its fragment ions produced upon collision-induced dissociation (V_{exc} = 0.70 V).

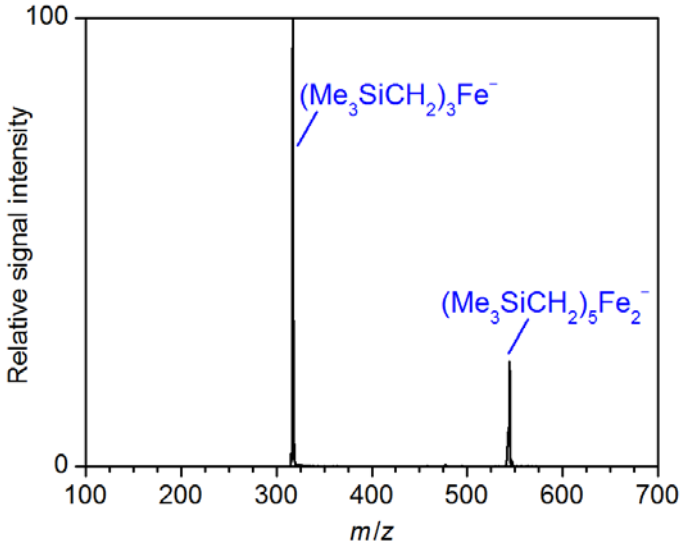

Figure S129. Mass spectrum of mass-selected $(Me_3SiCH_2)_5Fe_2^-$ (m/z 547) and its fragment ions produced upon collision-induced dissociation (V_{exc} = 0.50 V).

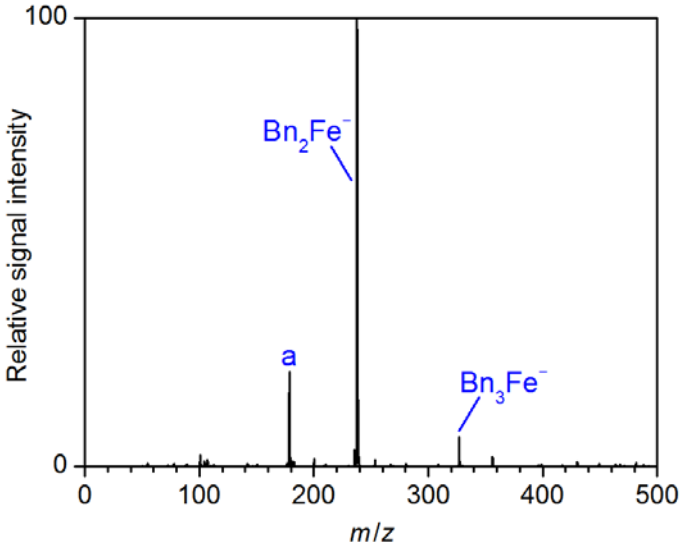

Figure S130. Mass spectrum of mass-selected Bn_3Fe^- (*m*/*z* 329) and its fragment ions produced upon collision-induced dissociation (V_{exc} = 0.55 V); a = $[Fe,Bn,O_2]^-$.

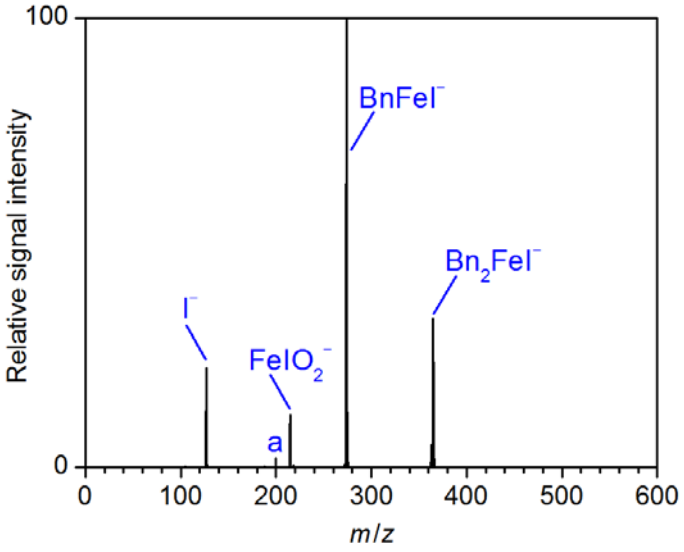

Figure S131. Mass spectrum of mass-selected Bn_2FeI^- (*m*/*z* 365) and its fragment ions produced upon collision-induced dissociation (V_{exc} = 0.50 V); a = $FeI(OH)^-$.

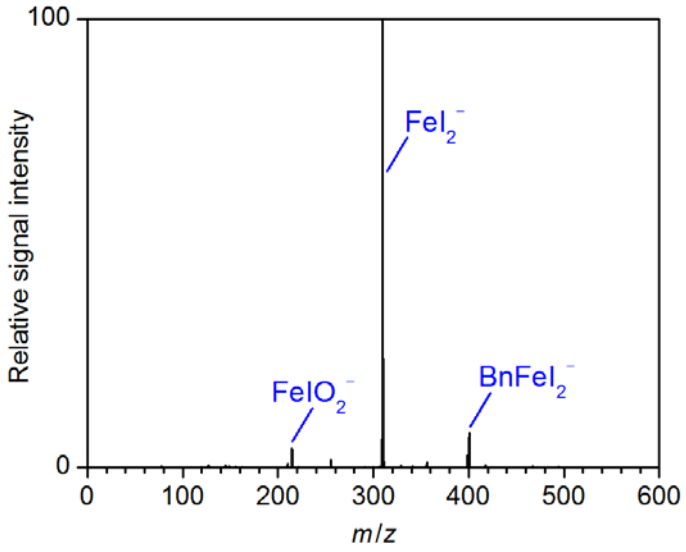

Figure S132. Mass spectrum of mass-selected $BnFeI_2^-$ (*m*/*z* 401) and its fragment ions produced upon collision-induced dissociation (V_{exc} = 0.90 V).

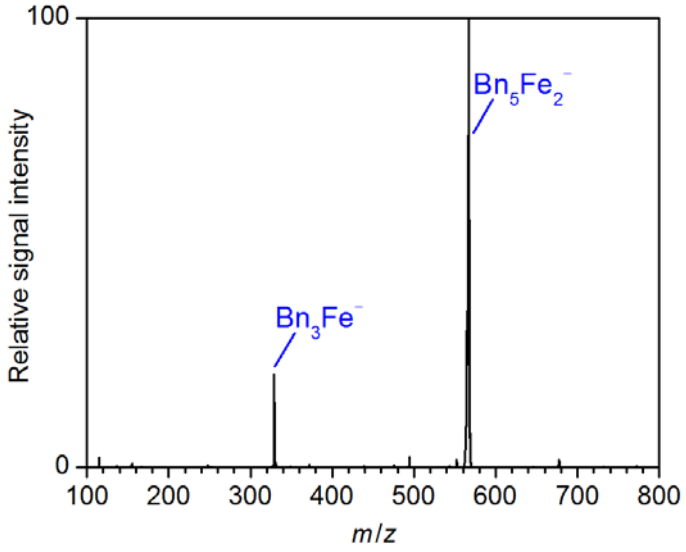

Figure S133. Mass spectrum of mass-selected $Bn_5Fe_2^-$ (*m*/*z* 567) and its fragment ions produced upon collision-induced dissociation (V_{exc} = 0.35 V).

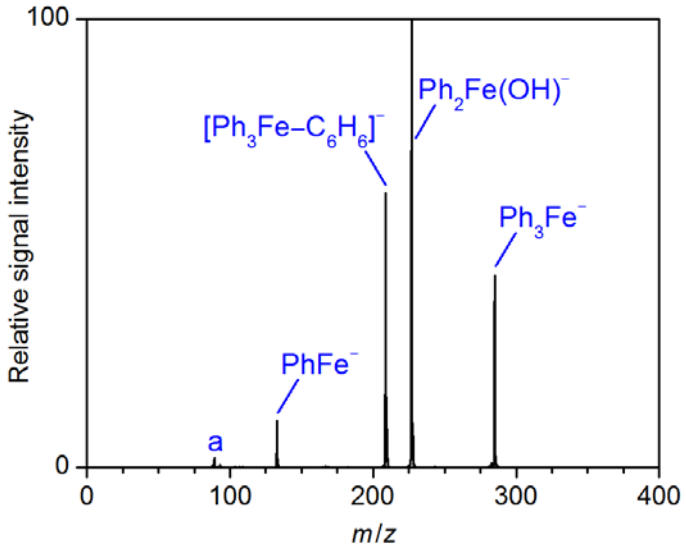

Figure S134. Mass spectrum of mass-selected Ph_3Fe^- (*m*/*z* 287) and its fragment ions produced upon collision-induced dissociation (V_{exc} = 0.60 V); a = $C_6H_5O^-$. The resulting $Ph_2Fe(OH)^-$ ion originated from an ion-molecule reaction with traces of water present in the vacuum system of the mass spectrometer.

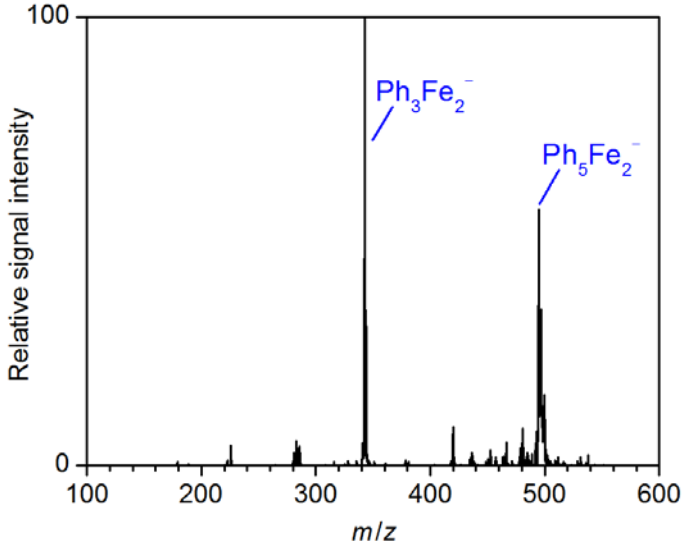

Figure S135. Mass spectrum of mass-selected $Ph_5Fe_2^-$ (*m*/*z* 497) and its fragment ions produced upon collision-induced dissociation (V_{exc} = 0.40 V).

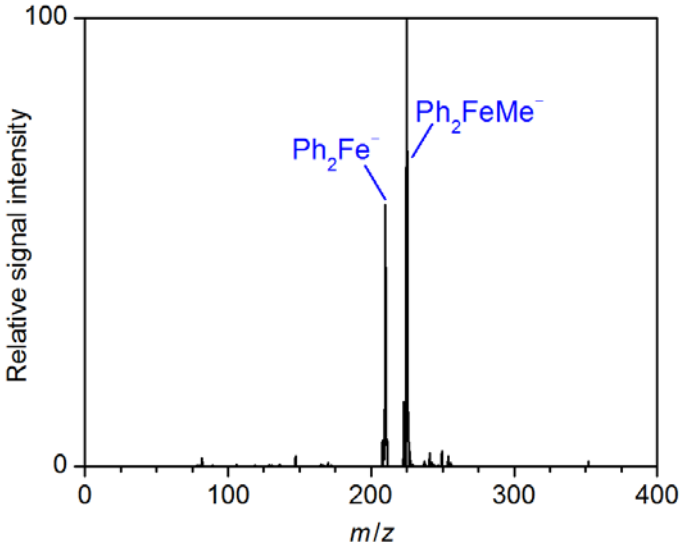

Figure S136. Mass spectrum of mass-selected Ph_2FeMe^- (m/z 225) and its fragment ions produced upon collision-induced dissociation (V_{exc} = 0.70 V).

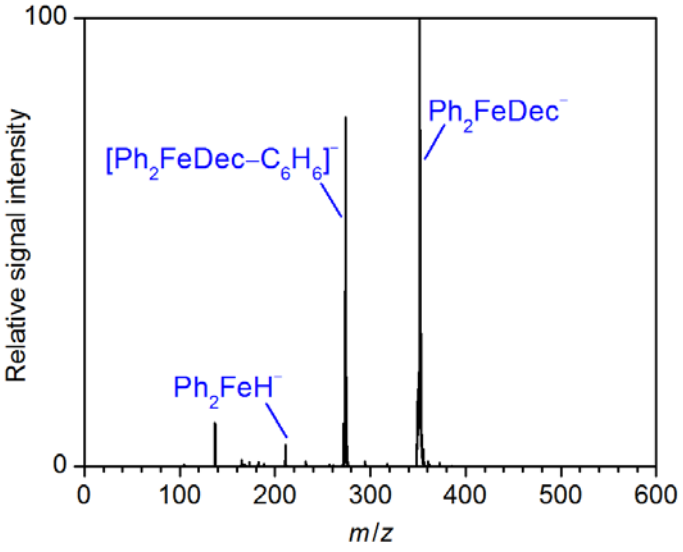

Figure S137. Mass spectrum of mass-selected Ph_2FeDec^- (m/z 351) and its fragment ions produced upon collision-induced dissociation (V_{exc} = 0.45 V).

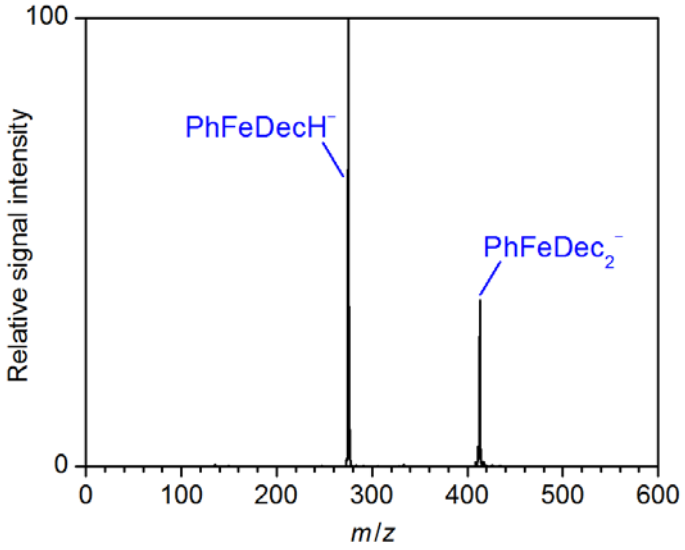

Figure S138. Mass spectrum of mass-selected $PhFeDec_2^-$ (m/z 415) and its fragment ions produced upon collision-induced dissociation (V_{exc} = 0.60 V).

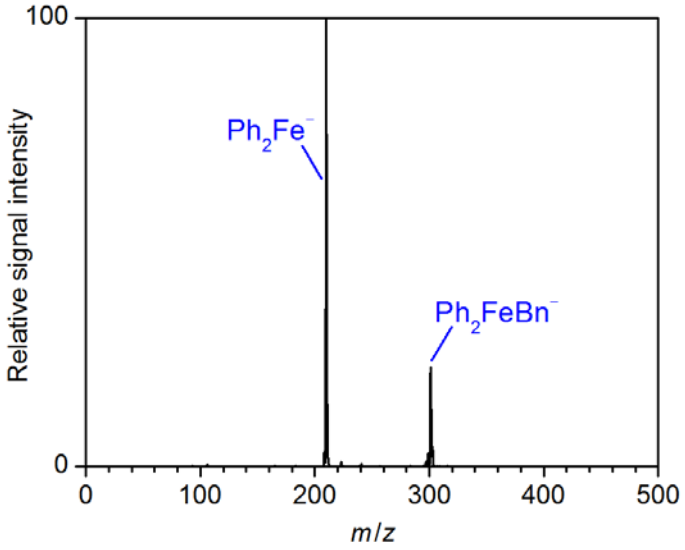

Figure S139. Mass spectrum of mass-selected Ph_2FeBn^- (m/z 301) and its fragment ions produced upon collision-induced dissociation (V_{exc} = 0.85 V).

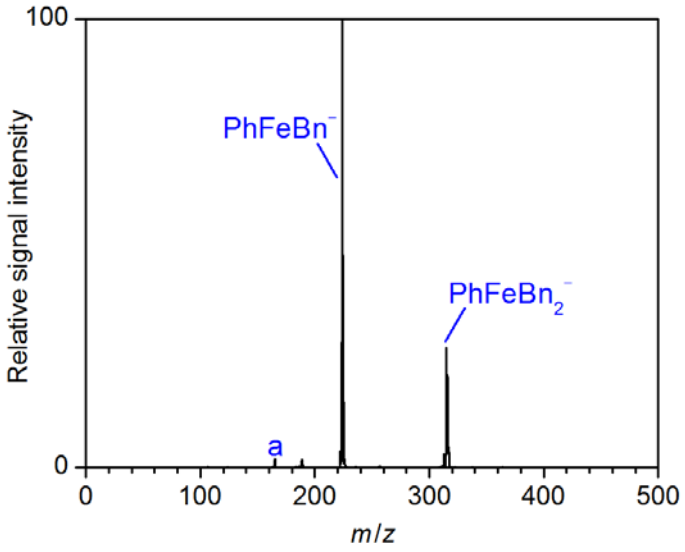

Figure S140. Mass spectrum of mass-selected $PhFeBn_2^-$ (*m*/*z* 315) and its fragment ions produced upon collision-induced dissociation (V_{exc} = 0.85 V); a = $[Fe,Ph,O_2]^-$.

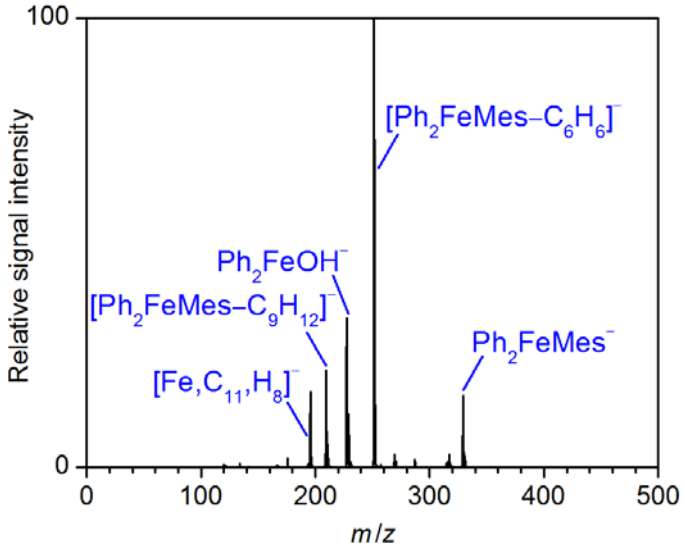

Figure S141. Mass spectrum of mass-selected Ph_2FeMes^- (*m*/*z* 329) and its fragment ions produced upon collision-induced dissociation (V_{exc} = 0.90 V). The resulting Ph_2FeOH^- ion originated from an ion-molecule reaction with traces of water present in the vacuum system of the mass spectrometer.

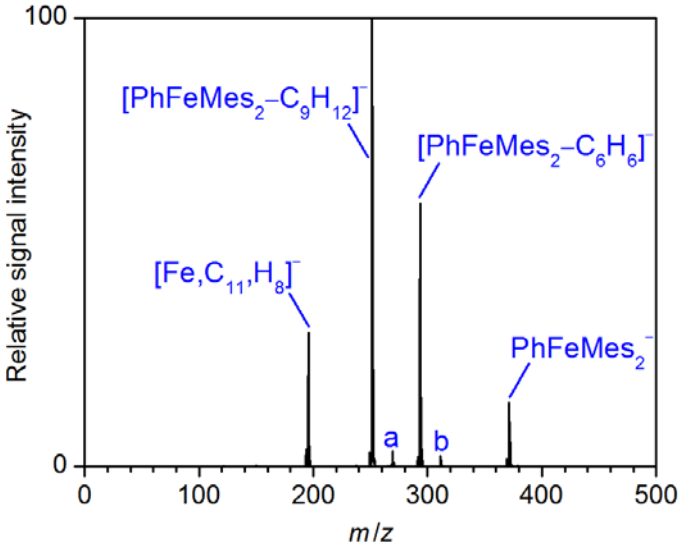

Figure S142. Mass spectrum of mass-selected $PhFeMes_2^-$ (m/z 371) and its fragment ions produced upon collision-induced dissociation (V_{exc} = 1.00 V); a = $PhFeMes(OH)^-$, b = $FeMes(OH)_2^-$.

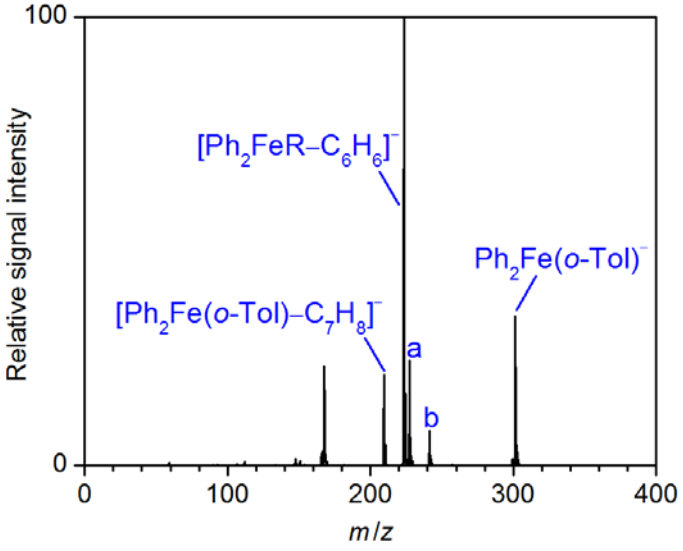

Figure S143. Mass spectrum of mass-selected Ph_2FeR^- (m/z 301) and its fragment ions produced upon collision-induced dissociation (V_{exc} = 0.80 V); a = Ph_2FeOH^-, b = PhFe(*o*-Tol)$(OH)^-$.

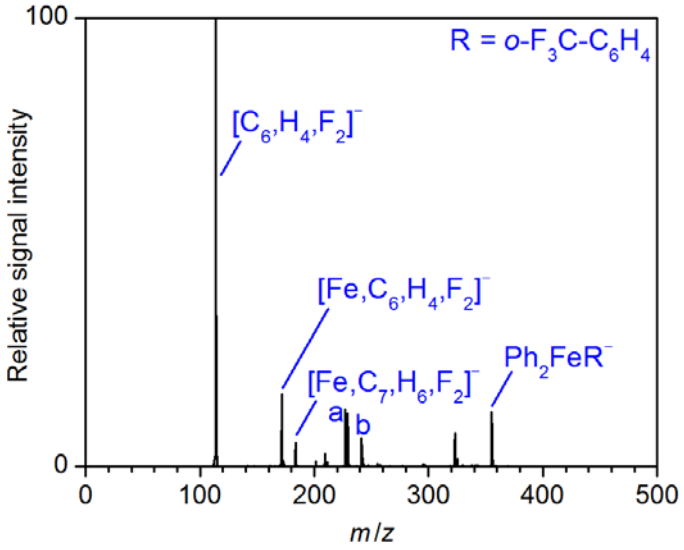

Figure S144. Mass spectrum of mass-selected Ph_2FeR^- (m/z 355) and its fragment ions produced upon collision-induced dissociation (V_{exc} = 0.85 V); a = $[Fe,C_{12},H_8,F]^-$ + $[Fe,C_{12}H_{10},F]^-$, b = $[Fe,C_{13},H_{10},F]^-$; R = o-F_3C-C_6H_4.

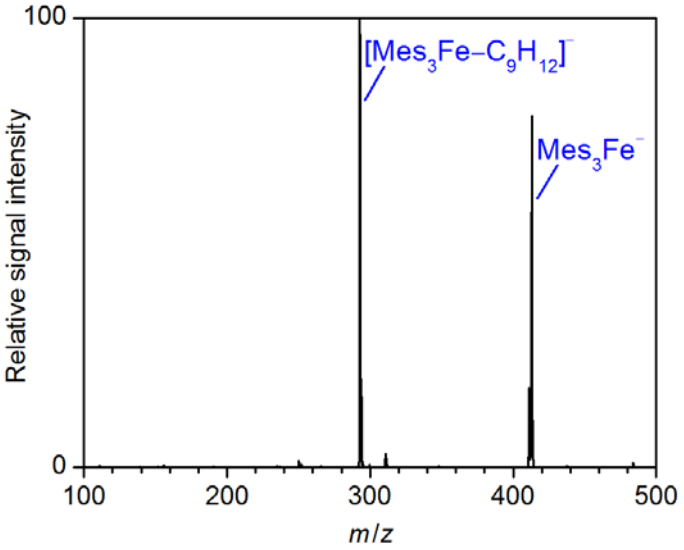

Figure S145. Mass spectrum of mass-selected Mes_3Fe^- (m/z 416) and its fragment ions produced upon collision-induced dissociation (V_{exc} = 0.80 V).

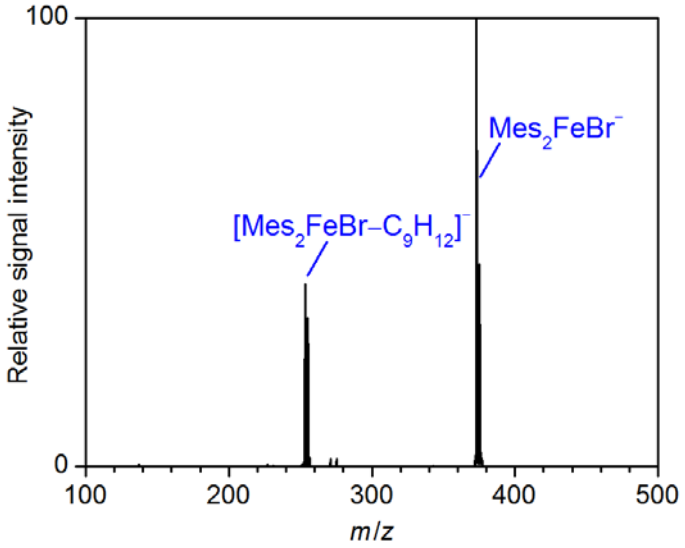

Figure S146. Mass spectrum of mass-selected Mes_2FeBr^- (*m*/*z* 373) and its fragment ions produced upon collision-induced dissociation (V_{exc} = 0.90 V).

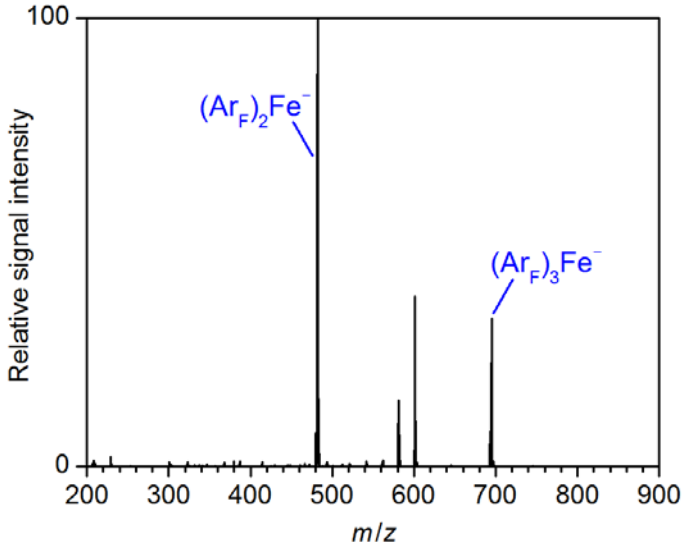

Figure S147. Mass spectrum of mass-selected $(Ar_F)_3Fe^-$ (*m*/*z* 695) and its fragment ions produced upon collision-induced dissociation (V_{exc} = 1.40 V); Ar_F = 3,5-$(CF_3)_2$-C_6H_3.

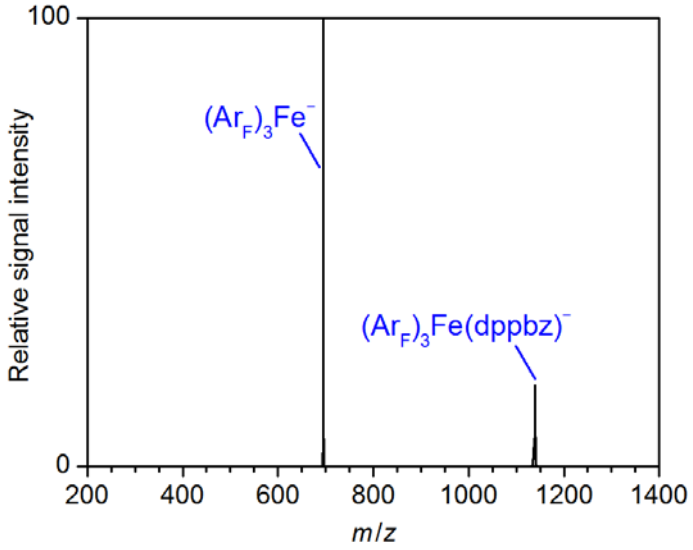

Figure S148. Mass spectrum of mass-selected $(Ar_F)_3Fe(dppbz)^-$ (*m*/*z* 1141) and its fragment ions produced upon collision-induced dissociation (V_{exc} = 0.25 V); Ar_F = 3,5-$(CF_3)_2$-C_6H_3.

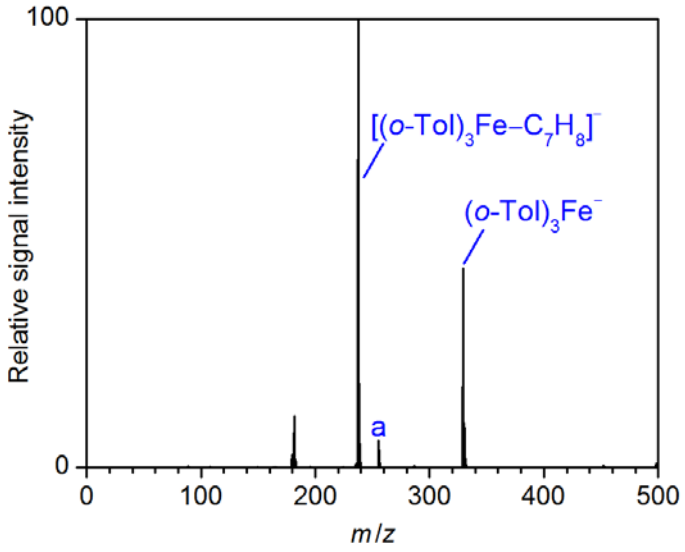

Figure S149. Mass spectrum of mass-selected $(o\text{-Tol})_3Fe^-$ (*m*/*z* 329) and its fragment ions produced upon collision-induced dissociation (V_{exc} = 0.80 V); a = $(o\text{-Tol})_2FeOH^-$.

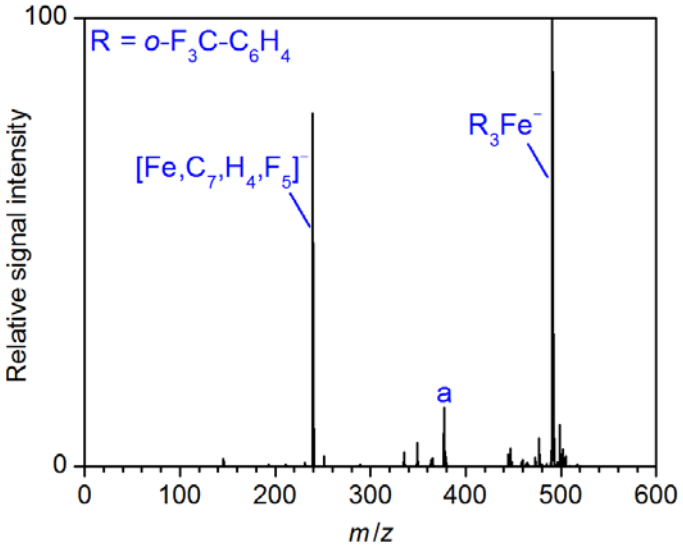

Figure S150. Mass spectrum of mass-selected R_3Fe^- (m/z 491) and its fragment ions produced upon collision-induced dissociation (V_{exc} = 0.80 V); a = $[Fe,C_{15},H_8,F_7]^-$; R = o-F_3C-C_6H_4.

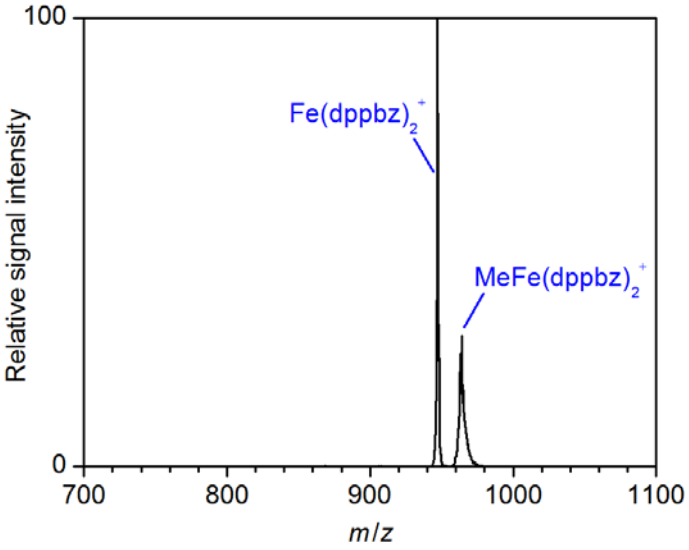

Figure S151. Mass spectrum of mass-selected $MeFe(dppbz)^+$ (m/z 963) and its fragment ions produced upon collision-induced dissociation (V_{exc} = 0.25 V).

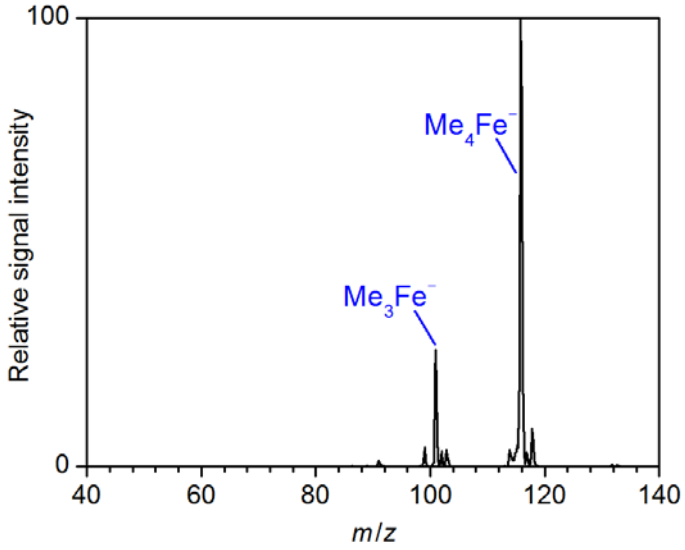

Figure S152. Mass spectrum of mass-selected Me_4Fe^- (*m*/*z* 116) and its fragment ions produced upon collision-induced dissociation (V_{exc} = 0.40 V).

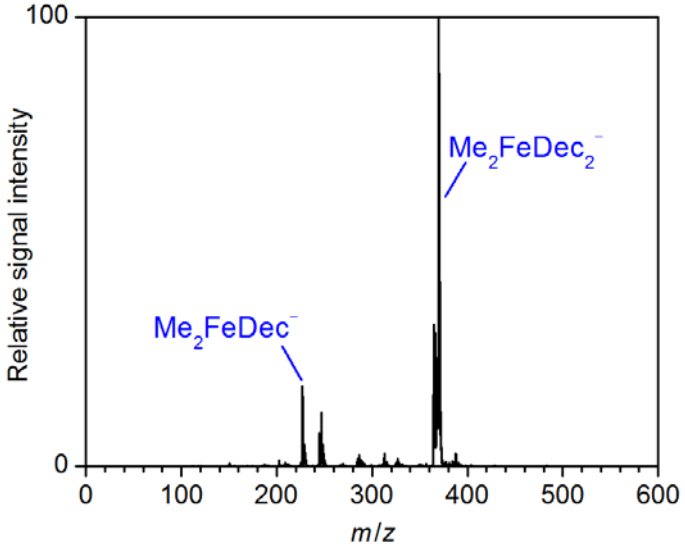

Figure S153. Mass spectrum of mass-selected $Me_2FeDec_2^-$ (*m*/*z* 368) and its fragment ions produced upon collision-induced dissociation (V_{exc} = 0.60 V).

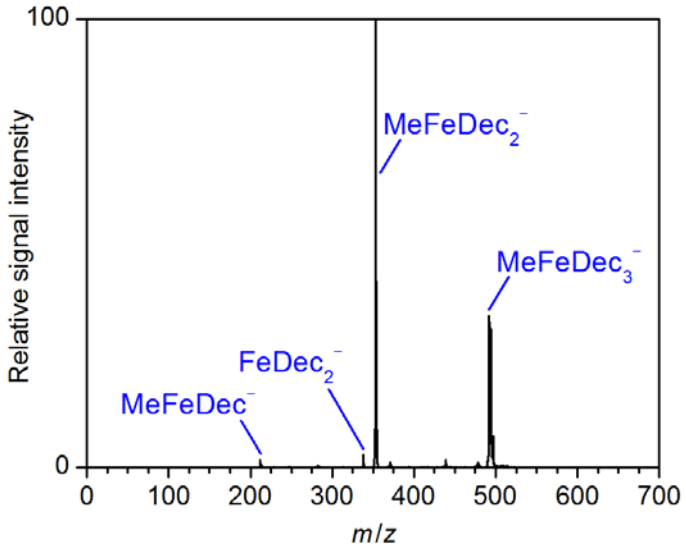

Figure S154. Mass spectrum of mass-selected $MeFeDec_3^-$ (*m*/*z* 494) and its fragment ions produced upon collision-induced dissociation (V_{exc} = 0.55 V).

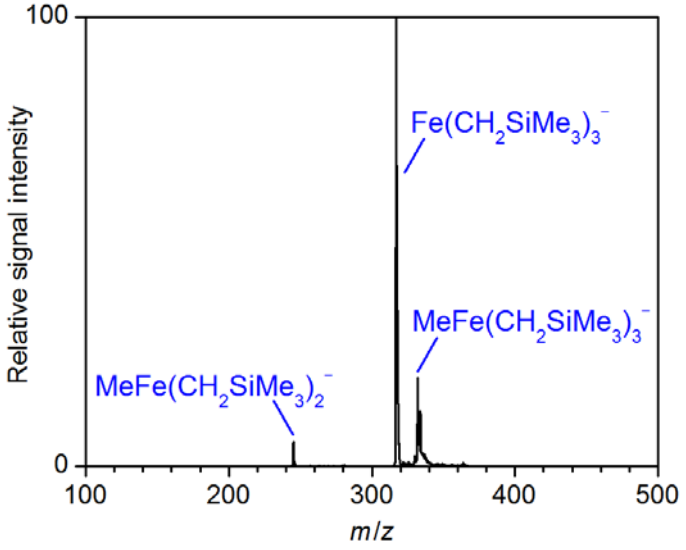

Figure S155. Mass spectrum of mass-selected $MeFe(CH_2SiMe_3)_3^-$ (*m*/*z* 332) and its fragment ions produced upon collision-induced dissociation (V_{exc} = 0.30 V).

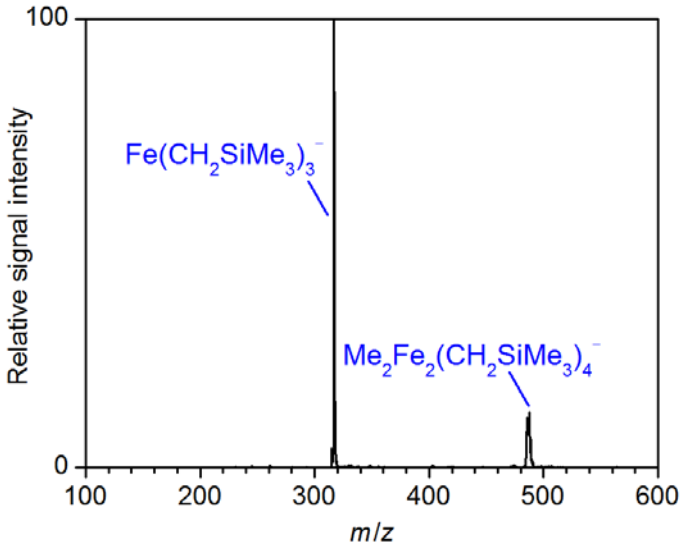

Figure S156. Mass spectrum of mass-selected $Me_2Fe_2(CH_2SiMe_3)_4^-$ (*m*/*z* 490) and its fragment ions produced upon collision-induced dissociation (V_{exc} = 0.50 V).

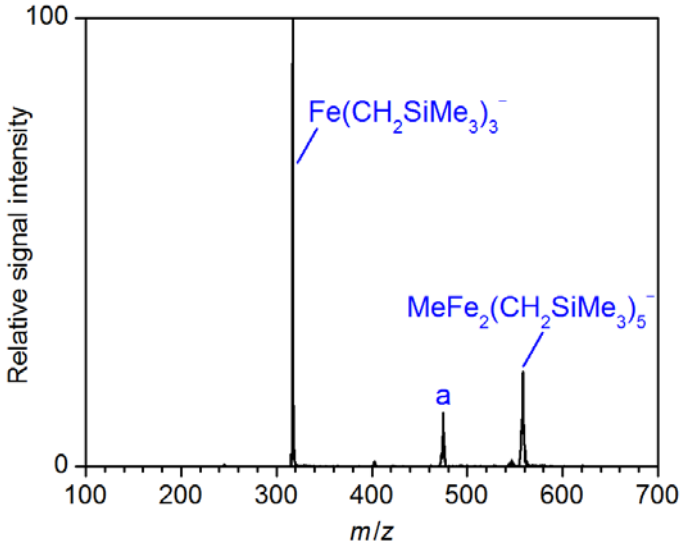

Figure S157. Mass spectrum of mass-selected $MeFe_2(CH_2SiMe_3)_5^-$ (*m*/*z* 562) and its fragment ions produced upon collision-induced dissociation (V_{exc} = 0.45 V); a = $MeFe(CH_2SiMe_3)_4^-$.

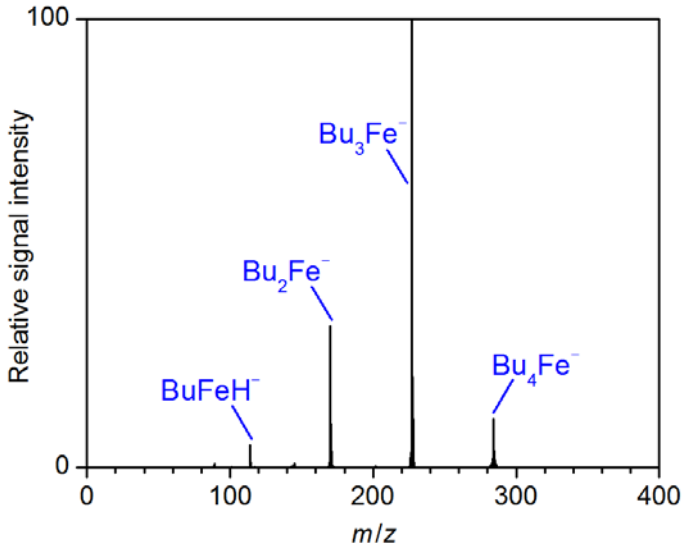

Figure S158. Mass spectrum of mass-selected Bu_4Fe^- (*m*/*z* 284) and its fragment ions produced upon collision-induced dissociation (V_{exc} = 0.20 V).

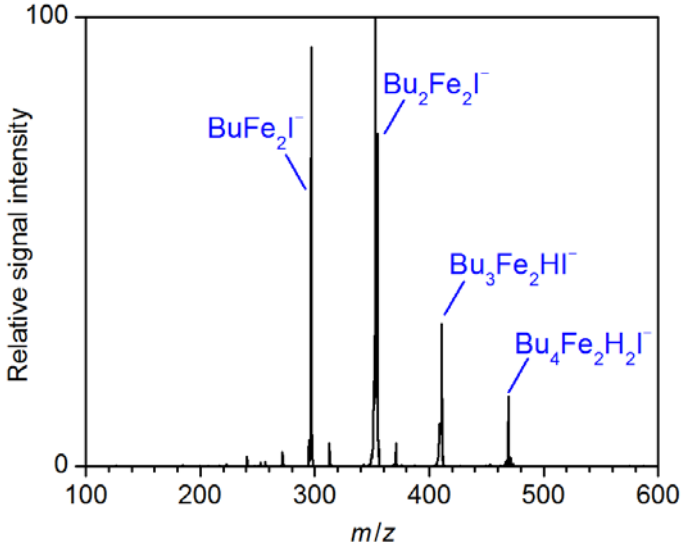

Figure S159. Mass spectrum of mass-selected $Bu_4Fe_2H_2I^-$ (*m*/*z* 469) and its fragment ions produced upon collision-induced dissociation (V_{exc} = 0.40 V).

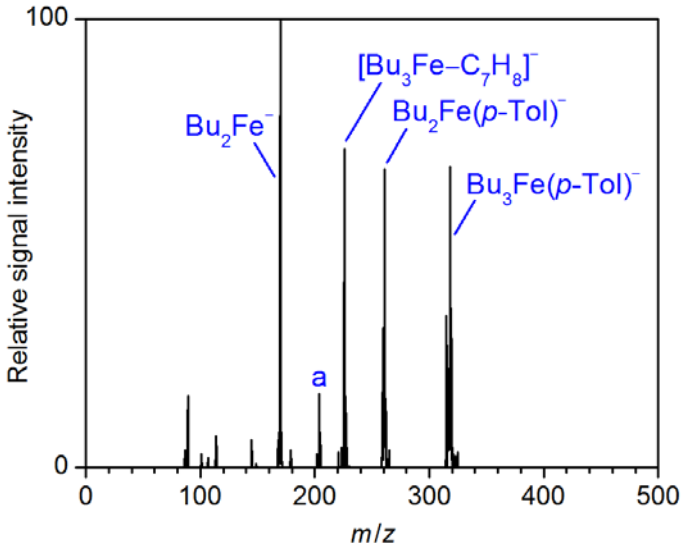

Figure S160. Mass spectrum of mass-selected $Bu_3Fe(p\text{-Tol})^-$ (m/z 318) and its fragment ions produced upon collision-induced dissociation (V_{exc} = 0.35 V); a = $BuFe(p\text{-Tol})^-$.

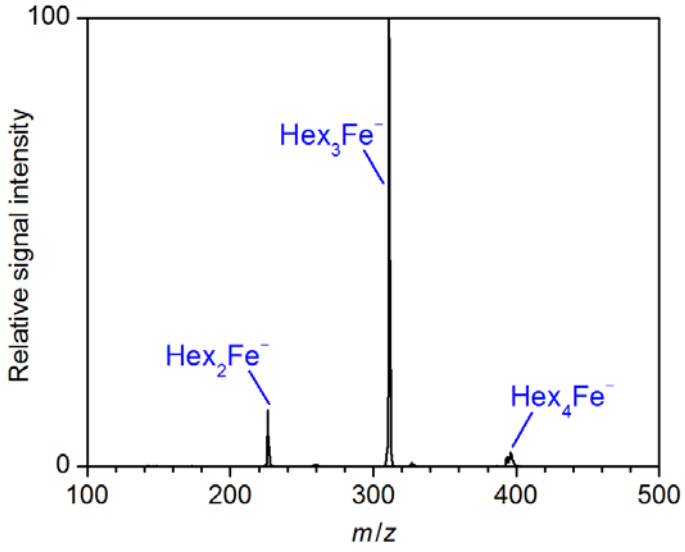

Figure S161. Mass spectrum of mass-selected Hex_4Fe^- (m/z 396) and its fragment ions produced upon collision-induced dissociation (V_{exc} = 0.55 V).

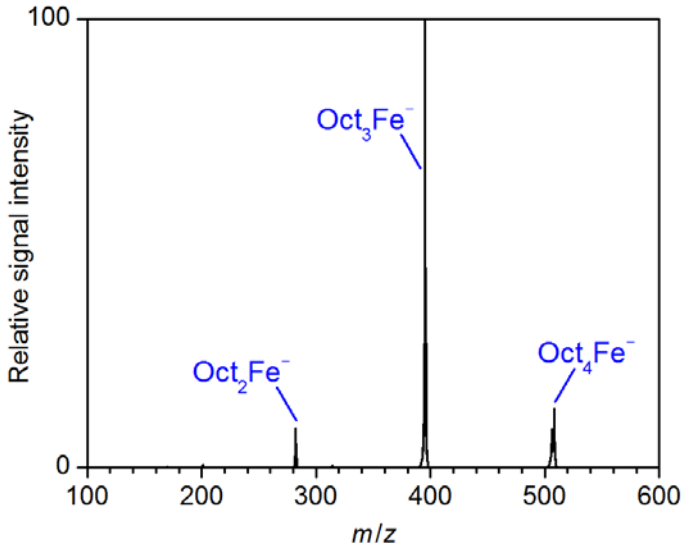

Figure S162. Mass spectrum of mass-selected Oct_4Fe^- (*m*/*z* 508) and its fragment ions produced upon collision-induced dissociation (V_{exc} = 0.55 V).

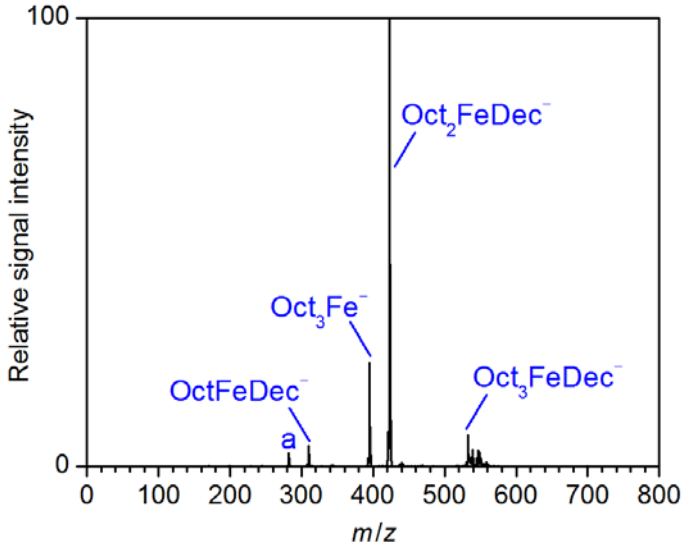

Figure S163. Mass spectrum of mass-selected Oct_3FeDec^- (*m*/*z* 536) and its fragment ions produced upon collision-induced dissociation (V_{exc} = 0.70 V); a = Oct_2Fe^-.

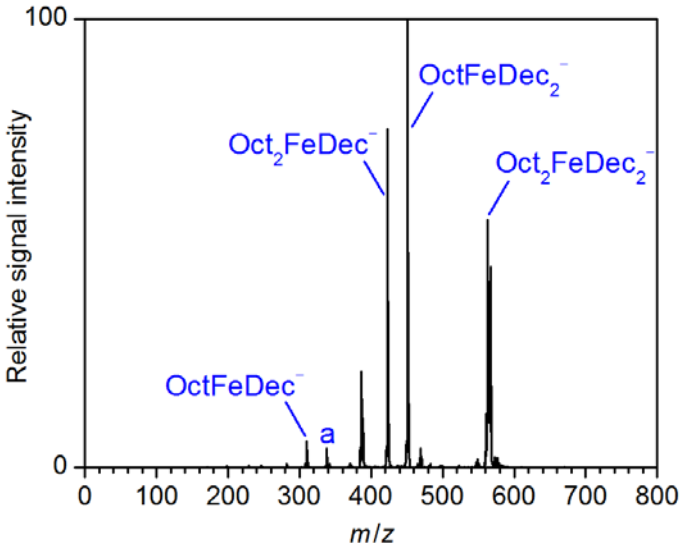

Figure S164. Mass spectrum of mass-selected $Oct_2FeDec_2^-$ (m/z 564) and its fragment ions produced upon collision-induced dissociation (V_{exc} = 0.70 V); a = $FeDec_2^-$.

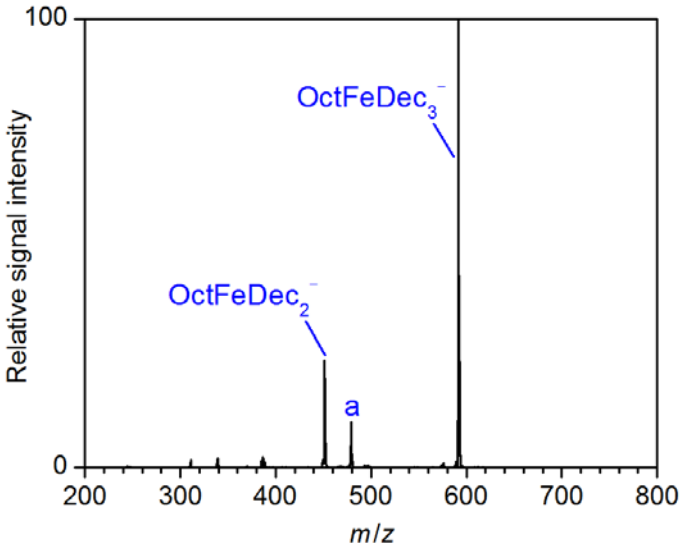

Figure S165. Mass spectrum of mass-selected $OctFeDec_3^-$ (m/z 592) and its fragment ions produced upon collision-induced dissociation (V_{exc} = 2.20 V); a = $FeDec_3^-$.

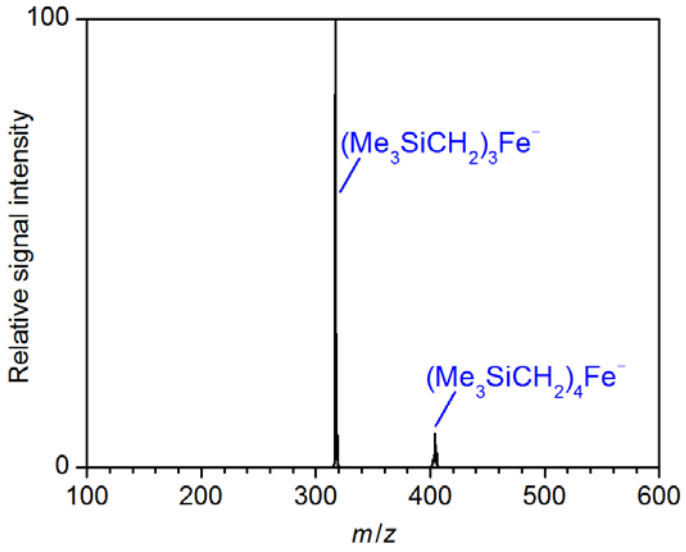

Figure S166. Mass spectrum of mass-selected $(Me_3SiCH_2)_4Fe^-$ (m/z 404) and its fragment ions produced upon collision-induced dissociation (V_{exc} = 0.40 V).

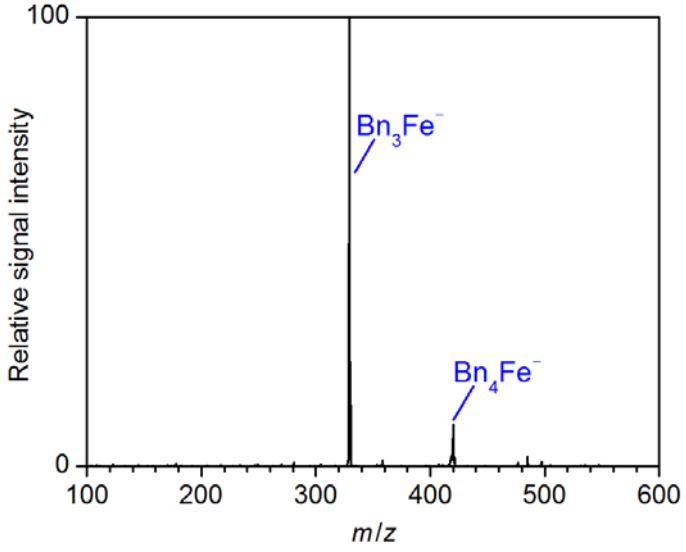

Figure S167. Mass spectrum of mass-selected Bn_4Fe^- (m/z 420) and its fragment ions produced upon collision-induced dissociation (V_{exc} = 0.30 V).

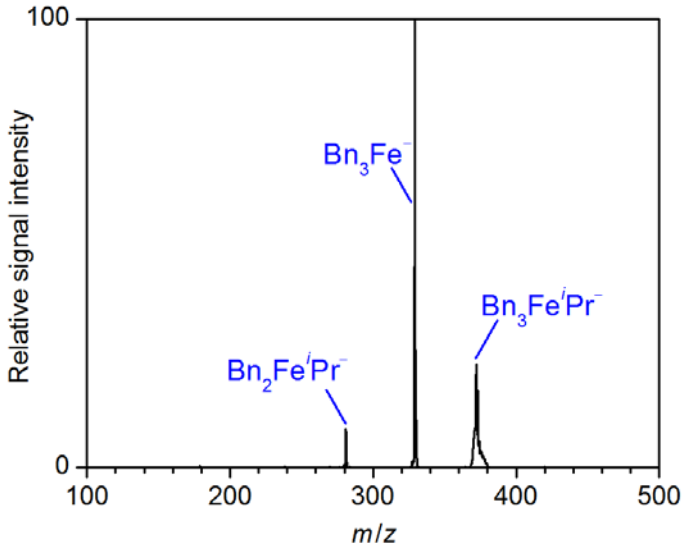

Figure S168. Mass spectrum of mass-selected $Bn_3Fe^iPr^-$ (m/z 372) and its fragment ions produced upon collision-induced dissociation (V_{exc} = 0.20 V).

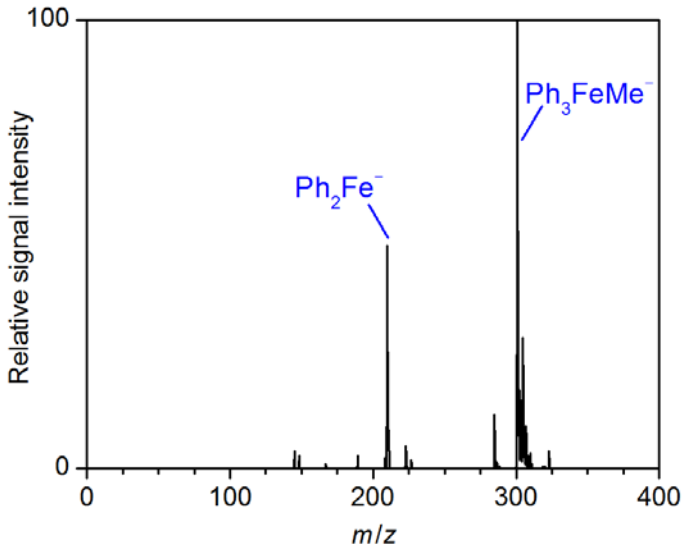

Figure S169. Mass spectrum of mass-selected Ph_3FeMe^- (m/z 302) and its fragment ions produced upon collision-induced dissociation (V_{exc} = 0.70 V).

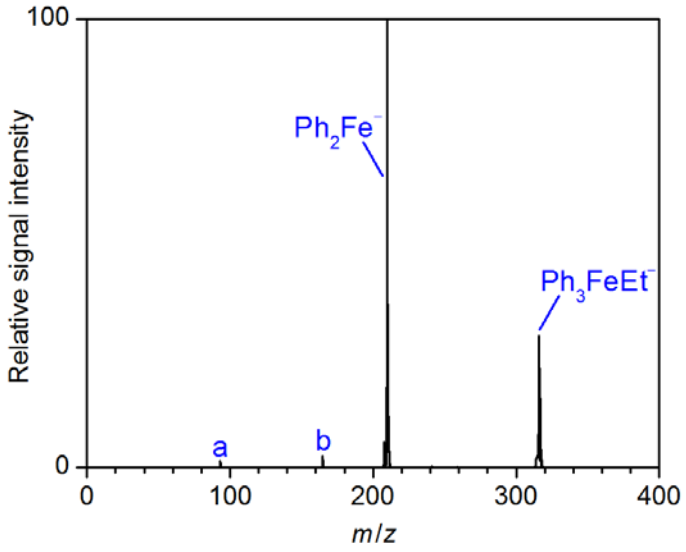

Figure S170. Mass spectrum of mass-selected Ph_3FeEt^- (m/z 316) and its fragment ions produced upon collision-induced dissociation (V_{exc} = 0.30 V); a = PhO^-, b = $[Ph,Fe,O_2]^-$.

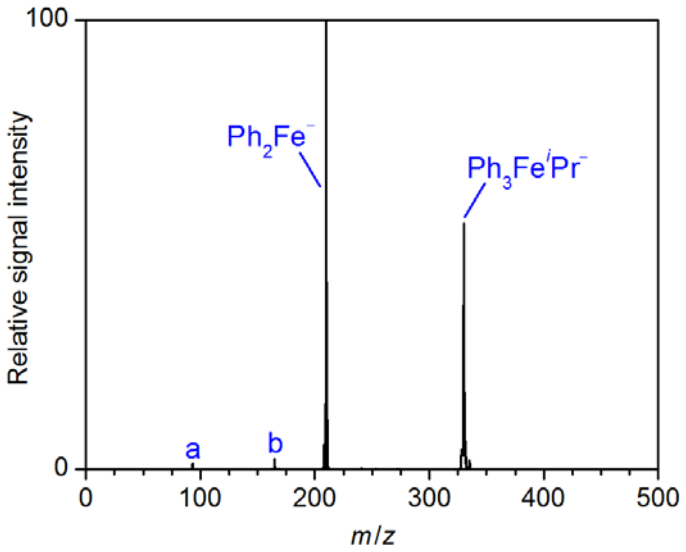

Figure S171. Mass spectrum of mass-selected $Ph_3Fe^iPr^-$ (m/z 330) and its fragment ions produced upon collision-induced dissociation (V_{exc} = 0.60 V); a = PhO^-, b = $[Ph,Fe,O_2]^-$.

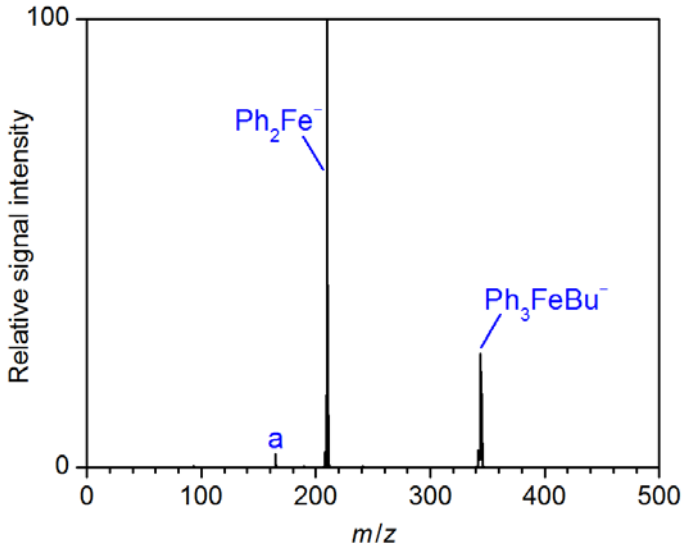

Figure S172. Mass spectrum of mass-selected Ph_3FeBu^- (m/z 344) and its fragment ions produced upon collision-induced dissociation (V_{exc} = 0.30 V); a = $[Ph,Fe,O_2]^-$.

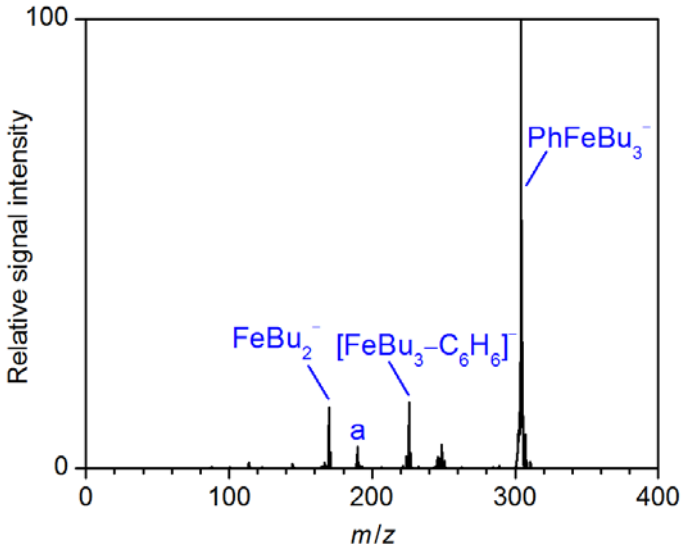

Figure S173. Mass spectrum of mass-selected $PhFeBu_3^-$ (m/z 304) and its fragment ions produced upon collision-induced dissociation (V_{exc} = 0.30 V); a = $PhFeBu^-$.

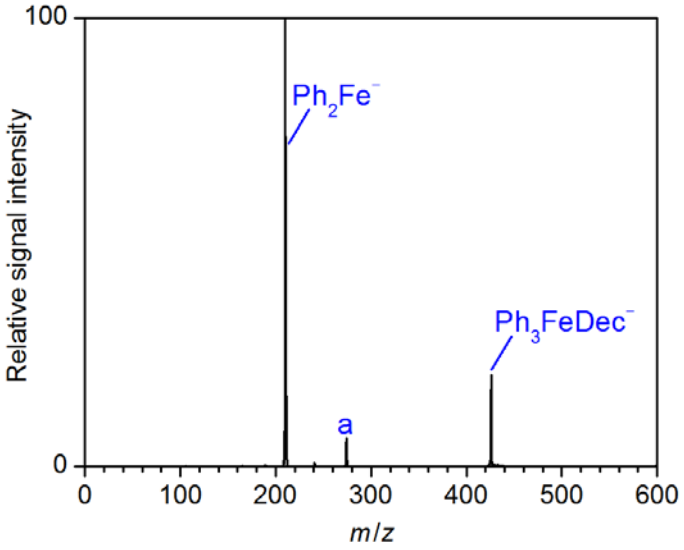

Figure S174. Mass spectrum of mass-selected Ph_3FeDec^- (*m*/*z* 428) and its fragment ions produced upon collision-induced dissociation (V_{exc} = 0.55 V); a = $PhFeDec^-$.

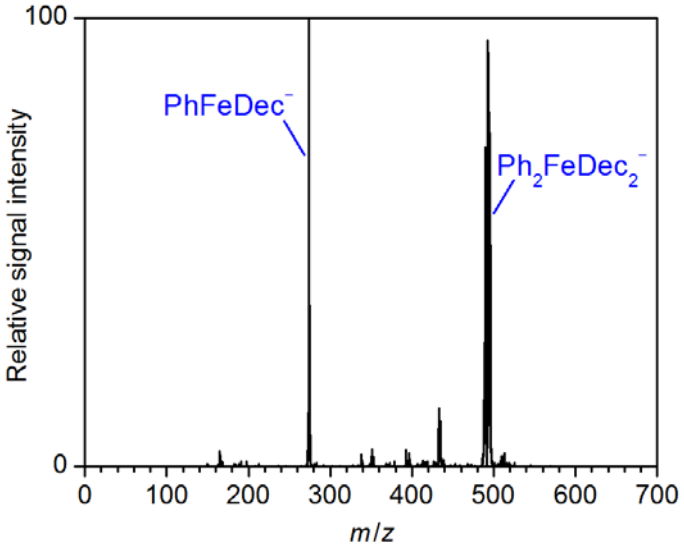

Figure S175. Mass spectrum of mass-selected $Ph_2FeDec_2^-$ (*m*/*z* 492) and its fragment ions produced upon collision-induced dissociation (V_{exc} = 0.65 V).

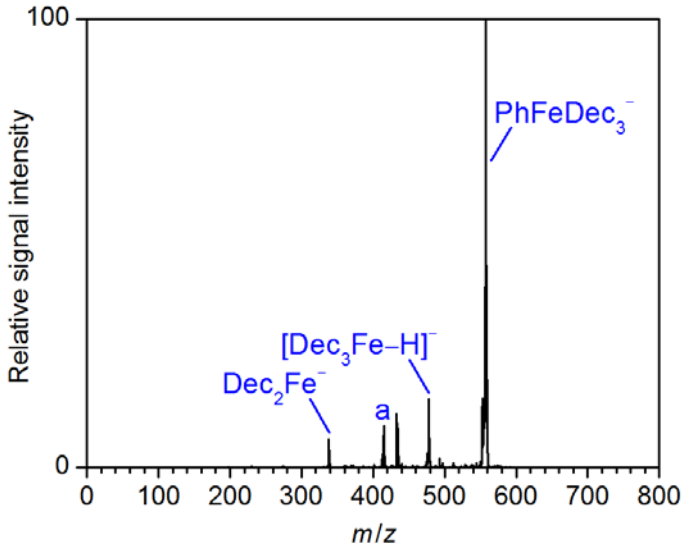

Figure S176. Mass spectrum of mass-selected $PhFeDec_3^-$ (*m*/*z* 556) and its fragment ions produced upon collision-induced dissociation (V_{exc} = 0.50 V); a = $PhFeDec_2^-$.

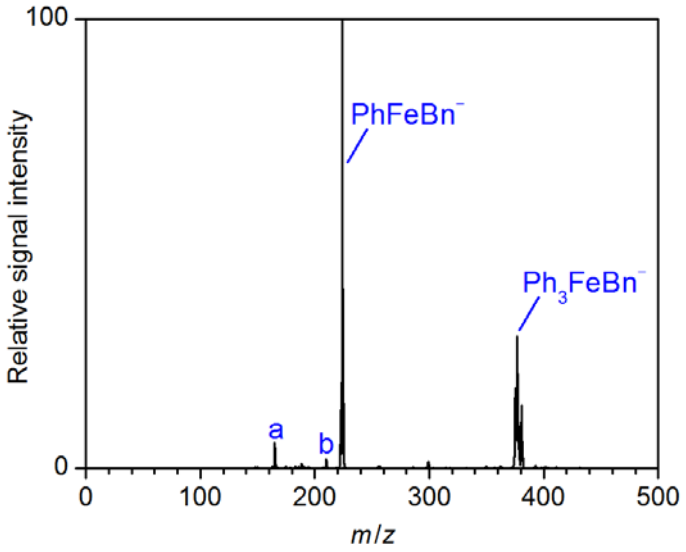

Figure S177. Mass spectrum of mass-selected Ph_3FeBn^- (*m*/*z* 378) and its fragment ions produced upon collision-induced dissociation (V_{exc} = 0.60 V); a = $[Ph,Fe,O_2]^-$, b = Ph_2Fe^-.

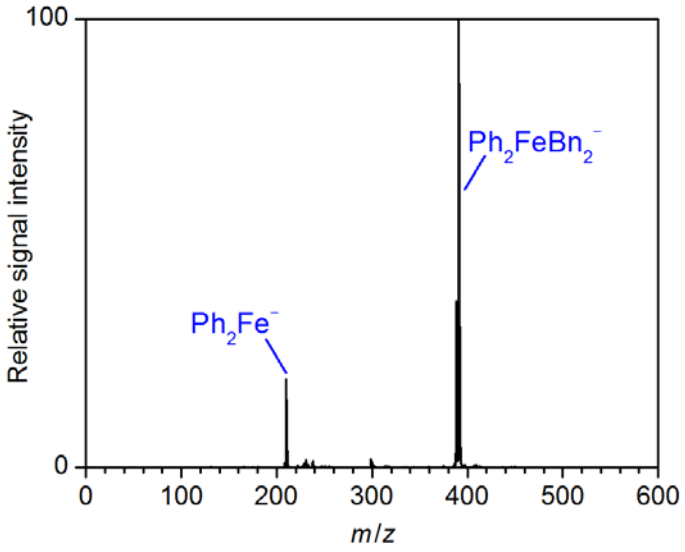

Figure S178. Mass spectrum of mass-selected $Ph_2FeBn_2^-$ (*m*/*z* 392) and its fragment ions produced upon collision-induced dissociation (V_{exc} = 0.80 V).

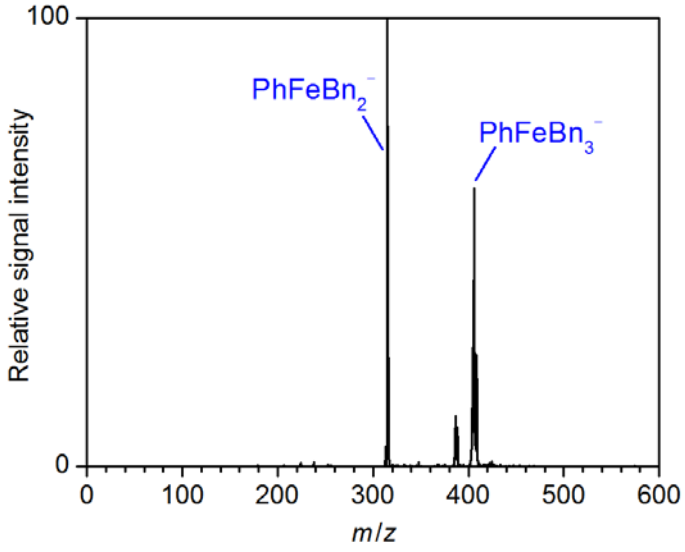

Figure S179. Mass spectrum of mass-selected $PhFeBn_3^-$ (*m*/*z* 406) and its fragment ions produced upon collision-induced dissociation (V_{exc} = 0.50 V).

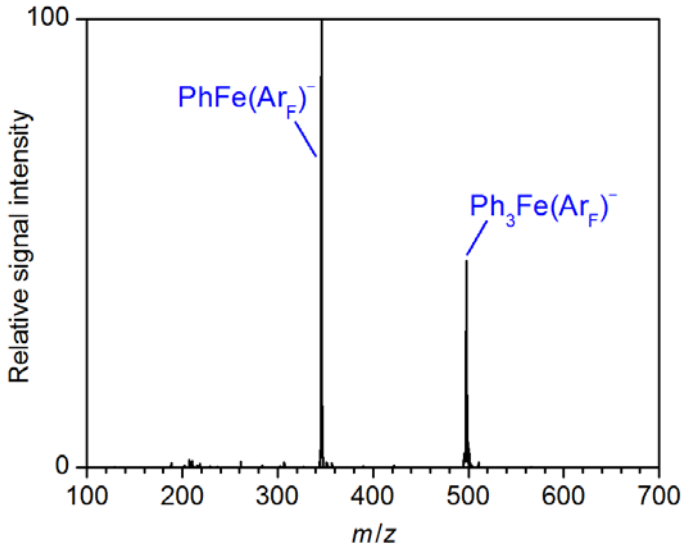

Figure S180. Mass spectrum of mass-selected $Ph_3Fe(Ar_F)^-$ (*m*/*z* 500) and its fragment ions produced upon collision-induced dissociation (V_{exc} = 0.70 V); Ar_F = 3,5-$(CF_3)_2$-C_6H_3.

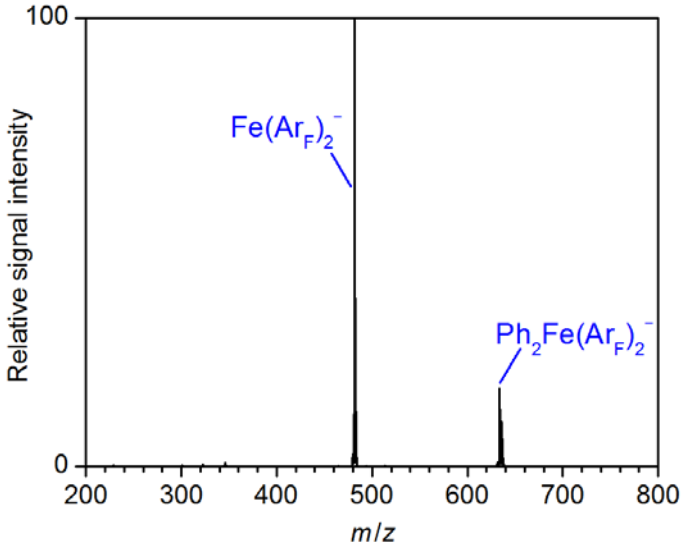

Figure S181. Mass spectrum of mass-selected $Ph_2Fe(Ar_F)_2^-$ (*m*/*z* 636) and its fragment ions produced upon collision-induced dissociation (V_{exc} = 0.70 V); Ar_F = 3,5-$(CF_3)_2$-C_6H_3.

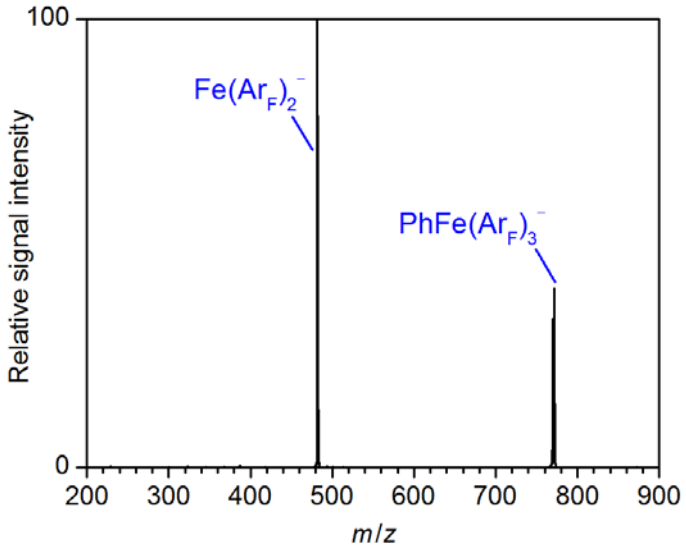

Figure S182. Mass spectrum of mass-selected PhFe$(Ar_F)_3^-$ (*m*/*z* 772) and its fragment ions produced upon collision-induced dissociation (V_{exc} = 0.90 V); Ar_F = 3,5-$(CF_3)_2$-C_6H_3.

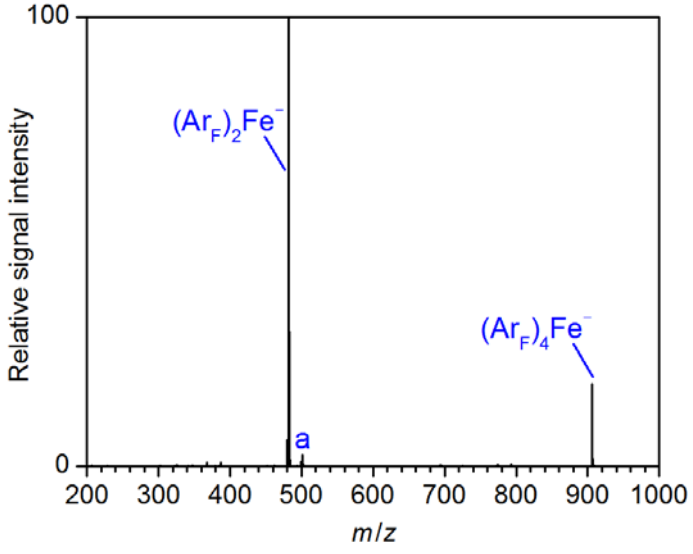

Figure S183. Mass spectrum of mass-selected $(Ar_F)_4Fe^-$ (*m*/*z* 908) and its fragment ions produced upon collision-induced dissociation (V_{exc} = 1.90 V); a = $(Ar_F)_2Fe(H_2O)^-$; Ar_F = 3,5-$(CF_3)_2$-C_6H_3.

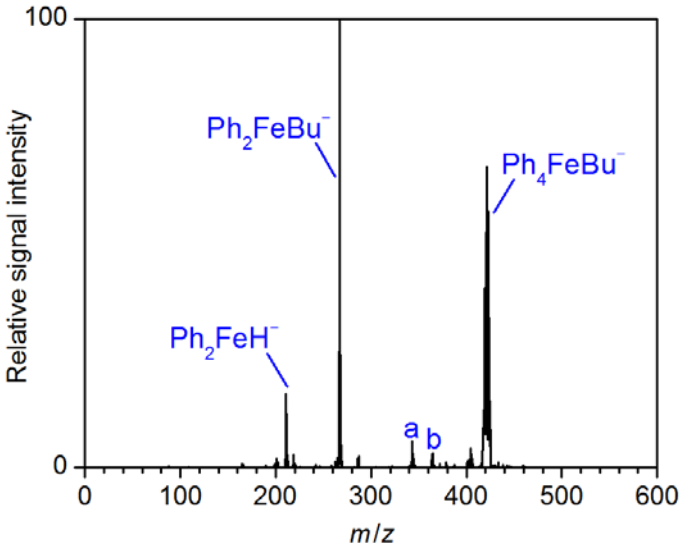

Figure S184. Mass spectrum of mass-selected Ph_4FeBu^- (m/z 421) and its fragment ions produced upon collision-induced dissociation (V_{exc} = 0.20 V); a = $[Ph_4FeBu–C_6H_6]^-$; b = Ph_4Fe^- + Ph_4FeH^-.

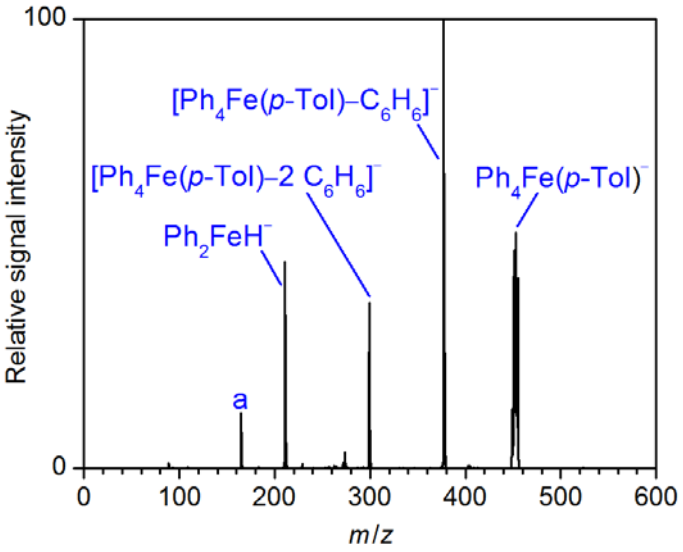

Figure S185. Mass spectrum of mass-selected $Ph_4Fe(p\text{-Tol})^-$ (m/z 455) and its fragment ions produced upon collision-induced dissociation (V_{exc} = 0.70 V); a = $[Ph,Fe,O_2]^-$.

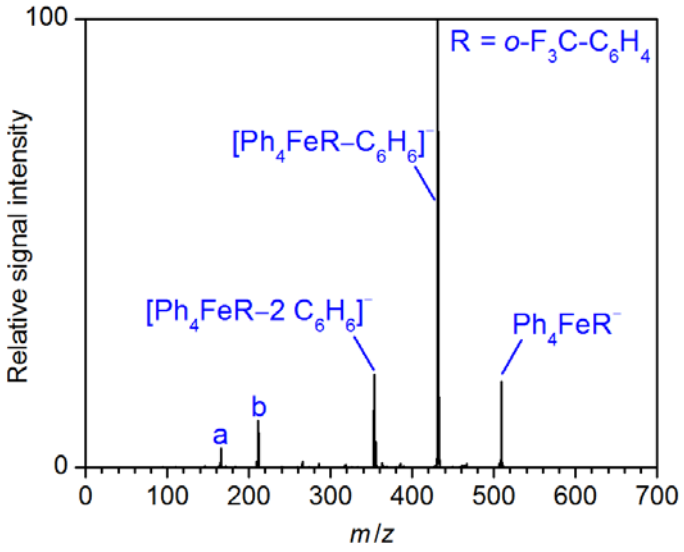

Figure S186. Mass spectrum of mass-selected Ph_4FeR^- (m/z 509) and its fragment ions produced upon collision-induced dissociation (V_{exc} = 0.60 V); a = $[Ph,Fe,O_2]^-$, b = Ph_2FeH^-; R = *o*-F_3C-C_6H_4.

7.) References

[1] Schnegelsberg, C.; Blümke, T. D.; Koszinowski, *J. Mass Spectrom*. **2015**, *50*, 1393-1395.
[2] Muñoz, S. B. III; Daifuku, S. L.; Sears, J. D.; Baker, T. M.; Carpenter, S. H.; Brennessel, W.W.; Neidig, M. L. *Angew. Chem. Int. Ed.* **2018**, *57*, 6496-6500; *Angew. Chem.* **2018**, *130*, 6606-6610.